HafenCity Universität Hamburg

Kumulative Dissertation

Titel der Dissertation

Physikalische Beschreibung der Wasser- und Energiebilanz von Gründächern

zur Erlangung des akademischen Grades
Doktor-Ingenieur
(Dr.-Ing.)

Datum der Einreichung
27.12.2025

Datum der Verteidigung
15.07.2026

Publikationsdatum
14.08.2026

vorgelegt von:
Dominik Gößner
Matrikelnummer: 6114931
dominik.goessner@hcu-hamburg.de

Erstgutachter:
Prof. Dr.-Ing. Wolfgang Dickhaut
wolfgang.dickhaut@hcu-hamburg.de

Zweitgutachter:
Prof. Dr.-Ing. Nicole Pfoser
nicole.pfoser@hfwu.de

Beratende Funktion:
Dr. Wolfgang Karl Hofbauer
wolfgang.hofbauer@ibp.fraunhofer.de

Dissertation, HafenCity Universität Hamburg
Forschungsgebiet: Bauingenieurwesen
Gutachter:innen: Prof. Dr.-Ing. Wolfgang Dickhaut
Prof. Dr.-Ing. Nicole Pfoser
Eingereicht am: 27.12.2025
Verteidigung am: 15.07.2026

Impressum

HafenCity Universität Hamburg
Henning-Voscherau-Platz 1
20457 Hamburg

Gößner, Dominik: *Physikalische Beschreibung der Wasser- und Energiebilanz von Gründächern*

Veröffentlichungsdatum: 14.08.2026

 Sofern nicht anders angegeben steht dieses Werk unter der Creative Commons Lizenz CC BY 4.0, www.creativecommons.org/licenses/by/4.0.

Zusammenfassung

Die vorliegende kumulative Dissertation widmet sich der physikalischen Beschreibung der Wasser- und Energiebilanz marktüblicher extensiver Gründachsysteme und schließt damit zentrale Forschungslücken in der urbanen Klimaanpassung. Auf Basis einer zweijährigen Lysimeter-Messkampagne wurden vier unterschiedliche Dachaufbauten (Economy-, Nature-, Garden- und Retention Roof) unter realen Witterungsbedingungen kontinuierlich untersucht. Dabei konnten signifikante Unterschiede in der Evapotranspiration (ET) sowie der Substrat- und Lufttemperaturen nachgewiesen werden, die direkt auf technische Systemparameter wie Speichervolumen, Substratdicke und Vegetationszusammensetzung zurückzuführen sind.

Ein Schwerpunkt der Arbeit lag auf der erstmaligen systematischen Erhebung vegetationsphysiologischer Steuergrößen auf Gründächern. Stomatäre Leitfähigkeit, Interzeptionskapazität sowie dynamische Parameter wie Plant Area Index (PAI) und Soil Cover Fraction (SCF) wurden Arten- bzw. Gründachspezifisch quantifiziert. Die Ergebnisse belegen, dass diese Größen entscheidend zur Steuerung von Transpirationsleistung, Interzeption und Temperaturregimen beitragen und die funktionale Differenzierung technischer Dachsysteme maßgeblich erklären.

Die gewonnenen Daten bildeten die Grundlage für die Entwicklung und Validierung eines praxistauglichen Simulationsmodells, das ET und Substrattemperatur mit hoher zeitlicher Auflösung prognostiziert. Das Modell integriert dynamische Stomatäre Widerstände, PAI-abhängige Interzeptionsspeicher und die hydraulische Kopplung zwischen Substrat- und Retentionsebene. Mit einem prozentualen Bias (PBIAS) von -1% für die Evapotranspirationsmodellierung erreicht es eine im Vergleich zu etablierten Ansätzen deutlich höhere Prognosegüte.

Die Dissertation zeigt, dass sich marktübliche Gründachsysteme nicht nur bautechnisch, sondern auch funktional stark unterscheiden und dass diese Unterschiede durch eine Kombination aus hochauflösenden Messungen und prozessintegrierter Modellierung präzise erfassbar sind. Damit wird sowohl ein methodischer Beitrag zur Weiterentwicklung der Gründachforschung als auch ein praktisches Instrument für Planung, Simulation und Bewertung grüner Infrastrukturen geleistet. Perspektivisch eröffnet die Arbeit Anknüpfungspunkte für die Übertragung auf andere Klimazonen, Vegetationstypen und Gebäudekontexte sowie für die Kopplung mit energetischen und städtebaulichen Modellen.

Abstract

The present cumulative dissertation focuses on the physical characterization of the water and energy balance of commercially available extensive green roof systems, thereby addressing key research gaps in urban climate adaptation. Based on a two-year lysimeter measurement campaign, four different roof configurations (Economy Roof, Nature Roof, Garden Roof, and Retention Roof) were continuously investigated under real meteorological conditions. Significant differences in evapotranspiration (ET) as well as in substrate and air temperatures were identified, which can be directly attributed to technical system parameters such as water storage capacity, substrate thickness, and vegetation composition.

A central focus of the dissertation was the first systematic assessment of vegetation-physiological control variables on green roofs. Stomatal conductance, interception capacity, and dynamic parameters such as Plant Area Index (PAI) and Soil Cover Fraction (SCF) were quantified in a species- and system-specific manner. The results demonstrate that these variables play a decisive role in controlling transpiration performance, interception processes, and temperature regimes, and substantially explain the functional differentiation of technical green roof systems.

The collected data formed the basis for the development and validation of a practice-oriented simulation model capable of predicting evapotranspiration and substrate temperature at high temporal resolution. The model integrates dynamic stomatal resistances, PAI-dependent interception storage, and the hydraulic coupling between the substrate and retention layers. With a percentage bias (PBIAS) of −1% for evapotranspiration modeling, it achieves a markedly higher predictive accuracy compared to established approaches.

The dissertation demonstrates that commercially available green roof systems differ not only in their structural design but also substantially in their functional performance, and that these differences can be precisely captured through a combination of high-resolution measurements and process-integrated modeling. The work thus provides both a methodological contribution to the advancement of green roof research and a practical tool for the planning, simulation, and assessment of green infrastructure. From a forward-looking perspective, the findings open pathways for transfer to other climate zones, vegetation types, and building contexts, as well as for integration with energetic and urban-scale model.

Inhaltsverzeichnis

TEIL 1: MANTELTEXT

1. EINLEITUNG: WISSENSCHAFTLICHE ERKENNTNISZIELE UND NEUARTIGKEIT DER FRAGESTELLUNG 1

1.1 Zielsetzung der Arbeit 1
1.2 Neuartigkeit der Fragestellung 1
1.3 Wissenschaftlicher Mehrwert 2
1.4 Übergeordnete Zielperspektive 2

2. STAND DER FORSCHUNG 3

2.1 Technische Heterogenität und fehlende Systemdifferenzierung 3
2.2 Pflanzliche Steuergrößen und Vegetationsdynamik 3
2.3 Datengrundlagen und Messzeiträume 3
2.4 Modellierungsansätze: Zwischen Vereinfachung und Komplexität 4
2.5 Zusammenfassung der Forschungslücken 4

3. FACHLICHER ZUSAMMENHANG DER EINZELNEN VERÖFFENTLICHUNGEN 5

3.1 Fachartikel 1 (Land, 2021): Evapotranspiration und klimatische Wirksamkeit verschiedener Gründächer 5
3.2 Fachartikel 2 (Building and Environment, 2025): Vegetationsphysiologie, Stomata und Interzeption 6
3.3 Fachartikel 3 (Urban Science, 2025): Modellierung der Wasser- und Energiebilanz 7

4. ERGEBNISSE 8

4.1 Empirische Differenzierung technischer Gründachsysteme 8
4.2 Integration vegetationsphysiologischer Steuergrößen 9
4.3 Entwicklung eines validierten Simulationsmodells 10

5 DISKUSSION UND OFFENE FORSCHUNGSFRAGEN 11

5.1 Beurteilung der Ergebnisse 11
5.1.1 Datenerhebung 11
5.1.2 Modellgüte 12
5.2 Weiterer Forschungsbedarf 13
5.2.1 Einschränkungen in der Temperaturmodellierung 13
5.2.2 Generalisierbarkeit auf andere Klimazonen und Vegetationstypen 13
5.2.3 Noch nicht vollständig abgebildete stomatäre Dynamik 14

6. STELLUNG IM RAHMEN VON KOAUTORENSCHAFTEN 15

6.1 Fachartikel 1 (Land, 2021): Evapotranspiration Measurements and Assessment of Driving Factors 15
6.2 Fachartikel 2 (Building and Environment, 2025): Green Roof Performance Monitoring 15
6.3 Fachartikel 3 (Urban Science, 2025): Evaporation and Substrate Temperature Modelling 15

7. SYNTHESE UND AUSBLICK 16

7.1 Zusammenführung der Kernergebnisse 16
7.2 Praxisrelevanz und Anwendungsfelder 16
7.3 Perspektiven für zukünftige Forschung 17
7.4 Schlussbemerkung 17

LITERATURVERZEICHNIS 18

TEIL 2: FACHARTIKEL

FACHARTIKEL 1 (LAND, 2021): EVAPOTRANSPIRATION MEASUREMENTS AND ASSESSMENT OF DRIVING FACTORS: A COMPARISON OF DIFFERENT GREEN ROOF SYSTEMS DURING SUMMER IN GERMANY 22

FACHARTIKEL 2 (BUILDING AND ENVIRONMENT, 2025): GREEN ROOF PERFORMANCE MONITORING: INSIGHTS ON PHYSICAL PROPERTIES OF 4 EXTENSIVE GREEN ROOF TYPES AFTER 2 YEARS OF MICROCLIMATIC MEASUREMENTS 44

FACHARTIKEL 3 (URBAN SCIENCE, 2025): YEAR-ROUND MODELING OF EVAPORATION AND SUBSTRATE TEMPERATURE OF TWO DISTINCT GREEN ROOF SYSTEMS 60

TEIL 1
MANTELTEXT

1. Einleitung: Wissenschaftliche Erkenntnisziele und Neuartigkeit der Fragestellung

Die zunehmende Versiegelung urbaner Räume und die spürbaren Folgen des Klimawandels – insbesondere in Form häufigerer Starkregenereignisse und sommerlicher Hitzeextreme – stellen Städte weltweit vor erhebliche Herausforderungen. Gründächer gelten in diesem Zusammenhang als wichtige Bausteine der städtischen Klimaanpassung. Sie tragen zur Reduktion des urbanen Wärmeinseleffekts bei, verbessern das Mikroklima, bieten Lebensraum für Flora und Fauna und können als dezentrale Retentionsräume zur Entlastung kommunaler Entwässerungssysteme beitragen [1–4]. Entsprechend erfahren sie eine wachsende Verbreitung, gefördert durch kommunale Förderprogramme, planerische Zielvorgaben und baurechtliche Vorgaben [5,6].

Trotz dieser Entwicklung bestehen erhebliche Wissenslücken im Hinblick auf eine umfassende physikalische Beschreibung ihrer Wirkmechanismen. Die meisten vorliegende Studien beleuchten oft nur einzelne Wirkdimensionen – wie den thermischen oder hydrologischen Nutzen bestimmter Aufbauten – und beschränken sich meist auf kurze Messzeiträume. Eine integrative, ganzjährige und auf marktübliche Systeme übertragbare Beschreibung der Wasser- und Energiebilanz von Gründächern unter realen Witterungsbedingungen fehlt bislang weitgehend [7].

1.1 Zielsetzung der Arbeit

Vor diesem Hintergrund verfolgt die vorliegende kumulative Dissertation das Ziel, marktübliche extensive Gründachsysteme physikalisch fundiert zu charakterisieren und zu modellieren. Die Untersuchung basiert auf empirischen Langzeitmessungen, pflanzenphysiologischen Analysen und modellgestützten Prognosen. Unter „marktüblich“ werden Gründachaufbauten mit gängigen Drän- oder Retentionselementen und typischen Vegetationsformen (Sedum, Gräser, Kräuter) verstanden [5].

Im Zentrum stehen folgende wissenschaftliche Erkenntnisziele:

1. **Ganzjährige, schichtübergreifende Analyse** der physikalischen Eigenschaften und klimatologischen Effekte von vier marktgängigen extensiven Gründachsystemen unter natürlichen Witterungsbedingungen.
2. **Systematische Erfassung vegetationsphysiologischer Parameter** wie Plant Area Index (PAI), Soil Cover Fraction (SCF), Interzeptionskapazität und stomatärer Widerstand, einschließlich ihrer saisonalen Dynamik und systemabhängigen Unterschiede.
3. **Entwicklung und Validierung eines praxistauglichen Prognosemodells**, das Evapotranspiration (ET) und Substrattemperatur als die wesentlichen Variablen für die Ermittlung sowohl der hydrologischen Leistung als auch der städtischen Kühlkapazität von Gründächern mit hoher zeitlicher Auflösung und unter Nutzung frei verfügbarer meteorologischer Eingangsdaten realistisch abbildet.

1.2 Neuartigkeit der Fragestellung

Die Neuartigkeit dieser Arbeit ergibt sich aus den umfassenden Messungen der untersuchten Gründachaufbauten in Kombination mit der darauf basierenden Erstellung und Validierung

eines Vorhersagemodells. Bestandteil der Messungen ist die langfristige, kontinuierliche Lysimeter-basierte Messung klimarelevanter Wasser- und Energieflüsse über mindestens zwei Vegetationsjahre, sowie die Erhebung bislang vernachlässigter pflanzenphysiologischer Steuergrößen (stomatärer Widerstand, Interzeption, PAI/SCF) unter praxisrelevanten Bedingungen. Die empirischen Befunde wurden dann in ein schlankes, validiertes Modell, das die unterschiedlichen technischen Aufbauten gängiger Gründachtypen berücksichtigt überführt, ohne hohe Rechenressourcen oder Spezialsoftware zu erfordern.

Das Modell simuliert sowohl hydrologische als auch thermische Prozesse über den Zeitraum von einem Jahr. Besondere Merkmale sind die explizite Berücksichtigung der Interzeption, die Integration saisonaler Vegetationsdynamiken, die Simulation der hydraulischen Kopplung zwischen Substrat- und Retentionsebene sowie die Validierung durch erhobene ET- und Temperaturdaten.

1.3 Wissenschaftlicher Mehrwert

Diese Herangehensweise erlaubt eine differenzierte Betrachtung extensiver Gründachsysteme. Durch die Quantifizierung technischer Unterschiede und deren Auswirkung auf Wasser- und Energiebilanzen werden präzisere Prognosen und Planungsgrundlagen möglich. Die Ergebnisse umfassen:

- Nachweis niedrigerer Lufttemperaturen auf Vegetationsebene, geringerer Substrattemperaturen und höherer ET-Raten in Systemen mit größerer Wasserspeicherfähigkeit.
- Artenspezifische (Sedum, Gräser, Kräuter) Erhebung der stomatären Leitwerte unter Realbedingungen zum Vergleich der Transpirationsleistungen
- Experimentelle Bestimmung der Interzeptionskapazitäten verschiedener Arten
- Ganzjährige Erhebung des Plant Area Index (PAI) und der Soil Cover Fraction (SCF) zur korrekten Modellierung der Pflanzentwicklung und damit der Verdunstungs- und Interzeptionsleistung über den Jahresverlauf
- Ableitung von Regressionsmodellen, die den Einfluss einzelner Umweltfaktoren (z. B. Lufttemperatur, Einstrahlung, Windgeschwindigkeit) auf die Gründachparameter quantifizieren.
- Darstellung das konstruktive Unterschiede von Gründachaufbauten auch zu deutlich unterschiedlichen klimatischen Effekten führen

1.4 Übergeordnete Zielperspektive

Langfristig zielt die Arbeit darauf, die Erkenntnisse in die Entwicklung von Gestaltungsstrategien für optimierte Gründächer einfließen zu lassen. Die Ergebnisse sollen helfen, Dachsysteme so auszulegen, dass sie ihre mikroklimatische Kühlwirkung und ihr Retentionspotenzial maximieren – insbesondere in dicht bebauten, klimaexponierten Stadtbereichen. Die gewonnenen Modelle und Daten dienen als Grundlage für Planung, Simulation und Bewertung grüner Infrastrukturmaßnahmen im Kontext des Klimawandels.

2. Stand der Forschung

Gründächer sind in den letzten beiden Jahrzehnten zunehmend Gegenstand wissenschaftlicher Untersuchungen geworden – sowohl im Hinblick auf ihr Potenzial zur Rückhaltung von Regenwasser als auch auf ihre Fähigkeit zur mikroklimatischen Verbesserung durch Verdunstungskühlung [8–10]. Die positiven Effekte gelten in der Fachwelt als weitgehend anerkannt. Dennoch bleibt die Forschung in weiten Teilen fragmentiert. Einzelaspekte wie Wasserrückhalt, Wärmedämmung, Pflanzenentwicklung oder Energieflüsse wurden zwar vielfach untersucht, jedoch fehlt bislang eine integrative, ganzheitliche Betrachtung marktüblicher Gründachaufbauten unter realen, praxisrelevanten Bedingungen [7].

2.1 Technische Heterogenität und fehlende Systemdifferenzierung

Ein zentrales Defizit besteht in der unzureichenden Berücksichtigung der technischen Heterogenität. In vielen Studien erfolgt lediglich eine grobe Unterteilung in „extensive“ und „intensive“ Systeme, ohne die erheblichen Unterschiede in Substrataufbau, Schichtdicke, Speicherschichten, Drainage- und Retentionselementen oder Vegetationszusammensetzung zu berücksichtigen. Diese Parameter beeinflussen maßgeblich den Wasser- und Energiehaushalt eines Gründaches [9,11]. Vergleichende Studien, die gezielt unterschiedliche marktübliche Systeme gegenüberstellen, sind selten und fokussieren meist auf einzelne Wirkdimensionen wie die Abflussverzögerung oder die Wärmedämmung. Eine systematische Verknüpfung mikroklimatischer Effekte mit spezifischen Systemparametern auf Basis umfassender Wasser- und Energiebilanzmessungen über längere Zeiträume ist bislang nicht vorhanden [7].

2.2 Pflanzliche Steuergrößen und Vegetationsdynamik

Besonders unterrepräsentiert ist die empirische Erhebung pflanzenphysiologischer Steuergrößen unter Freilandbedingungen. Der stomatäre Widerstand – eine Schlüsselgröße der Transpiration – wird häufig modellhaft angesetzt, jedoch selten unter realen Klimabedingungen gemessen. Gleiches gilt für die Interzeptionsleistung der Vegetation sowie die dynamische Entwicklung des Plant Area Index (PAI) und des Soil Cover Fraction (SCF). Nur wenige Modelle (z. B. Tabares-Velasco et al. 2012; de Munck et al. 2013) integrieren validierte, saisonale Schwankungen dieser Parameter, obwohl diese für eine realistische Evapotranspirationsmodellierung entscheidend sind [7,12,13].

Erste Studien zur Interzeption urbaner Vegetation [14–16] zeigen deren potenziell hohen Beitrag zum Wasserhaushalt, insbesondere bei häufigen, kleineren Regenereignissen. Eine systematische Quantifizierung bei niedrigwüchsigen, für extensive Gründächer typischen Pflanzengesellschaften steht jedoch weitgehend aus.

2.3 Datengrundlagen und Messzeiträume

Viele Untersuchungen beschränken sich auf Sommermonate oder kurze Messperioden. Dadurch bleibt das saisonale Verhalten von Gründächern, insbesondere in Übergangszeiten oder bei Frost, unzureichend beschrieben. Vollständige Jahresdatensätze mit hoher zeitlicher Auflösung und parallel erfassten hydrologischen, thermischen und vegetationsphysiologischen Parametern sind rar. Nur vereinzelt existieren Studien, die Evapotranspiration, Interzeption, Substratfeuchte und -temperatur ganzjährig und systemübergreifend erfassen [7].

2.4 Modellierungsansätze: Zwischen Vereinfachung und Komplexität

Der Stand der Modellierung ist geprägt von zwei Extremen:

1. **Stark vereinfachte Modelle**, oft auf Basis des Penman–Monteith-Ansatzes mit konstanten Widerständen oder von Bucket-Modellen, die wichtige Steuergrößen wie Interzeption, Vegetationsdynamik oder hydraulische Kopplung zwischen Substrat und Retentionsschicht vernachlässigen.
2. **Komplexe, gekoppelte Wärme- und Feuchtetransportmodelle** (z. B. hygrothermische Simulationen mit HYDRUS-1D), die detaillierte Eingangsparameter, numerische Solver und hohe Rechenressourcen erfordern [17]. Diese liefern zwar hochaufgelöste Ergebnisse, sind jedoch für Planungs- und Praxisanwendungen oft ungeeignet.

Eine besondere Lücke besteht bei der Abbildung der hydraulischen Kopplung zwischen Substrat und Drainage- bzw. Retentionsebenen. In modernen, mehrschichtigen Systemen beeinflussen laterale Flüsse, kapillare Aufwärtsströmungen und Wasserspeicherung in Unterlagen die Verdunstungs- und Temperaturdynamik erheblich. Keines der in der Literatur identifizierten, praxistauglichen Modelle bildet diese Prozesse explizit ab [7].

Darüber hinaus fehlt es an Modellen, die alle wesentlichen Parameter – Interzeption, stomatärer Widerstand, PAI/SCF, Substrat-Retentionskopplung – integrieren und für eine ganzjährige Simulation empirisch validiert sind. Die wenigen vorhandenen Validierungen von Evapotranspiration (z. B. Takebayashi & Moriyama 2007; Tabares-Velasco et al. 2012) beschränken sich meist auf einzelne Jahreszeiten oder Wetterlagen.

2.5 Zusammenfassung der Forschungslücken

Zusammenfassend lassen sich folgende wesentliche Lücken im Stand der Forschung festhalten:

- Fehlende integrative Studien, die hydrologische, thermische und vegetationsphysiologische Prozesse marktüblicher Systeme unter realen Bedingungen ganzjährig erfassen.
- Unterrepräsentation empirisch validierter Steuergrößen wie Interzeption, stomatärer Widerstand und saisonale Vegetationsparameter in Modellen.
- Unzureichende Berücksichtigung der hydraulischen Kopplung zwischen Substrat- und Retentionsebenen.
- Mangel an praxistauglichen Modellen, die geringe Rechenressourcen benötigen, ganzjährig einsetzbar und für Planungsprozesse geeignet sind.

Die vorliegende Dissertation setzt an dieser Schnittstelle an. Ziel ist es, durch die Kombination langfristiger, systemübergreifender Messungen mit der Erfassung bislang vernachlässigter pflanzenphysiologischer Parameter und deren Integration in ein validiertes, rechenökonomisches Prognosemodell eine wissenschaftlich fundierte und praxisrelevante Beschreibung der Wasser- und Energiebilanz extensiver Gründachsysteme zu entwickeln.

3. Fachlicher Zusammenhang der einzelnen Veröffentlichungen

Die kumulative Dissertation basiert auf drei eigenständigen, peer-reviewten Fachartikeln, die jeweils unterschiedliche Aspekte der physikalischen Wasser- und Energiebilanz marktüblicher Gründachsysteme adressieren. Inhaltlich, methodisch und konzeptionell bauen die Arbeiten aufeinander auf und sind als integrierte Forschungssequenz zu verstehen. In ihrer Gesamtheit verfolgen sie das Ziel, die klimarelevanten Wirkungen extensiver Gründächer nicht nur zu messen und zu bewerten, sondern auch in ein valides, praxistaugliches Prognosemodell zu überführen.

3.1 Fachartikel 1 (Land, 2021): Evapotranspiration und klimatische Wirksamkeit verschiedener Gründächer

Die erste Publikation (siehe S. 21–42) bildet den empirischen Ausgangspunkt der Dissertation. Untersucht wurden vier marktübliche extensive Gründachsysteme – sog. Garden Roof, Economy Roof, Nature Roof und Retention Roof (s. Abbildung 1) - mit unterschiedlichen Substratdicken und Wasserspeicherkapazitäten über eine Vegetationsperiode unter realen Witterungsbedingungen. Ziel war es, die Evapotranspiration (ET), Substrattemperaturen und Wasserhaushaltsgrößen vergleichend zu quantifizieren und zentrale Steuergrößen zu identifizieren. Grundlage bildet eine Lysimeter-Versuchsplattform in Göggingen-Krauchenwies, die kontinuierliche Substratfeuchte, Substrat- und Lufttemperaturen, Wärmeflüsse sowie Abflussvolumina erfasste.

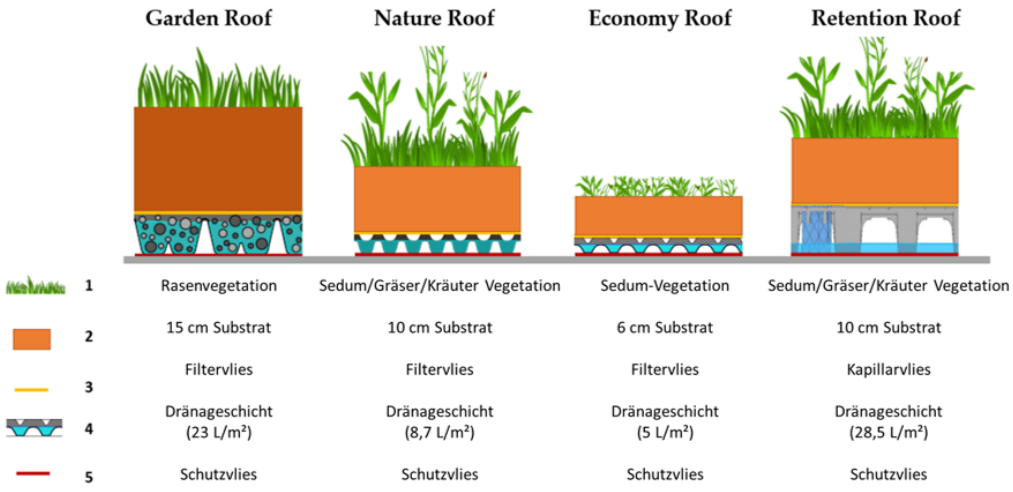


Abbildung 1: Beschreibung der vier untersuchten Systemaufbauten.

Zentrale Beiträge dieser Arbeit waren:

- Eine deutlich erhöhte Evapotranspiration im Retention- und Garden Roof (bis zu etwa 5 mm d^{-1}) gegenüber den anderen Systemen (häufig unter 3 mm d^{-1}).
- Signifikante Unterschiede in Substrat- und Lufttemperaturen, mit dem Economy Roof als wärmstem (Temperaturspitzen von über 35 °C) und dem Retention Roof als kühlstem Aufbau (um 5–8 K darunter). Nachts kehrte sich dieser Effekt teilweise um, wobei speicherstarke Systeme aufgrund der höheren Wärmespeicherkapazität langsamer abkühlten.

- Erhebung des Plant Area Index (PAI) und der Soil Cover Fraction (SCF) im Verlauf der Vegetationsperiode
- Erste Hinweise auf den Einfluss von Wasserverfügbarkeit, Vegetationstyp und Substratschicht auf das Verdunstungsverhalten

Diese Erkenntnisse lieferten die Grundlage für die Hypothese, dass sich Gründachsysteme nicht nur durch ihren bautechnischen Aufbau, sondern auch durch ihre pflanzenphysiologische Rückkopplung funktional stark unterscheiden – eine Annahme, die in den Folgearbeiten systematisch untersucht wurde.

3.2 Fachartikel 2 (Building and Environment, 2025): Vegetationsphysiologie, Stomata und Interzeption

Die zweite Veröffentlichung (siehe S. 43–58) baut auf den in Fachartikel 1 gewonnenen Erkenntnissen auf und erweitert die Untersuchung um eine zweijährige Messkampagne mit ganzjähriger Datenerfassung. Neben den hydrologischen und thermischen Parametern lag ein besonderer Fokus auf der detaillierten Erfassung pflanzenphysiologischer Steuergrößen **(**stomatäre Leitwerte und Interzeptionskapazität in Abhängigkeit des Plant Area Index (PAI)) und deren Wechselwirkungen mit den physikalischen Eigenschaften der Dachsysteme.

Wesentliche Beiträge dieser Arbeit waren:

- Quantifizierung des Stomatawiderstands verschiedener Dachpflanzen (Teppichsedum/*Sedum spurium,* Echter Schaf-Schwingel/*Festuca ovina,* Oregano/*Origanum vulgare*) unter realen Bedingungen:

  Artenreiche, kraut- und grasdominierte Vegetationsbestände wiesen im Mittel höhere stomatäre Leitfähigkeiten auf als Sedum-dominierten Bestände. Diese Unterschiede wirkten sich unmittelbar auf die Transpirationsleistung aus, besonders in gut mit Wasser versorgten Phasen.

- Empirische Korrelation zwischen Wasserverfügbarkeit, solarer Einstrahlung und stomatärer Aktivität:

  Die Analysen zeigten, dass stomatäre Leitwerte in gut wasserversorgten Phasen signifikant mit zunehmender Strahlungsintensität anstiegen, während unter Trockenstress eine deutliche Limitierung eintrat. Damit wurde bestätigt, dass die kombinierte Wirkung von Substratfeuchte und Einstrahlung eine zentrale Steuergröße für die Transpirationsleistung und die mikroklimatische Kühlwirkung darstellt.

- Nachweis signifikanter Unterschiede in der Interzeptionskapazität pflanzlicher Biomasse in Abhängigkeit vom PAI:

  Die Interzeptionsspeichergröße korrelierte signifikant mit dem PAI und variierte saisonal. Hohe PAI-Werte in den Sommermonaten führten zu einem erhöhten Anteil direkt verdunstenden Wassers ohne Durchgang ins Substrat, was besonders bei häufigen Kleinniederschlägen relevant sein kann.

Die statistische Auswertung unterstrich den Einfluss meteorologischer Faktoren – insbesondere globaler Strahlung, Dampfdruckdefizit und Lufttemperatur – auf die ET.

Gleichzeitig wurde deutlich, dass vegetationsphysiologische Parameter eine vergleichbare Bedeutung besitzen, um die Differenzen zwischen den Systemen zu erklären.

Die in Fachartikel 2 gewonnenen Erkenntnisse erweitern somit nicht nur das Verständnis der Interaktion physikalischer und biologischer Prozesse auf Gründächern, sondern liefern auch die für die Modellentwicklung in Fachartikel 3 notwendigen Eingangsdaten und Validierungsparameter.

3.3 Fachartikel 3 (Urban Science, 2025): Modellierung der Wasser- und Energiebilanz

Die dritte Arbeit (siehe S. 59–82) schließt den empirischen Teil der Dissertation ab und überführt die in den vorangegangenen Studien gewonnenen Erkenntnisse in ein praxisorientiertes Excel-basiertes Simulationsmodell, dass mit öffentlich zugänglichen Wetterdaten anwendbar ist. Das Ziel war, Evapotranspiration (ET) und Substrattemperatur über einen vollständigen Jahreszyklus für zwei repräsentative Systemtypen – ein frei drainiertes „Economy Roof“ und ein kapillar rückbefeuchtetes „Retention Roof“ – mit hoher zeitlicher Auflösung vorherzusagen.

Hauptmerkmale des Modells:

- Transpirationsberechnung durch Verknüpfung eines modifizierten Penman-Monteith-Ansatzes mit einem Dynamischer stomatärer Widerstand, kalibriert aus den in Fachartikel 2 ermittelten Leitwerten verschiedener Pflanzenarten.
- Differenzierte Simulation der Interzeption welche die PAI-abhängige Speichergröße sowie die Verdunstungsrate aus der Vegetationsoberfläche explizit berücksichtigt.
- Hydraulische Kopplung zwischen Substrat und Retentionsschicht, abgebildet durch einen empirisch kalibrierten Resättigungsfluss.
- Substratverdunstungskomponente, deren Oberflächenwiderstand feuchteabhängig skaliert wird.
- Substrattemperaturmodell auf Basis einer vereinfachten Energiebilanz mit feuchteabhängiger effektiver Wärmekapazität.

Validierungsergebnisse:

- **Evapotranspiration**: Für das Retention Roof erreichte das Modell eine sehr hohe Übereinstimmung mit den Messdaten (Bestimmtheitsmaß $R^2 = 0{,}87$, PBIAS = –1 %). Im Economy-System lag die Modellgüte etwas niedriger, was insbesondere auf stärkere Abweichungen in den wasserlimitierten Sommerphasen zurückzuführen ist.
- **Substrattemperatur**: Die Vorhersagegüte war im frei drainierten Dach hoch ($R^2 > 0{,}8$), zeigte im Retentionssystem jedoch in Frost- und Hochfeuchtephasen systematische Abweichungen. Ursache hierfür ist die noch fehlende explizite Modellierung von Phasenwechselprozessen und deren Einfluss auf die Wärmebilanz.
- **Saisonale Dynamik**: Das Modell konnte die saisonalen Unterschiede in ET und Temperaturverhalten reproduzieren, einschließlich der höheren winterlichen Substrattemperaturen in speicherstarken Systemen und der gesteigerten sommerlichen ET-Leistung bei höherem PAI.

Fachartikel 3 zeigt, dass ein vergleichsweise einfaches, in Tabellenkalkulation umsetzbares Modell die wesentlichen hydrologischen und thermischen Prozesse auf extensiven Gründächern realistisch abbilden kann, sofern zentrale pflanzenphysiologische und

systemtechnische Parameter berücksichtigt werden. Damit wird eine wichtige Forschungslücke geschlossen, da bisherige Modelle entweder stark vereinfacht und/oder unvollständig oder zu komplex und ressourcenintensiv waren.
Die Studie identifiziert zugleich Entwicklungsfelder – insbesondere die Integration feuchteabhängiger Wärmeleitfähigkeiten und latenter Wärmeflüsse bei Gefrier-/Tauprozessen – um die Prognosegüte unter winterlichen Bedingungen zu verbessern.

Durch die Integration der in Fachartikel 1 und 2 gewonnenen Erkenntnisse in ein Rechenmodell wird das zentrale Ziel der Dissertation eingelöst: die nutzbare, modelltheoretisch unterfütterte Beschreibung der Gründachwirkung als Klimaanpassungsmaßnahme.

4. Ergebnisse

4.1 Empirische Differenzierung technischer Gründachsysteme

Die zweijährige Erfassung relevanter physikalischer Größen (Evapotranspiration, Substratfeuchte, Substrat- und Lufttemperaturen) belegt erstmals empirisch, dass sich marktübliche extensive Gründachsysteme – trotz gleicher Klassifizierung – deutlich in ihrem mikroklimatischen Verhalten unterscheiden.

Substratfeuchte: Die Wasserspeicherfähigkeit erwies sich als entscheidender Faktor. Das Retention Roof wies mit Spitzenwerten über 35 % volumetrischer Wassergehalt ganzjährig die höchsten Feuchten auf, selbst in Trockenperioden selten unter 10 %. Dies ist auf die kapillare Rückbefeuchtung aus der Retentionsebene zurückzuführen. Vergleichbare Systeme ohne Retentionsschicht (z. B. Nature Roof) erreichten deutlich niedrigere Werte.

Evapotranspiration: Die Unterschiede in der Wasserverfügbarkeit der Systeme spiegelten sich klar in den täglichen Evapotranspirationsraten wider. Systeme mit großer Substrat- und Speichermächtigkeit erreichten während der Sommermonate Spitzenwerte von über 5 mm d^{-1} (Retention Roof und Garden Roof, Juni 2021) im Monatsmittel und lagen damit deutlich über den Werten der speicherarmen Aufbauten (Nature Roof: 3,87 mm d^{-1}, Economy Roof: 3,78 mm d^{-1}). Im Jahresmittel zeigte das Garden Roof mit rund 2,12 mm d^{-1} die höchste ET-Leistung, gefolgt vom Retention Roof (1,72 mm d^{-1}), dem Nature Roof (1,31 mm d^{-1}) und dem Economy Roof (1,27 mm d^{-1}). Die Ergebnisse belegen, dass zusätzliche Wasserspeicherung und kapillare Rückbefeuchtung in Retentionssystemen eine stabilere Verdunstungsleistung auch in Trockenperioden ermöglicht, während Systeme mit geringer Speicherfähigkeit eine deutlich höhere Anfälligkeit gegenüber Wasserstress aufweist.

Substrattemperatur: Die mittäglichen Maximaltemperaturen unterschieden sich je nach System um bis zu 8 K. Im Juni lag die Substrattemperatur des Retention Roofs Nachmittags bei nur 22 °C, während das Economy Roof 30 °C erreichte. Die tägliche Temperaturamplitude war beim Retention Roof am geringsten.

Lufttemperatur (Vegetationsniveau): Auch auf Vegetationsebene traten deutliche Unterschiede auf. Im Juni betrug die Mittagstemperatur über dem Retention Roof 26 °C und war damit bis zu 4 K niedriger als beim Economy Roof. Das Garden Roof zeigte in den Nachmittagsstunden die stärkste Kühlwirkung gegenüber den anderen Dachtypen.

Hinsichtlich des Abflussverhaltens zeigte sich, dass Systeme mit größerem Wasserspeicher signifikant geringere Abflussvolumina und verzögerte Abflussspitzen aufwiesen. Dies unterstreicht den Beitrag solcher Systeme zur Regenwasserbewirtschaftung und Überflutungsvorsorge.

Die multivariate Regressionsanalyse identifizierte die globale Strahlung, das Dampfdruckdefizit (VPD) und die Substratfeuchte als dominierende Einflussgrößen auf die ET. In wasserlimitierten Phasen war die ET in den Systemen mit geringer Speicherkapazität stärker durch sinkende Substratfeuchten begrenzt. Dies deutet auf eine höhere Anfälligkeit dieser Systeme gegenüber längeren Trockenperioden hin.

Insgesamt belegt dieser Datensatz, dass selbst innerhalb der Kategorie „extensiv" bau- und vegetationsbedingte Unterschiede von Substratdicke, Speichervolumen und Pflanzenzusammensetzung erhebliche Effekte auf Wasserhaushalt, Temperaturregime und mikroklimatische Leistungsfähigkeit haben. Diese quantitativen Unterschiede sind zentral für die Bewertung und Optimierung von Gründachsystemen als Klimaanpassungsmaßnahme.

4.2 Integration vegetationsphysiologischer Steuergrößen

Die erste und zweite Studie lieferte erstmals für extensive Gründächer in diesem Umfang erhobene und ganzjährig validierte Daten zu stomatärer Leitfähigkeit**,** Interzeptionskapazität**,** PAI und SCF. Damit wurde eine wesentliche Lücke zwischen vegetationsökologischer Grundlagenforschung und bautechnischer Anwendung geschlossen.

Stomatäre Leitfähigkeit: Die gemessenen Werte variierten stark zwischen den untersuchten Arten:

- Echter Schaf-Schwingel *(Festuca ovina)*: Ø 344,5 mmol m^{-2} s^{-1}
- Oregano *(Origanum vulgare)*: Ø 491,3 mmol m^{-2} s^{-1}
- Kamtschatkafetthenne *(Sedum kamtschaticum)*: Ø 143,0 mmol m^{-2} s^{-1}
- Teppichsedum *(Sedum spurium)*: Ø 141,5 mmol m^{-2} s^{-1}

Diese Unterschiede beeinflussten die Transpirationsleistung signifikant. Die Leitfähigkeit korrelierte positiv mit Substratfeuchte und Dampfdruckdefizit (VPD), wobei das Ausmaß system- und artabhängig war.

Interzeption: Die Interzeptionskapazität reichte von ca. 0,3 l m^{-2} (*Origanum vulgare*) bis über 1,5 l m^{-2} (Graues Heiligenkraut/*S. chamaecyparissus*). Zwischen PAI und Interzeptionskapazität bestand eine enge lineare Beziehung (R^2 = 0,91). Das abgeleitete empirische Modell ermöglicht eine Abschätzung der Interzeptionsleistung für Sedum-dominierte Bestände und kleine Sträucher.

Vegetationsentwicklung: Der SCF erreichte in allen Systemen im Mittel Werte um und über 90 %. Der PAI variierte zwischen den Systemen stark (max. ca. 8 beim Nature Roof, 4 beim Garden Roof) und spiegelte Unterschiede in Artenzusammensetzung und Wuchsform wider.

Substrattemperatur: Eine negative Korrelation zwischen Substratfeuchte und -temperatur wurde in allen Systemen festgestellt, besonders ausgeprägt bei trockenen Bedingungen (< 10 % Feuchte). Im Retention Roof führte eine Feuchte > 25 % zu einer mittäglichen Abkühlung von etwa 0,15 °C pro zusätzlichem Prozent Wassergehalt.

Insgesamt zeigt die Studie, dass vegetationsphysiologische Steuergrößen entscheidend für die mikroklimatische Leistungsfähigkeit von Gründächern sind und in praxistaugliche Prognosemodelle integriert werden sollten, um ET und Temperaturdynamik realistisch abzubilden.

4.3 Entwicklung eines validierten Simulationsmodells

Mit dem in Fachartikel 3 entwickelten Modell steht erstmals ein praxisorientiertes Werkzeug zur Verfügung, das Evapotranspiration (ET) und Substrattemperatur ganzjährig vorhersagen kann und zentrale Steuergrößen wie Interzeption, dynamischen stomatären Widerstand, saisonale Vegetationsdynamik und hydraulische Kopplung zwischen Substrat- und Retentionsebene integriert. Das Modell verwendet leicht zugängliche meteorologische Eingangsdaten und ist in Microsoft Excel implementiert, was zeigt das eine Anwendung in Planung und Forschung ohne hohe Rechenressourcen möglich ist.

Entsprechend dem Titel der Arbeit wurde im Modell die vollständige Energie- und Wasserbilanz abgebildet. Allerdings konnte diese nicht explizit validiert werden. Hintergrund ist, dass die für die Validierung der Energiebilanz benötigten Messwerte der Bodenwärmestromsensoren in den kleinen metallenen Messkammern (Lysimetern) keine durchgehend plausiblen Werte aufzeichneten und die Qualität der Abflussmessungen über Kippwagen zwar für die Verdunstungsquantifizierung ausreichend sind, aber nicht für die Ausweisung einer durchgehende Wasserbilanz. Insbesondere bei Starkregen kam es regelmäßig zu Verstopfungen der Kippwagen. Repräsentativ für die Energie- und Wasserbilanz wurden stattdessen die direkt praxisrelevanten Größen der Evapotranspiration und der Substrattemperatur zur Modellvalidierung verwendet.

Evapotranspiration:
Für das Retention Roof erreichte das Modell eine sehr hohe Güte (Jahres-R^2 = 0,87, PBIAS = –1 %) und saisonal R^2-Werte von 0,80 bis 0,96. Die mittlere tägliche ET wurde in allen Jahreszeiten gut erfasst, mit geringen Unterschätzungen im Frühjahr und leichten Überschätzungen im Herbst. Für das Economy Roof war die Modellgüte in Frühling und Sommer hoch (R^2 > 0,80), zeigte jedoch Überbewertungen im Herbst (PBIAS +78 %) und Schwächen im Winter (R^2 = 0,58), vermutlich bedingt durch eine unzureichende Abbildung reduzierter stomatärer Leitfähigkeit in der Vegetationsruhe. Im Mittel lag die modellierte ET des Retention Roofs 0,45 mm d^{-1} über der des Economy Roofs, was den Einfluss von Speicherhöhe und kapillarer Wasserbereitstellung bestätigt.

Substrattemperatur:
Die Vorhersagegüte variierte zwischen Systemen und Jahreszeiten. Für das Economy Roof lag R^2 von Frühling bis Herbst bei 0,88–0,92 (PBIAS = –5 bis –1 %), während die Wintervorhersagen ohne Frost-Tau-Prozesse unzureichend waren (PBIAS = –41 %). Für das Retention Roof zeigte sich in feuchten und winterlichen Perioden ein deutlicher Leistungsabfall (PBIAS = -90%), bedingt durch fehlende Phasenwechsel- und Feuchteeffekte in der Berechnung der Wärmekapazität. Dennoch lieferte das Modell in den warmen Jahreszeiten eine robuste Abbildung der Temperaturverläufe (PBIAS = -12 % bis -7 %).

Das Modell schließt die Lücke zwischen stark vereinfachten und hochkomplexen Simulationsansätzen, indem es wesentliche Prozesse integriert, empirisch validiert und in einer leicht anwendbaren Form bereitstellt. Damit bietet es Planern und Forschern ein

leistungsfähiges Werkzeug zur quantitativen Bewertung der mikroklimatischen Leistungsfähigkeit verschiedener Gründachsysteme.

5 Diskussion und offene Forschungsfragen

5.1 Beurteilung der Ergebnisse

Die im Rahmen dieser kumulativen Dissertation erzielten Ergebnisse leisten in mehrfacher Hinsicht einen substanziellen Beitrag zur Weiterentwicklung der Forschung im Bereich urbaner Begrünungssysteme. Im Zentrum steht dabei die quantitative, systemübergreifende Beschreibung der Wasser- und Energiebilanz extensiver Gründächer auf Basis technisch unterschiedlicher Aufbauten. Die Kombination aus Langzeitmessung, vegetationsphysiologischer Analyse und praxisnaher Modellbildung stellt eine methodische wie inhaltliche Erweiterung des bestehenden Kenntnisstandes dar.

5.1.1 Datenerhebung

Die vorliegende Studie stützt sich auf eine zweijährige, kontinuierliche Messkampagne, in der physikalische und vegetationsphysiologische Parameter marktüblicher extensiver Gründachsysteme erfasst wurden. Trotz der vergleichsweise kleinen Messflächen konnten potenzielle Randeffekte durch eine umlaufende Begrünung weitgehend minimiert werden. Abweichungen traten lediglich bei Wärmestrommessungen auf, vermutlich bedingt durch die metallische Unterkonstruktion. Für alle anderen Messgrößen ergaben sich keine Hinweise auf systematische Beeinträchtigungen der Ergebnisse.

Lufttemperatur auf Vegetationsebene: Kurzwellige Strahlung und Substrattemperatur erwiesen sich als die maßgeblichen Einflussgrößen. Im Juli lag die mittägliche Durchschnittstemperatur über dem Economy Roof bei 32,12 ± 7,52 °C, während das Retention Roof lediglich 27,35 ± 5,09 °C erreichte – ein Unterschied von mehr als 4,5 K. Über die gesamte Sommerperiode um 14:00 Uhr betrachtet, blieb das Retention Roof mit 26,36 ± 5,75 °C am kühlsten. Der Einfluss der kurzwelligen Strahlung variierte zwischen den Dachtypen (z. B. Garden Roof $\beta = 19{,}05$; Retention Roof $\beta = 10{,}35$; jeweils $p < 0{,}001$) [18]. Diese Ergebnisse stehen im Einklang mit früheren Arbeiten, die die Rolle der Wasserverfügbarkeit für die evaporative Kühlung betonen [19–22].

Stomatäre Leitfähigkeit: Die Messwerte liegen im Bereich oder oberhalb der in der Literatur berichteten Werte: *O. vulgare* zeigte die höchste Leitfähigkeit **(**Ø 491,3 mmol m^{-2} s^{-1}), gefolgt von *F. ovina* (Ø 344,5 mmol m^{-2} s^{-1}). Beide Sedum-Arten lagen bei ca. 140 mmol m^{-2} s^{-1}. Vergleichswerte aus der Literatur umfassen 190 mmol m^{-2} s^{-1} für die Prächtige Fetthenne/*Sedum spectabile* [23], 50–700 mmol m^{-2} s^{-1} für das Fuchsschwanzgewächs *Cyathula prostrata* [24] sowie 266–973 s m^{-1} stomatären Widerstand für *S. spurium* [25]. Demgegenüber berechnete Sailor [26] für Gründächer typische Widerstände von 50–300 s m^{-1}, während Tabares-Velasco und Srebric [27] 500–700 s m^{-1} für sukkulente Arten wie die Lesotho Mittagsblume/*Delosperma nubigenum* und *S. spurium* angaben. Diese Abweichungen verdeutlichen die Diskrepanz zwischen modellbasierten Annahmen und feldbasierten Messungen. Positiv bestätigte sich die in der Literatur mehrfach belegte Korrelation zwischen Leitfähigkeit, Substratfeuchte und Dampfdruckdefizit [12,28–31].

Evapotranspiration (ET): Die maximalen ET-Werte betrugen 6,79 mm d^{-1} (Retention Roof) und 6,75 mm d^{-1} (Garden Roof) und entsprechen damit den von Takebayashi und Moriyama [32] für ein 21 cm dickes, begrüntes System gemessenen 6,9 mm d^{-1} sowie den von Kaiser et al. [22] berichteten 5 mm d^{-1} bei bewässerten extensiven Dächern mit 9–21 cm Substrat. Der Zusammenhang zwischen hoher Wasserspeicherfähigkeit und stabiler ET-Leistung auch in Trockenperioden deckt sich mit Beobachtungen von Djedjig et al. [33] und Voyde et al. [34], die die Rolle ausreichender Substratfeuchte für eine kontinuierliche Verdunstungsleistung hervorheben. Als wesentliche Steuergrößen wurden Substratfeuchte, VPD und kurzwellige Strahlung identifiziert, was auch in anderen Studien bestätigt wird [12,29,35–37].

Interzeption: Die Interzeptionskapazität variierte stark (0,3 – >1,5 l m^{-2}) und korrelierte eng mit dem PAI (R^2 = 0,91). Diese Werte liegen im Rahmen bisheriger Studien: Kemp et al. [14] maßen für *S. spurium* 0,3–0,6 l m^{-2}, Smets et al. [38] für den echten Lavendel/*Lavandula angustifolia* 4,22 ± 1,83 l m^{-2}. Letztere Abweichung lässt sich durch unterschiedliche Berechnungsmethoden (Annahme 100 % Pflanzendeckung vs. tatsächlicher Deckungsgrad) erklären.

Substrattemperatur: Die Daten bestätigen frühere Ergebnisse, wonach dünnschichtige Systeme größere Temperaturamplituden aufweisen [39–41] und feuchtere Substrate zu niedrigeren Temperaturen führen [42].

Substratfeuchte: Die Werte lagen im Bereich anderer Studien: Tan et al. [24] berichteten 35 % Feuchte für ein 35 cm dickes Dach mit Retentionsschicht, gegenüber 22 % ohne. Heusinger und Weber [19] ermittelten für ein 8.600 m² großes, 9 cm dickes Dach ohne Drainschicht mittlere Trockenperioden-Feuchten um 10 % und Maximalwerte bis 42,3 %. Das Retention Roof dieser Studie wies mit bis zu 35 % Feuchte ganzjährig die höchsten und stabilsten Werte auf, selbst in längeren Trockenphasen selten unter 10 %.

Zusammenfassend zeigt die Datenerhebung, dass durch die Kombination hochauflösender, ganzjähriger Messungen mit detaillierter vegetationsphysiologischer Erfassung ein einzigartiger Datensatz entstanden ist, der nicht nur bestehende Literaturwerte bestätigt, sondern diese um praxisrelevante Kenngrößen erweitert und so eine belastbare Grundlage für die Modellierung der Wasser- und Energiebilanz extensiver Gründächer bietet.

5.1.2 Modellgüte

Im Vergleich zu bestehenden Modellierungsansätzen zeigt das entwickelte Modell punktuelle Leistungssteigerungen, insbesondere bei der Vorhersage der Evapotranspiration (ET) für das Retention Roof, während in anderen Bereichen – vor allem bei der Substrattemperatur und der ET des Economy-Dachs – die Modellgüte auf einem Niveau mit bisherigen Arbeiten liegt.

Für die Evapotranspiration des Retention Roofs erreicht das Modell eine hohe Übereinstimmung mit den Messdaten (R^2 = 0,87) bei gleichzeitig minimalem systematischen Fehler (PBIAS = –1 %). Diese Genauigkeit über den gesamten Jahresverlauf stellt einen klaren Fortschritt gegenüber etablierten Modellen dar, etwa denen von Feng (PBIAS 5–11 %, R^2 = 0,28–0,67) oder Tabares (PBIAS –24 % bis +4 %). Demgegenüber erzielt das Modell für das Economy Roof einen R^2 von 0,77 und einen PBIAS von +22 %, was auf eine moderate Überschätzung hinweist und im Bereich der vorgenannten Referenzmodelle liegt. Die Integration von Interzeptionsprozessen und einer expliziten Kopplung zwischen Substrat- und

Retentionsebene ist als methodische Verbesserung zu werten und zentraler Grund für die hohe hydrologische Prognosegüte des Retention Roofs.

Bei der Modellierung der Substrattemperatur liefert das Modell robuste, aber nicht außergewöhnliche Ergebnisse. Die Genauigkeit liegt insbesondere unter warmen und trockenen Bedingungen im Bereich der besten bisher publizierten Werte. Vergleichbare Leistungen werden beispielsweise von de Munck ($R^2 = 0,91$; RMSE = 4,32) oder Tabares (RMSE ≈ 2,0; PBIAS –4 % bis –6 %) [12,13] berichtet, womit das hier vorgestellte Modell für das Economy Roof im oberen Leistungsbereich liegt, diesen jedoch nicht signifikant übertrifft.

Zusammenfassend zeichnet sich das Modell weniger durch eine durchgehend überlegene quantitative Prognosegüte als vielmehr durch seine Prozessvollständigkeit und Transparenz aus. Einzigartige Merkmale wie die integrierte Interzeptionsmodellierung, dynamische Vegetationsparameter und die explizite hydraulische Kopplung der Retentionsebene erhöhen den Realismus und die Reproduzierbarkeit. Die deutlichsten Leistungsgewinne werden im Bereich der hydrologischen Modellgüte für retentionstechnisch optimierte Systeme erzielt, während bei vereinfachten Dachtypen die Vorhersagequalität auf dem Niveau bestehender Ansätze verbleibt.

5.2 Weiterer Forschungsbedarf

5.2.1 Einschränkungen in der Temperaturmodellierung

Die Modellierung der Substrattemperatur zeigte über weite Teile des Jahres – insbesondere während der Sommer- und Übergangszeiten – eine hohe Übereinstimmung mit den Messwerten. Unter extremen Bedingungen, wie gefrorenem Substrat oder vollständig wassergesättigten Substratprofilen, traten jedoch systematische Abweichungen auf. Besonders ausgeprägt war diese Diskrepanz beim Retention Roof während der Wintermonate, wo die simulierten Temperaturen deutlich von den gemessenen Werten abwichen.

Ursächlich hierfür sind Limitierungen in den thermischen Annahmen des Modells. Insbesondere fehlen bislang eine feuchteabhängige Wärmeleitfähigkeit, eine realitätsnahe Abbildung der spezifischen Wärmekapazität bei hohen Wassergehalten sowie die explizite Berücksichtigung von Gefrier-Tau-Prozessen und latenter Wärmefreisetzung. Diese Prozesse sind entscheidend, um die thermische Pufferwirkung und Phasenwechsel-bedingte Energieflüsse realitätsnah zu simulieren. In der aktuellen Modellformulierung werden sie jedoch stark vereinfacht.

Für eine künftige Weiterentwicklung des Modells ist daher eine Erweiterung des thermischen Moduls erforderlich. Die Integration von gefrier- und feuchteabhängigen Materialeigenschaften würde nicht nur die Prognosegüte in winterlichen und hochfeuchten Phasen verbessern, sondern auch eine realistischere Abbildung von Extremereignissen ermöglichen. Dies ist insbesondere für die Übertragbarkeit der Modellergebnisse auf kalte Klimazonen sowie für die Bewertung der ganzjährigen mikroklimatischen Leistungsfähigkeit von Gründächern von zentraler Bedeutung.

5.2.2 Generalisierbarkeit auf andere Klimazonen und Vegetationstypen

Die vorliegende Untersuchung wurde unter humiden mitteleuropäischen Klimabedingungen durchgeführt, die sich durch gemäßigte Temperaturen, eine ausgeglichene

Niederschlagsverteilung und vergleichsweise hohe Luftfeuchtigkeit auszeichnen. Unter ariden, semiariden oder submediterranen Klimaverhältnissen ist anzunehmen, dass sich sowohl das Verdunstungsverhalten als auch die physiologischen Reaktionen der Vegetation signifikant unterscheiden. Dies betrifft insbesondere den Einfluss von Wasserverfügbarkeit, Strahlungsintensität und Extremtemperaturen auf Evapotranspiration, stomatäre Leitfähigkeit und Interzeptionsleistung.

Ein weiterer Aspekt der Übertragbarkeit betrifft die Vegetationsstruktur. In dieser Studie wurden ausschließlich niedrigwüchsige Pflanzenarten untersucht, wie sie für extensive Gründächer typisch sind. Eine Übertragung der Modellergebnisse auf intensivere Dachbegrünungssysteme mit höherwüchsiger, artenreicher Vegetation oder auf andere Pflanzengattungen ist methodisch prinzipiell möglich, erfordert jedoch zusätzliche empirische Datenerhebungen sowie eine gezielte Anpassung und Kalibrierung der Modellparameter. Unterschiede in Wurzelarchitektur, Blattflächenindex, Jahresganganpassung und Wasserverbrauchsstrategien könnten die Modellgüte in solchen Szenarien erheblich beeinflussen.

Zudem basiert die Parametrisierung auf Messdaten zweier spezifischer Standorte und Systemaufbauten, wenngleich marktübliche Konfigurationen gewählt wurden. Für eine robuste Generalisierung auf andere Klimazonen oder stark abweichende Vegetationszusammensetzungen sind daher ergänzende Langzeitmessungen und Validierungen erforderlich. Dies gilt insbesondere für Regionen mit grundlegend unterschiedlichen klimatischen Bedingungen, wie Trockengebieten mit ausgeprägten Dürren, subtropischen Klimazonen mit stark saisonalen Niederschlägen oder Gebieten mit anhaltender Schneebedeckung im Winter, dort können sich Prozesse unterschiedlich verhalten und eine Neukalibrierung oder Anpassung erfordern.

Durch eine gezielte Erweiterung der Datengrundlage und standortspezifische Kalibrierung ließe sich die Anwendbarkeit des Modells deutlich erhöhen und seine Aussagekraft für ein breiteres Spektrum an Klimaräumen und Vegetationstypen sichern.

5.2.3 Noch nicht vollständig abgebildete stomatäre Dynamik

Trotz der Integration empirisch erhobener, artspezifischer Werte zur stomatären Leitfähigkeit verbleiben relevante Unsicherheiten in der Modellierung der Transpirationsdynamik.

Besonders deutlich werden diese Limitierungen bei vereinfachten Dachaufbauten wie dem Economy Roof, wo in den Herbstmonaten eine systematische Überschätzung der Evapotranspiration auftritt. Hier zeigt sich, dass die gegenwärtige Parametrisierung die Übergänge zwischen aktiver Vegetationsphase und beginnender Ruheperiode (Dormanz) – insbesondere im Spätherbst – noch nicht realitätsnah abbildet.

Für eine künftige Verbesserung der Modellgüte ist daher die Weiterentwicklung der stomatären Widerstandsmodelle erforderlich. Diese sollten neben artspezifischen Basiswerten auch saisonale Alterungsprozesse berücksichtigen. Ergänzende experimentelle Untersuchungen könnten hierbei eine belastbare Datenbasis liefern, um die Parametrisierung zu verfeinern und die Übertragbarkeit des Modells auf unterschiedliche Vegetationstypen und Klimaszenarien zu erhöhen.

6. Stellung im Rahmen von Koautorenschaften

Die kumulative Dissertation basiert auf drei wissenschaftlichen Artikeln, deren Autorenschaften und individuelle Beiträge klar und vollständig in den jeweiligen Veröffentlichungen dokumentiert sind. Die Zuordnung der Autorenrollen erfolgte offiziell im Rahmen des Reviewverfahrens der jeweiligen Artikel und wurde von allen Beteiligten bestätigt.

6.1 Fachartikel 1 (Land, 2021): Evapotranspiration Measurements and Assessment of Driving Factors

Die Arbeit entstand in Zusammenarbeit von Dominik Gößner (D.G.), Milena Mohri (M.M.) und Justine Krespach (J.K.) wie folgt:

- **D.G.**: Konzeption, Entwicklung der Methodik (Messkonzept, Auswahl/Identifikation und Art der Analyse), Supervision, Projektleitung und Finanzierungsakquise. Validierung der Untersuchung und Ressourcenmanagement gemeinsam mit M.M. Durchführung der Untersuchung gemeinsam mit J.K. Review und fachliche Überarbeitung im Team.
- **M.M.**: Erstellen des Originalentwurfs und Teile der Methodik, Visualisierung sowie formale Analyse zusammen mit J.K. Beteiligung an Datenvalidierung und Ressourcenmanagement.
- **J.K.**: Verantwortlich für Software und Datenkuratierung, Mitwirkung an der Untersuchung sowie Visualisierung und Analyse. Überarbeitung und Review im Team.

Die detaillierte Aufgabenteilung wurde im Rahmen des Review-Prozesses transparent dokumentiert und durch alle Autoren bestätigt.

6.2 Fachartikel 2 (Building and Environment, 2025): Green Roof Performance Monitoring

Die Arbeit entstand in Zusammenarbeit von Dominik Gößner (D.G.), Maria Kunle (M.K.) und Milena Mohri (M.M.) wie folgt:

- **D.G.**: Schreiben – Korrektur & Überarbeitung, Projektadministration, Einwerbung von Drittmitteln, Konzeption, Durchführung der Untersuchungen, Methodik, Validierung, Betreuung, Ressourcenmanagement, Schreiben des Originalentwurfs.
- **M.K.**: Schreiben – Korrektur & Überarbeitung, Projektadministration, Datenverwaltung, formale Analyse, Durchführung der Untersuchungen, Methodik, Visualisierung, Software.
- **M.M.**: Schreiben – Korrektur & Überarbeitung, Projektadministration, formale Analyse, Durchführung der Untersuchungen, Methodik, Visualisierung, Software, Schreiben des Originalentwurfs.

Auch hier ist die Aufgabenverteilung und der individuelle Beitrag jedes Autors offiziell Bestandteil des veröffentlichten Artikels und wurde im Begutachtungsprozess bestätigt.

6.3 Fachartikel 3 (Urban Science, 2025): Evaporation and Substrate Temperature Modelling

Den dritten Beitrag hat Dominik Gößner als Alleinautor vollständig konzipiert, bearbeitet und verfasst.

7. Synthese und Ausblick

Die vorliegende kumulative Dissertation liefert eine umfassende, datenbasierte und praxisrelevante Analyse der physikalischen Wasser- und Energiebilanzen extensiver Gründächer. In der Verknüpfung empirischer Feldmessungen, vegetationsphysiologischer Detailuntersuchungen und anwendungsorientierter Modellierung liegt ihr zentrales Innovationspotenzial. Die Ergebnisse belegen eindrucksvoll, dass sich marktübliche Gründachsysteme nicht nur in ihren baulichen Eigenschaften, sondern auch in ihren funktionalen Umweltwirkungen signifikant unterscheiden – und dass diese Unterschiede präzise mess- und berechenbar sind.

7.1 Zusammenführung der Kernergebnisse

Die drei Arbeiten der Dissertation entfalten ihre Wirkung in einem engen fachlichen Zusammenspiel:

- **Fachartikel 1** quantifiziert erstmals die Unterschiede der mikroklimatischen und hydrologischen Leistungsfähigkeit gängiger Gründachsysteme im direkten Vergleich unter realen Witterungsbedingungen.
- **Fachartikel 2** analysiert die zugrunde liegenden pflanzenphysiologischen Steuergrößen – insbesondere die Rolle von Stomata, Interzeption und PAI – und liefert damit eine Erklärungsbasis für die beobachteten Unterschiede.
- **Fachartikel 3** operationalisiert diese Erkenntnisse in einem Modell, das praxistaugliche, transparente und valide Prognosen für Evapotranspiration und Substrattemperatur auf Systemebene ermöglicht.

Es konnte gezeigt werden, dass vegetationsphysiologische Parameter wie stomatäre Leitfähigkeit, Interzeptionskapazität, PAI und SCF entscheidende Steuergrößen darstellen. Diese wurden erstmals systematisch auf Gründächern unter Realbedingungen erhoben und erlauben eine verbesserte Parametrisierung von Prognosemodellen.

Durch die Kombination dieser drei Forschungsperspektiven wird ein Erkenntnisraum aufgespannt, der sowohl grundlagenwissenschaftlich als auch anwendungsnah hohe Relevanz besitzt. Die Arbeit trägt damit zur methodischen Weiterentwicklung der Gründachforschung ebenso bei wie zur strategischen Fundierung städtischer Klimaanpassungsmaßnahmen.

7.2 Praxisrelevanz und Anwendungsfelder

Das entwickelte Prognosemodell erlaubt eine differenzierte Bewertung von Gründachsystemen im Hinblick auf:

- Evapotranspirative Kühlleistung, etwa zur Abschätzung lokaler thermischer Entlastung,
- Verdunstungsbasierte Rückhaltung, z. B. zur Dimensionierung von Retentionsdächern im Kontext der Starkregenvorsorge,

- Planungs- und Genehmigungsverfahren, bei denen wasserwirtschaftliche oder energetische Kriterien zu berücksichtigen sind (z. B. nach DWA-A 102-1),
- sowie die Integration in städtische Simulationswerkzeuge wie ENVI-met oder urbane Wassermodellierungen.

Die einfache Implementierbarkeit in eine Software erhöht die Zugänglichkeit für Planende, Kommunen und Forschungseinrichtungen, ohne auf wissenschaftliche Tiefe zu verzichten. Besonders für Kommunen und Planungsbüros eröffnet sich die Möglichkeit, unterschiedliche Dachaufbauten hinsichtlich ihrer Kühlleistung und Retentionswirkung vergleichend zu bewerten. Durch die Systemdifferenzierung können Planungsentscheidungen fundierter getroffen werden. Die erhobenen Interzeptions- und Stomatadaten sind zudem für die Weiterentwicklung von Klima- und Wasserhaushaltsmodelle relevant.

7.3 Perspektiven für zukünftige Forschung

Auf Basis der Dissertation ergeben sich mehrere anschlussfähige Forschungslinien:

- **Modellerweiterung auf andere Vegetationstypen und Klimazonen**: Eine Überprüfung und Kalibrierung des Modells für aride, subtropische oder kontinentalere Klimate sowie intensivere Dachbegrünungen ist ebenso naheliegend wie die Ausweitung auf höhere Wuchsformen (z. B. Sträucher, Stauden).
- **Kopplung mit Energie- und Gebäudemodellen**: Die Integration des Gründachmodells in Gebäudesimulationsprogramme wie EnergyPlus oder TRNSYS würde eine Bewertung der Gesamtenergieeffizienz von Gebäuden mit Gründach ermöglichen.
- **Berücksichtigung weiterer physikalischer Prozesse**: Die Modellierung von Eisbildung, Sublimation und Schneeschmelze in Substraten sowie die Betrachtung von Zeitverzögerungen könnten die Prognosegüte in Übergangszeiten weiter erhöhen.
- **Langfriststudien zur Vegetationsentwicklung**: Da viele Dachpflanzen eine interannuelle Dynamik aufweisen, sind Studien über mehrere Jahre notwendig, um den Einfluss von Pflege, Alterung und Biodiversität auf die Dachleistung abzuschätzen.

Ein besonderer Forschungsbedarf ergibt sich aus der bislang nur unzureichend erfassten stomatären Dynamik während Übergangszeiten (Herbst, Frühjahr). Hier könnten kombinierte Langzeitmessungen von Gaswechsel, Biomasseentwicklung und Substratfeuchte neue Modellansätze ermöglichen. Darüber hinaus wäre die Übertragung der Methodik auf großmaßstäbliche Dächer in realen Stadtquartieren sinnvoll, um Skaleneffekte und Interaktionen mit der umgebenden Bebauung zu untersuchen.

7.4 Schlussbemerkung

Die Dissertation zeigt, dass technische Gründachsysteme in ihrer Umweltwirkung differenziert zu bewerten sind – und dass diese Differenzierung durch geeignete Mess- und Modellierungsansätze möglich und praktikabel ist. Die Arbeit verdeutlicht, dass eine integrative Betrachtung – von den Pflanzenprozessen über die Schichtaufbauten bis hin zum Modell – notwendig ist, um die multifunktionalen Leistungen von Gründächern verlässlich zu bewerten. Sie bietet damit eine Grundlage, Gründächer als planbare Infrastrukturkomponenten in klimaresiliente Städte systematisch einzubinden und leistet einen Beitrag zur Versachlichung der Debatte um urbane Begrünungsmaßnahmen.

Literaturverzeichnis

1. Santamouris, M. Heat Island Research in Europe: The State of the Art. *Advances in Building Energy Research* **2007**, *1*, 123–150, doi:10.1080/17512549.2007.9687272.
2. Berardi, U. The Outdoor Microclimate Benefits and Energy Saving Resulting from Green Roofs Retrofits. *Energy and Buildings* **2016**, *121*, 217–229, doi:10.1016/j.enbuild.2016.04.060.
3. Oberndorfer, E. et al. Green Roofs as Urban Ecosystems: Ecological Structures, Functions, and Services. *BioScience* **2007**, *57*, 823–833, doi:10.1641/B571005.
4. Rowe, D.B. Green Roofs as a Means of Pollution Abatement. *Environmental Pollution* **2011**, *159*, 2100–2110, doi:10.1016/j.envpol.2010.10.029.
5. Pitha, U.; Zluwa, I.; Scharf, B.; Lapin, K.; Besener, I.-M.; Virgolini, J.; Kapus, S.; Preiss, J.; Enzi, V.; Jesner, L.; et al. Leitfaden Dachbegrünung **2021**.
6. Brune, M.; Bender, S.; Groth, M. *Gebäudebegrünung Und Klimawandel. Anpassung an Die Folgen Des Klimawandels Durch Klimawandeltaugliche Begrünung*; Report; Climate Service Center Germany: Hamburg, **2017**;
7. Gößner, D. Year-Round Modeling of Evaporation and Substrate Temperature of Two Distinct Green Roof Systems. *Urban Science* **2025**, *9*, doi:10.3390/urbansci9100396.
8. Manso, M.; Teotónio, I.; Silva, C.M.; Cruz, C.O. Green Roof and Green Wall Benefits and Costs: A Review of the Quantitative Evidence. *Renewable and Sustainable Energy Reviews* **2021**, *135*, 110111, doi:10.1016/j.rser.2020.110111.
9. Richter, M.; Dickhaut, W. Retentionsgründächer als multifunktionale blau-grüne Infrastrukturen - Ergebnisse eines Langzeit-Monitorings in Hamburg. In Proceedings of the Grün statt grau; Eawag, Switzerland: Glattfelden, Switzerland, 14-15 November 2022, **2022**; pp. 54–61.
10. Alexandri, E.; Jones, P. Temperature Reduction Effect of Vegetation Coverage on Building Surfaces. *Energy and Buildings* **2008**, *40*, 280–288.
11. Gößner, D.; Mohri, M.; Krespach, J.J. Evapotranspiration Measurements and Assessment of Driving Factors: A Comparison of Different Green Roof Systems during Summer in Germany. *Land* **2021**, *10*, 1334, doi:10.3390/land10121334.
12. Tabares-Velasco, P.C.; Srebric, J. A Heat Transfer Model for Assessment of Plant Based Roofing Systems in Summer Conditions. *Building and Environment* **2012**, *49*, 310–323, doi:10.1016/j.buildenv.2011.07.019.
13. de Munck, C.S.; Lemonsu, A.; Bouzouidja, R.; Masson, V.; Claverie, R. The GREENROOF Module (v7.3) for Modelling Green Roof Hydrological and Energetic Performances within TEB. *Geosci. Model Dev.* **2013**, *6*, 1941–1960, doi:10.5194/gmd-6-1941-2013.
14. Kemp, S.; Hadley, P.; Blanuša, T. The Influence of Plant Type on Green Roof Rainfall Retention. *Urban Ecosyst* **2019**, *22*, 355–366, doi:10.1007/s11252-018-0822-2.
15. Muzylo, A.; Llorens, P.; Valente, F.; Keizer, J.J.; Domingo, F.; Gash, J.H.C. A Review of Rainfall Interception Modelling. *Journal of Hydrology* **2009**, *370*, 191–206, doi:10.1016/j.jhydrol.2009.02.058.
16. Dunkerley, D.L.; Booth, T.L. Plant Canopy Interception of Rainfall and Its Significance in a Banded Landscape, Arid Western New South Wales, Australia. *Water Resources Research* **1999**, *35*, 1581–1586, doi:10.1029/1999WR900003.
17. Simunek, J.; Sejna, M.; Saito, D.; Sakai, M.; van Genuchten, M. The HYDRUS-1D Soft- Ware Package for Simulating the One-Dimensional Movement of Water,Heat Ans Multiple So- Lutes in Variably-Satured Media. Version 4.17. **2013**.
18. Gößner, D.; Kunle, M.; Mohri, M. Green Roof Performance Monitoring: Insights on Physical Properties of 4 Extensive Green Roof Types after 2 Years of Microclimatic

Measurements. *Building and Environment* **2025**, *269*, 112356, doi:10.1016/j.buildenv.2024.112356.
19. Cirkel, D.; Voortman, B.; van Veen, T.; Bartholomeus, R. Evaporation from (Blue-)Green Roofs: Assessing the Benefits of a Storage and Capillary Irrigation System Based on Measurements and Modeling. *Water* **2018**, *10*, 1253, doi:10.3390/w10091253.
20. Feng, Y.; Burian, S.; Pardyjak, E. Observation and Estimation of Evapotranspiration from an Irrigated Green Roof in a Rain-Scarce Environment. *Water* **2018**, *10*, 262, doi:10.3390/w10030262.
21. Heusinger, J.; Weber, S. Comparative Microclimate and Dewfall Measurements at an Urban Green Roof versus Bitumen Roof. *Building and Environment* **2015**, *92*, 713–723, doi:10.1016/j.buildenv.2015.06.002.
22. Kaiser, D.; Köhler, M.; Schmidt, M.; Wolff, F. Increasing Evapotranspiration on Extensive Green Roofs by Changing Substrate Depths, Construction, and Additional Irrigation. *Buildings* **2019**, *9*, 173, doi:10.3390/buildings9070173.
23. Baraldi, R.; Neri, L.; Costa, F.; Facini, O.; Rapparini, F.; Carriero, G. Ecophysiological and Micromorphological Characterization of Green Roof Vegetation for Urban Mitigation. *Urban Forestry & Urban Greening* **2019**, *37*, 24–32, doi:10.1016/j.ufug.2018.03.002.
24. Tan, C.L.; Tan, P.Y.; Wong, N.H.; Takasuna, H.; Kudo, T.; Takemasa, Y.; Lim, C.V.J.; Chua, H.X.V. Impact of Soil and Water Retention Characteristics on Green Roof Thermal Performance. *Energy and Buildings* **2017**, *152*, 830–842, doi:10.1016/j.enbuild.2017.01.011.
25. Arriola-Cepeda, R.; Vera, S.; Albornoz, F.; Steinfort, U. Experimental Study on the Stomatal Resistance of Green Roof Vegetation of Semiarid Climates for Building Energy Simulations **2018**.
26. Sailor, D.J. A Green Roof Model for Building Energy Simulation Programs. *Energy and Buildings* **2008**, *40*, 1466–1478, doi:10.1016/j.enbuild.2008.02.001.
27. Tabares-Velasco, P.C.; Srebric, J. Experimental Quantification of Heat and Mass Transfer Process through Vegetated Roof Samples in a New Laboratory Setup. *International Journal of Heat and Mass Transfer* **2011**, *54*, 5149–5162, doi:10.1016/j.ijheatmasstransfer.2011.08.034.
28. Avissar, R.; Pielke, R.A. The Impact of Plant Stomatal Control on Mesoscale Atmospheric Circulations. *Agricultural and Forest Meteorology* **1991**, *54*, 353–372, doi:10.1016/0168-1923(91)90013-G.
29. Lee, L.S.H.; Jim, C.Y. Thermal-Cooling Performance of Subtropical Green Roof with Deep Substrate and Woodland Vegetation. *Ecological Engineering* **2018**, *119*, 8–18, doi:10.1016/j.ecoleng.2018.05.014.
30. Noilhan, J.; Planton, S. A Simple Parameterization of Land Surface Processes for Meteorological Models. *Mon. Wea. Rev.* **1989**, *117*, 536–549, doi:10.1175/1520-0493(1989)117%3C0536:ASPOLS%3E2.0.CO;2.
31. Ogle, K.; Reynolds, J.F. Desert Dogma Revisited: Coupling of Stomatal Conductance and Photosynthesis in the Desert Shrub, *Larrea Tridentata*. *Plant Cell & Environment* **2002**, *25*, 909–921, doi:10.1046/j.1365-3040.2002.00876.x.
32. Takebayashi, H.; Moriyama, M. Surface Heat Budget on Green Roof and High Reflection Roof for Mitigation of Urban Heat Island. *Building and Environment* **2007**, *42*, 2971–2979, doi:10.1016/j.buildenv.2006.06.017.
33. Djedjig, R.; Ouldboukhitine, S.-E.; Belarbi, R.; Bozonnet, E. Development and Validation of a Coupled Heat and Mass Transfer Model for Green Roofs. *International Communications in Heat and Mass Transfer* **2012**, *39*, 752–761, doi:10.1016/j.icheatmasstransfer.2012.03.024.

34. Voyde, E.; Fassman, E.; Simcock, R.; Wells, J. Quantifying Evapotranspiration Rates for New Zealand Green Roofs. *J. Hydrol. Eng.* **2010**, *15*, 395–403, doi:10.1061/(ASCE)HE.1943-5584.0000141.
35. He, H.; Jim, C.Y. Simulation of Thermodynamic Transmission in Green Roof Ecosystem. *Ecological Modelling* **2010**, *221*, 2949–2958, doi:10.1016/j.ecolmodel.2010.09.002.
36. Qin, M.; Walton, G.; Belarbi, R.; Allard, F. Simulation of Whole Building Coupled Hygrothermal-Airflow Transfer in Different Climates. *Energy Conversion and Management* **2011**, *52*, 1470–1478, doi:10.1016/j.enconman.2010.10.010.
37. Susca, T.; Gaffin, S.R.; Dell'Osso, G.R. Positive Effects of Vegetation: Urban Heat Island and Green Roofs. *Environmental Pollution* **2011**, *159*, 2119–2126, doi:10.1016/j.envpol.2011.03.007.
38. Smets, V.; Akkermans, W.; Verbeiren, B.; Hermy, M.; Somers, B. Ex-Situ Estimation of Interception Storage Capacity of Small Urban Plant Species. *Journal of Hydrology* **2019**, *572*, 869–883, doi:10.1016/j.jhydrol.2019.03.047.
39. Eksi, M.; Rowe, D.B.; Wichman, I.S.; Andresen, J.A. Effect of Substrate Depth, Vegetation Type, and Season on Green Roof Thermal Properties. *Energy and Buildings* **2017**, *145*, 174–187, doi:10.1016/j.enbuild.2017.04.017.
40. Pianella, A.; Aye, L.; Chen, Z.; Williams, N. Substrate Depth, Vegetation and Irrigation Affect Green Roof Thermal Performance in a Mediterranean Type Climate. *Sustainability* **2017**, *9*, 1451, doi:10.3390/su9081451.
41. Reyes, R.; Bustamante, W.; Gironás, J.; Pastén, P.A.; Rojas, V.; Suárez, F.; Vera, S.; Victorero, F.; Bonilla, C.A. Effect of Substrate Depth and Roof Layers on Green Roof Temperature and Water Requirements in a Semi-Arid Climate. *Ecological Engineering* **2016**, *97*, 624–632, doi:10.1016/j.ecoleng.2016.10.025.
42. Jim, C.Y.; Peng, L.L.H. Substrate Moisture Effect on Water Balance and Thermal Regime of a Tropical Extensive Green Roof. *Ecological Engineering* **2012**, *47*, 9–23, doi:10.1016/j.ecoleng.2012.06.020.

TEIL 2
FACHARTIKEL

land

MDPI

Article

Evapotranspiration Measurements and Assessment of Driving Factors: A Comparison of Different Green Roof Systems during Summer in Germany

Dominik Gößner *, Milena Mohri and Justine Jasmin Krespach

Optigrün International AG, 72505 Krauchenwies, Germany; m.mohri@optigruen.de (M.M.); j.stoetzner@optigruen.de (J.J.K.)

* Correspondence: d.goessner@optigruen.de; Tel.: +49-7576-772-150

Abstract: Green roofs have proven to be a space-saving solution to mitigate peak temperatures and control floods in urban areas through evaporative cooling and storm water retention. To encourage a sustainable city design with large-scale green infrastructure networks, a better differentiation between the diverse existing green roof systems is needed. The aim of this study is to demonstrate differences among green roof systems based on comprehensive microclimatic measurements on four small experimental roofs and to assess differences in evapotranspiration with a partial least square regression. The results show that short-wave solar radiation, relative humidity and water availability are the most important drivers of evapotranspiration. The roof system with permanent water storage maintained significantly higher substrate moisture compared to the other roofs and produced peak evapotranspiration rates of 4.88 mm d^{-1}. The highest total evapo-transpiration of 526 mm from April to September was recorded for the roof system with the thickest substrate layer and grass vegetation. In summer, the shallowest roof showed the highest substrate temperature and air temperature at vegetation level. These findings highlight the importance of specifying the characteristics of the various green roofs in order to turn them into useful planning tools for the design of climate-change-resilient cities.

Keywords: blue–green roof; evapotranspiration; blue–green infrastructure; urban heat island; green roof; green infrastructure; retention roof

check for updates

Citation: Gößner, D.; Mohri, M.; Krespach, J.J. Evapotranspiration Measurements and Assessment of Driving Factors: A Comparison of Different Green Roof Systems during Summer in Germany. *Land* **2021**, *10*, 1334. https://doi.org/10.3390/land10121334

Academic Editor: Nir Krakauer

Received: 29 October 2021
Accepted: 30 November 2021
Published: 3 December 2021

Publisher's Note: MDPI stays neutral with regard to jurisdictional claims in published maps and institutional affiliations.

Copyright: © 2021 by the authors. Licensee MDPI, Basel, Switzerland. This article is an open access article distributed under the terms and conditions of the Creative Commons Attribution (CC BY) license (https://creativecommons.org/licenses/by/4.0/).

1. Introduction

Hot weather extremes such as heatwaves or droughts as well as the intensity and frequency of heavy rain events have increased during in recent decades and, due to climate change, they are expected to intensify [1]. Urban areas are especially sensitive to these weather extremes because they already exhibit higher temperatures [2,3] and increased precipitation compared to the rural surroundings [4]. The high percentage of sealed surfaces and lack of green space both contribute to the urban heat island effect, resulting, on average, in a 1–3 °C difference between the city center and countryside with peak differences of up to 10 °C [5–8]. At the same time, urbanization also increases the precipitation over the city by more than 15% [4]. The consequences are floods from overloaded sewage systems and health implications due to heat stress [9,10]. Studies have shown that people living in cities are more likely to be affected by floods [11] and to die a premature death due to heat [12] than the rural population. As the majority of the world population at present lives in urban areas [13], measures for heat mitigation and flood prevention must be implemented in cities.

The expansion of vegetated areas as part of a green infrastructure network is highly effective in lowering temperatures through evaporative cooling as well as controlling floods through storm water retention [5]. Green roofs are a particularly suitable green infrastructure type for dense cities, because they do not take up precious ground space.

Their cooling effect arises from the evaporation of water from the soil and the transpiration of water by vegetation, and the measured reduction in the ambient air temperature through green roofs was found to be, on average, 1.34 °C [14]. Models conducted on a meso-scale achieve similar results, with a vegetation cooling efficiency between 1 and 3 °C, while micro-scale results only detect a 0.5 °C cooling [15]. Moreover, green roofs are effectively controlling floods [16]: storm water slowly infiltrates into the substrate layer where it partly remains until it evaporates, while excess water can be temporarily stored in the drainage layer before it flows off with a delay. This lowers the burden on the sewer system, especially during the peaks of heavy rain events. Extensive green roofs can reduce the storm water runoff by about 60% and intensive green roofs by 80%, while the outflow is, on average, 70% delayed compared to non-vegetated roofs [14]. Apart from cooling the ambient air temperature and substantially reducing the storm water runoff, green roofs provide further environmental benefits such as increased biodiversity [17], noise protection [14], building insulation [18] and various social and economic benefits including improved aesthetics of the townscape, resulting in better mental recovery [19,20] and increased property value [14].

Municipalities increasingly acknowledge these benefits and the green roof coverage expands yearly by over 1.5 million m^2 in central Europe [21]. Still, many cities lack a holistic and integrated spatial planning approach, which is needed to face today's environmental challenges [22]. An important basis for solutions implemented at the city scale is detailed knowledge about green roof services, which can partly be obtained from urban climate simulations [23]. However, most scientific studies with models only differentiate between extensive and intensive green roofs [24–27], which does not adequately reflect the variety of existing green roofs: the growing demand for green infrastructure solutions has led to the development of a broad range of green roof systems. Thus, the simple differentiation between extensive and intensive green roofs, based only on the thickness of the substrate layer, can be considered outdated. Today's green roofs differ not only in substrate height, but also in substrate type, vegetation, drainage/water retention layer and roof outlet characteristics. Further, some green roof systems even include water storage elements such as retention storages or cisterns, which can be used for passive or active irrigation. These different designs strongly affect the green roofs' water household and their potential evaporative cooling and storm water retention capacity [28]. Even though scientific studies increasingly differentiate between green roof designs to measure evapotranspiration [29,30], present data do not adequately reflect the existing diversity of systems with their different effects.

Mitigating extreme summer temperatures and floods in urban areas has become one of the central goals of sustainable city planning [31]. With evapotranspiration as a key to the urban heat island mitigation [28], precise numbers are needed regarding the quantity of water returned to the atmosphere via green roofs. The best possible strategies to counter climate change in cities can only be developed when specific information about the services provided by different green roof systems is available. The obtained data can subsequently be used to validate urban climate simulations, which facilitate the implementation of research findings about green infrastructure.

The present study includes comprehensive microclimatic measurements on four small experimental roofs situated in Germany. The focus of the study lies on the evapotranspiration, which is measured using the gravimetric method. The presented results include the data of one summer season, and both single measured parameters and their relation and contribution to the evapotranspiration process will be evaluated. The aim of this study is (I) to encourage better differentiation between various green roof types by providing detailed data on microclimatic characteristics of four different green roof systems; (II) to quantify the evapotranspiration rate among the green roofs as a central tool for cooling the ambient air temperature and mitigating the urban heat island effect and (III) to better understand which environmental and climatic factors have the greatest influence on evapotranspiration.

2. Materials and Methods

2.1. Site Description

The study site is located in Göggingen-Krauchenwies, Germany (48°0′20.27916″ N, 9°12′5.33952″ E) at 623 m altitude and belongs to the warm summer, humid continental climate zone according to the Köppen-Geiger classification [32]. The lowest mean, minimum and maximum temperatures occur in January and are −0.7 °C (−4.2 °C; 2.7 °C) respectively. The highest mean, minimum and maximum temperatures are 17.9 °C (10.7 °C; 24.5 °C) in July, and the precipitation is evenly distributed throughout the year, reaching an average total of 699 mm (reference period: 2016–2021, station Sigmaringen-Laiz at 581 m altitude, 8.5 km distance from the study site [33]).

2.2. Experimental Setup

The experimental site is located at ground-level at the side of a parking lot at the aforementioned coordinates, with a few trees throwing shade evenly across the area in late afternoon. Lysimeters with four different green roofs, each with an area of 0.5 m^2, were set up together with a local climate station in spring 2021. To minimize the edge effects from the pavement, a green roof of about 16 m^2 was constructed around the experimental roofs (Figure 1). The measurement period and data used in this study range from the 1 April 2021 until the 5 October 2021. Details about the measured parameters and installed devices are given in Table 1. Measurements were taken at 5 min intervals.

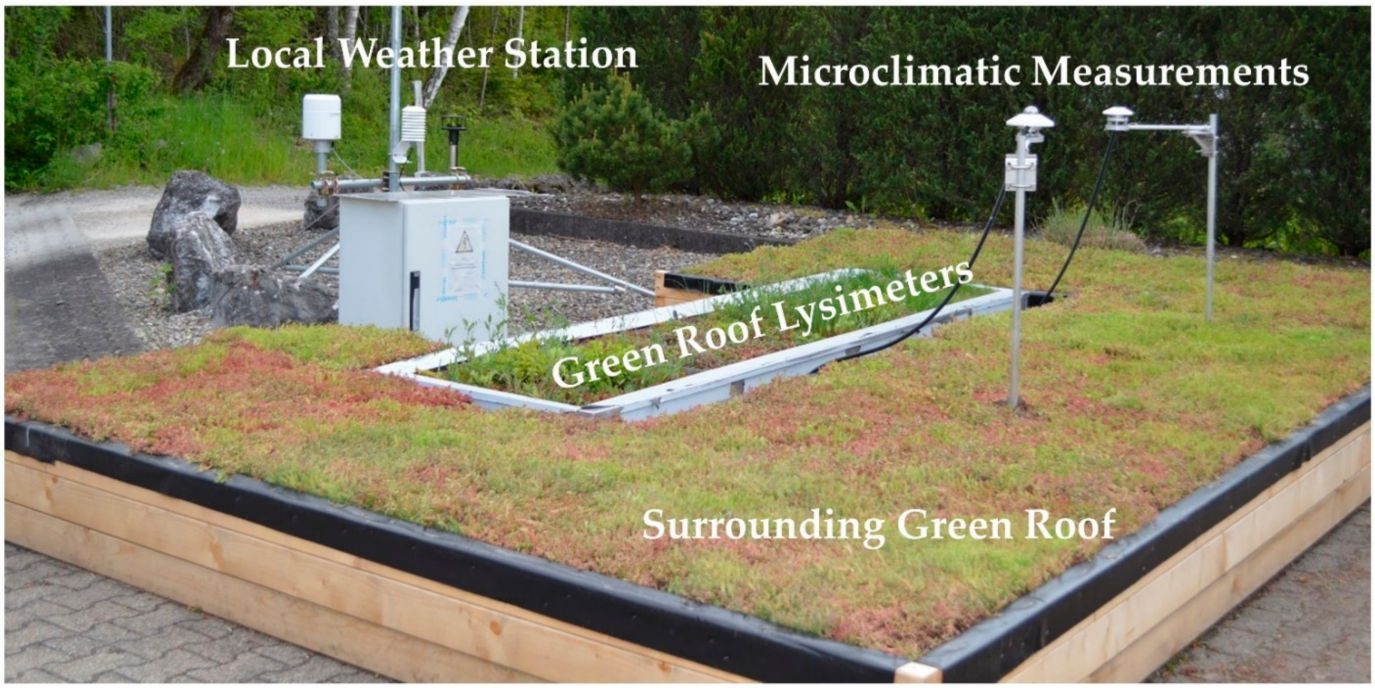


Figure 1. Experimental setup in Göggingen-Krauchenwies, Germany (48°0′20.27916″ N, 9°12′5.33952″ E).

Table 1. List of parameters measured, the installed measurement devices and approximate position of the sensors.

Layer	Parameter	Measurement Device	Manufacturer
Atmospheric Layer	Precipitation	rain[e]	LAMBRECHT meteo GmbH, Göttingen, Germany
	Air Temperature	CS215 Temperature and Relative Humidity Probe	Campbell Scientific Inc., Logan, UT, USA
	Relative Humidity	CS215 Temperature and Relative Humidity Probe	Campbell Scientific Inc., Logan, UT, USA
	Short-Wave Solar Radiation	CMP10 Pyranometer	Kipp & Zonen B.V., Delft, The Netherlands
	Long-Wave Radiation	CGR3 Pyrgeometer (facing the sky)	Kipp & Zonen B.V., The Netherlands
	Wind Speed	WindSonic4 Two-Dimensional Sonic Anemometer	Campbell Scientific Inc., USA
Vegetation Layer	Leaf Temperature + Air Temperature	Leaf-&-Air-Temperature Type LAT-B2, Broadleaf	ECOMATIK GmbH, Dachau, Germany
Substrate Layer	Volumetric Water Content	CS655 soil water content reflectometer	Campbell Scientific Inc., Logan, UT, USA
	Substrate Temperature	105E Temperature Probe	Campbell Scientific Inc., Logan, UT, USA
	Heat Flux	HFP01 Heat Flux Plate	Hukseflux Thermal Sensors B.V., Delft, The Netherlands
Total Setup	Weight	Scale 9392.15.140 (1×) and Scale 9392.16.140 (3×)	Soehnle Industrial Solutions GmbH, Backnang, Germany
	Outflow	Small Rain Gauge 100.054	Pronamic ApS, Ringkoebing, Denmark

2.3. Green Roof Systems Description

The four green roof systems included in this study are the *Garden Roof*, *Economy Roof*, *Nature Roof* and *Retention Roof*, which are commercially available from Optigrün international AG, Germany. They can be distinguished based on vegetation, substrate type and depth, filter fleece, and the water retention and drainage layer (Figure 2).

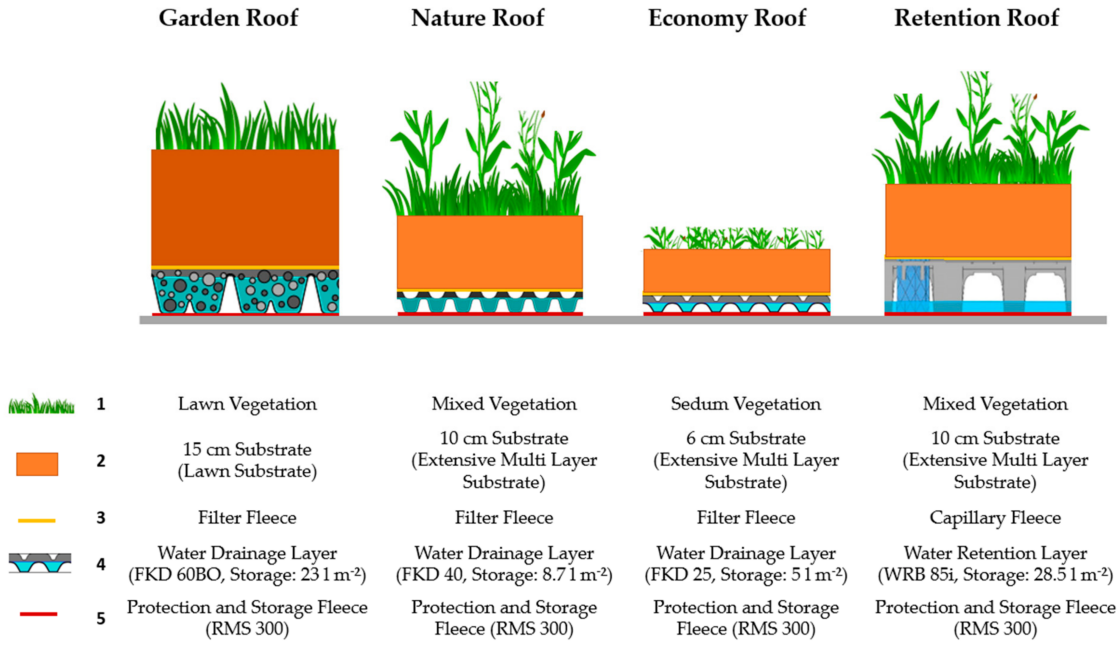


Figure 2. Description of the four different green roof systems used in this study.

The vegetation is comprised of typical lawn species (*Garden Roof*), *Sedum* species (*Economy Roof*), and mixed vegetation with succulents and herbs (*Nature* and *Retention Roof*).

The lawn vegetation was transferred from a pre-grown *Garden Roof* onto the lysimeter, the *Economy Roof* received sprouts of different *Sedum* species and other low-growing perennials. Both the *Nature* and *Retention Roof* were planted with *Sedum* sprouts and seeds of various herbs in 2019.

The Optigrün Lawn Substrate of the *Garden Roof* consists of expanded shale, expanded clay, lava, pumice, crushed brick and green waste compost, while the Optigrün Extensive Multi-Layer Substrate used in the other systems also includes Porlith.

The fleece layer of the *Garden*, *Nature* and *Economy Roof* is a filter fleece with a thickness of 1.1 mm, while the *Retention Roof* contains a capillary fleece of 3.6 mm, which is able to quickly distribute water.

The drainage layers differ among all green roof systems: the *Garden Roof* is equipped with the Optigrün Drainage and Storage Board FKD 60BO from recycled high-density polyethylene, consisting of a 6 cm high chamber network filled with a drainage material. About 23 L m^{-2} of water can be stored in this system. The *Nature Roof* has the Optigrün Drainage and Storage Board FKD 40, which is about 4 cm high, with a water storage of 8.7 L m^{-2}. The *Economy Roof* contains the shallow Optigrün Drainage and Storage board FKD 25 similar to the *Nature Roof*, but is only 2.5 cm high, and thus has a water reservoir function of only 5 L m^{-2}. The *Retention Roof* contains the Optigrün Water Retention Box WRB 85i from recycled polypropylene, which can temporarily contain a water volume of up to 80 L m^{-2}. In this study, a permanent water accumulation is reached in the *Retention Roof* by positioning the outflow at 3 cm height instead of at the bottom of the system, leading to a water storage capacity of 28.5 L m^{-2}. Further, it contains capillary bridges, which allow for the vertical transportation of water between the drainage level and substrate layer through capillary forces.

The Optigrün Protection and Storage Fleece RMS 300, with a thickness of approximately 3.6 mm, protects the roof's waterproofing.

2.4. Roof Maintenance

The green roofs were maintained according to the green roof guidelines [34]. In mid-April 2021, fertilizer (Slow Release Fertiliser Opticote, Optigrün AG, Krauchenwies, Germany) was added with 50 g m^{-2} to the *Garden Roof* and 35 g m^{-2} to the other three roofs. The *Garden Roof* was watered twice until field capacity (once in April, once in May). Weeding was carried out whenever needed and, due to the removal of plant biomass, the weight of each weeded roof was set to "not-a-number" (NaN) on the respective day. The grass of the *Garden Roof* was cut four times (in May, twice in July and once in September). The *Nature Roof* was weeded five times (in May, July, and three times in September), the *Economy Roof* had to be weeded only three times (in May, and twice in September) and the *Retention Roof* was weeded twice (once in May and once in September).

2.5. Data Processing

The hours at which maintenance work such as weeding, broken sensor replacements or cleaning of outflow sensors was carried out at the lysimeter station were excluded from the dataset. Additionally, the weight, outflow and soil moisture were set to NaN on the days where the *Garden Roof* was irrigated.

After inspecting the raw data (i.e., measurements in the interval of 5 min), reasonable minimum and maximum values were defined in order to exclude outliers: precipitation 0–2.5 mm, air temperature −10–40 °C, relative humidity 0–100%, short-wave solar radiation 0–1250 W m^{-2}, long-wave radiation 250–450 W m^{-2}, wind speed 0–3 m s^{-1}, leaf temperature −20–55 °C, substrate temperature −10–45 °C, volumetric water content ≥0–1 m^3 m^{-3} and heat flux −16–40 W m^{-2}.

The weights of all fields were smoothened to hourly values due to strong variations, especially at the scale of the *Garden Roof*. Continuous increases and decreases in the weight would have led to an overestimation of weight loss, and thus in evapotranspiration.

2.6. Calculation of Vegetation Cover and Plant Area Index

For the estimation of the vegetation cover and the plant area index (PAI), triplicate photos were taken of each roof approximately once per week with a digital camera (D3200, Nikon, Düsseldorf, Germany and 8 mm/3.5 Fish-Eye II Lens Walimex pro, Studioexpress Vertriebs GmbH, Wiernsheim, Germany). The calculation of the vegetation cover and PAI was performed with the freeware CAN-EYE (INRAE, Paris, France). The PAI was calculated as the ratio of the plant area over the ground area, above which plants were growing.

2.7. Determination of Evapotranspiration

The daily evapotranspiration was calculated based on precipitation, outflow and smoothened weight of the roofs. Each of the smoothened weight values consisted of the mean of one hour calculated from 12 single-weight datapoints (the first ranging from 00:00 to 00:55 o'clock, the second from 01:00 to 01:55, etc.). Thus, each day contained a total of 24-hourly values and only complete days with 24 weight values were considered for the calculation. Equation (1) gives the calculation of the evapotranspiration for one specific day and one specific field

$$\text{Evapotranspiration} = \text{Weight}_{00} - \text{Weight}_{23} - \text{Outflow} + \text{Precipitation} \times 0.5 \quad (1)$$

where Weight_{00} and Weight_{23} are the weights at the beginning and at the end of the day, respectively, and the outflow and the precipitation are the sum over the entire day. Both weight and outflow are based on the area of a single roof ($\triangleq$0.5 m^2) and are, therefore, expressed as kg per 0.5 m^2 and l per 0.5 m^2, while the precipitation is measured per m^2, and thus needs to be divided by half. The calculated evapotranspiration has the unit l per 0.5 m^2; however, all results presented in this study are scaled up to 1 m^2.

Due to clogging and malfunctioning of the rain sensor, no precipitation data are available from the 7 June until the 16 August, and this gap could not be filled with data from any nearby weather station. Therefore, the evapotranspiration was calculated differently for the period without the rain sensor (Equation (2)); the units are as described above:

$$\text{Evapotranspiration} = \text{Weight}_{00} - \text{Weight}_{23} - \text{Outflow} \quad (2)$$

Days with negative evapotranspiration values are excluded, as this means that more rain has fallen than was evapotranspirated or lost as outflow. On days where only little rain fell, the evapotranspiration is slightly underestimated by the amount of the rain that was not incorporated into the calculation.

For the calculation of monthly and yearly sums of evapotranspiration, data for different roof systems must remain comparable, despite short-term sensor failures. Therefore, data were extrapolated onto the same number of days when needed, i.e., when only 28 days in one month were recorded for the *Garden Roof*, the monthly sum was extrapolated to 30 or 31 days depending on the month to allow for comparison to the other roofs containing data for the full month. Any extrapolation in the results is highlighted.

2.8. Statistical Analysis

All statistical analysis was done in RStudio Desktop Version 1.3.1093 [35] and R Version 4.0.3 [36]. To find out which factors play an important part in the evapotranspiration, a partial least square (PLS) regression was performed using the R-package "pls" and the function "plsr". The regression was performed separately for each roof. Cross-validation was used to validate the model, as suggested in [37]. The PLS summary was used to choose the number of components based on the explained variance in the evapotranspiration, as well as the root mean squared error of prediction, with the aim of maximizing the explained variance and minimizing the error to neither underfit nor overfit the model [37]. The following variables, most of which are also used by [30], were considered in the PLS regression: soil moisture, soil heat flux, soil temperature, leaf temperature, relative humidity, wind speed, short-wave solar radiation, long-wave radiation, precipitation.

Short-wave and long-wave radiation as well as precipitation were included as daily sums, and all other variables as daily means. As changes in the vegetation cover and PAI are generally very slow, these two variables were recorded only once per week. Consequently, the difference in measurement interval makes it impossible for the regression to relate the day-to-day variation in the evapotranspiration rate to the vegetation cover or PAI, which is why these two variables were excluded from the PLS regression. Further, the regression was only performed for the period in which the rain sensor was functioning. Based on the regression, the Variable Importance in Projection (VIP) was determined using the R function "VIP" of the package "plsVarSel". For the determination of differences in means, a repeated measures analysis of variance (ANOVA) was chosen, and in case the assumptions were not met, the Friedman Test was used. The level of significance was set to 0.05.

3. Results

3.1. Weather Conditions

Overall, the summer months in Göggingen were slightly colder and much wetter (Appendix A, Figure A1) compared to the reference period data of 2016–2021 [33]. More precisely, April, May, July and August were colder and only June and September were a little warmer than usual. The precipitation of the summer months of May, June and July was a lot higher, as it rained, in total, over 400 mm instead of 275 mm [33], while April, August and September were drier compared to the reference climate.

3.2. Vegetation Development

The survey of the vegetation development showed clear differences among the green roof systems (Figure 3). The *Garden Roof* was the first to reach 90% cover in the beginning of June, while the *Nature Roof* grew steadily and came to 90% shortly afterwards. Even though the *Retention Roof* started at 50% vegetation cover, together with the *Economy Roof*, it rapidly increased its cover and reached the 90% mark in the same week as the *Nature Roof*. The slowest development was registered for the *Economy Roof*, which showed little growth in the first 2 months, but quickly gained cover from the end of May onwards. However, it stagnated in July and only reached 90% cover by the end of July. The slight decreases in the cover of the *Garden Roof* in June, as well as of the *Retention Roof*, the *Economy Roof* and the *Nature Roof* in September, can be attributed to roof maintenance and weeding of unwanted species.

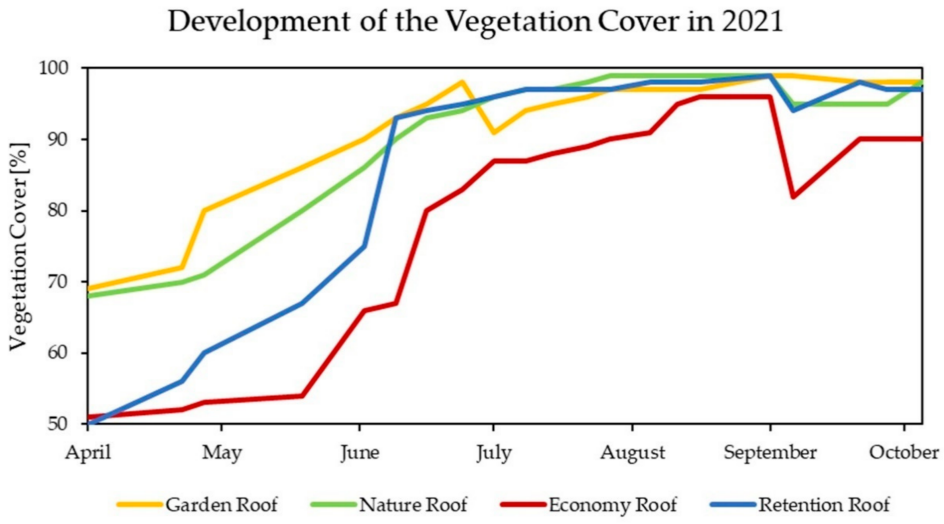


Figure 3. Development of the vegetation cover of the four different green roofs from April to October 2021. Exemplary photos can be found in Appendix A (Figure A2).

The plant area index (PAI) mostly increased slowly during the first months and more rapidly from June onwards (Figure 4). The *Nature Roof* reached the highest PAI of about 8; the *Retention Roof* was just below, with 7. The *Economy Roof* came up to 5 and the *Garden Roof* remained at around 4. Similar to the plant cover, the weeding of the *Garden Roof* also led to a decrease in the PAI.

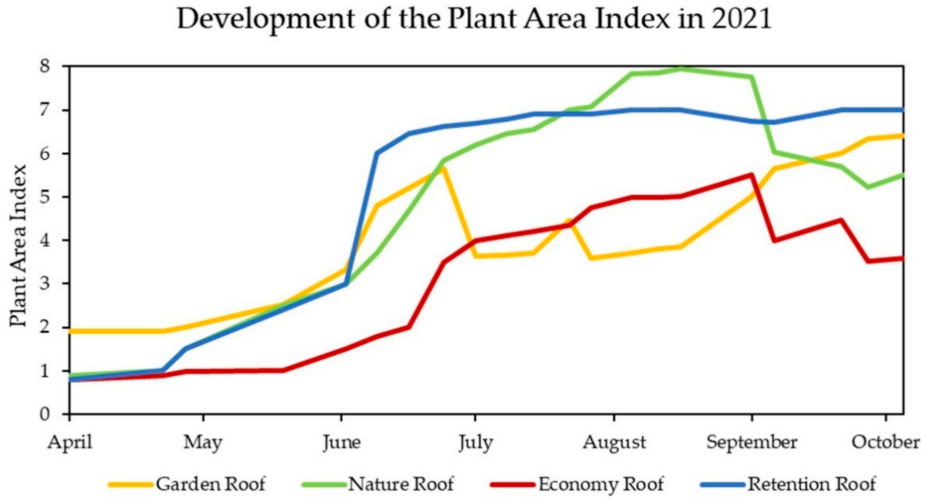


Figure 4. Development of the plant area index of the four different green roofs from April to October 2021.

Regarding the plant species, the *Garden Roof* was dominated by various grass species. The *Economy Roof* was covered by a mixture of succulent species such as *Sedum album* and *Sedum reflexum*. Even though the *Nature* and *Retention Roof* had the same vegetation mixture when set up, different species dominated at the peak stage of plant development. The *Nature Roof* exhibited a broad range of species with *Origanum vulgare*, *Sedum kamtschaticum* und *Sedum telephium*, while the *Retention Roof* was mostly covered by *Sedum kamtschaticum.*

3.3. Substrate Moisture

The substrate moisture showed great variations over time due to the influence of precipitation and evapotranspiration; however, it can be noted that all roofs mostly remained above 10% (Figure 5). The *Retention Roof* had the highest substrate moisture with peaks of over 35%. Except for a few hot and dry summer days, during which the moisture content dropped below 10%, it generally maintained a considerably higher soil moisture compared to the other roofs. The moisture values of the *Garden* and *Economy Roof* differed only slightly, and the *Nature Roof* was mostly between the *Retention* and *Economy Roof*. Regarding the moisture ranges, the *Garden Roof* and the *Economy Roof* were the systems with the most stable moisture conditions, with only around 12% difference between their minimum and maximum value, while the *Nature Roof* and the *Retention Roof* had much larger differences of around 15% and 30%, respectively.

When the values are averaged over the entire growth period to a daily mean, the differences between the roofs become even more evident. The soil moisture of the *Retention Roof*, with 26.5%, is significantly higher than all other roofs. The *Nature Roof*, with an average of 16.5%, also has a significantly higher moisture level than the *Garden* and *Economy Roof*, which do not differ significantly, with 13.9% and 13.6%, respectively (Figure 6).

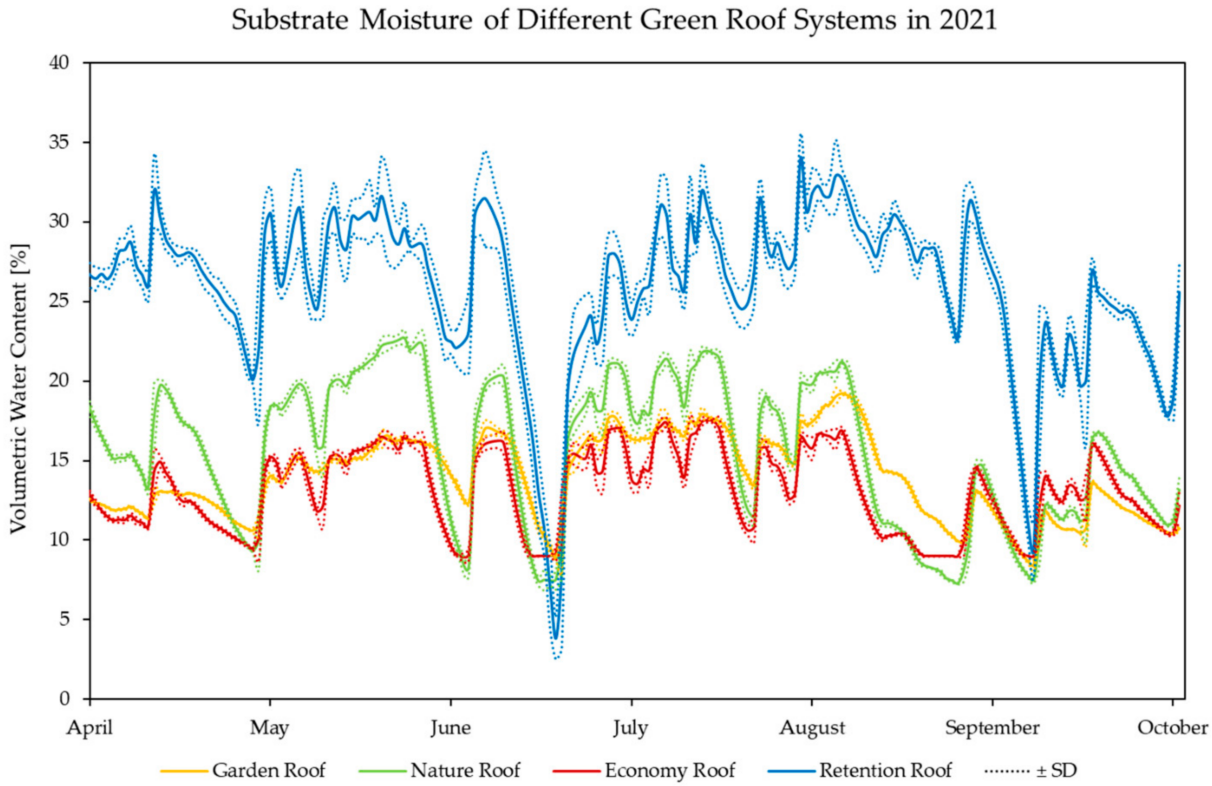


Figure 5. Daily averages ± standard deviation (SD) of the soil moisture of the four different green roofs from April to October 2021.

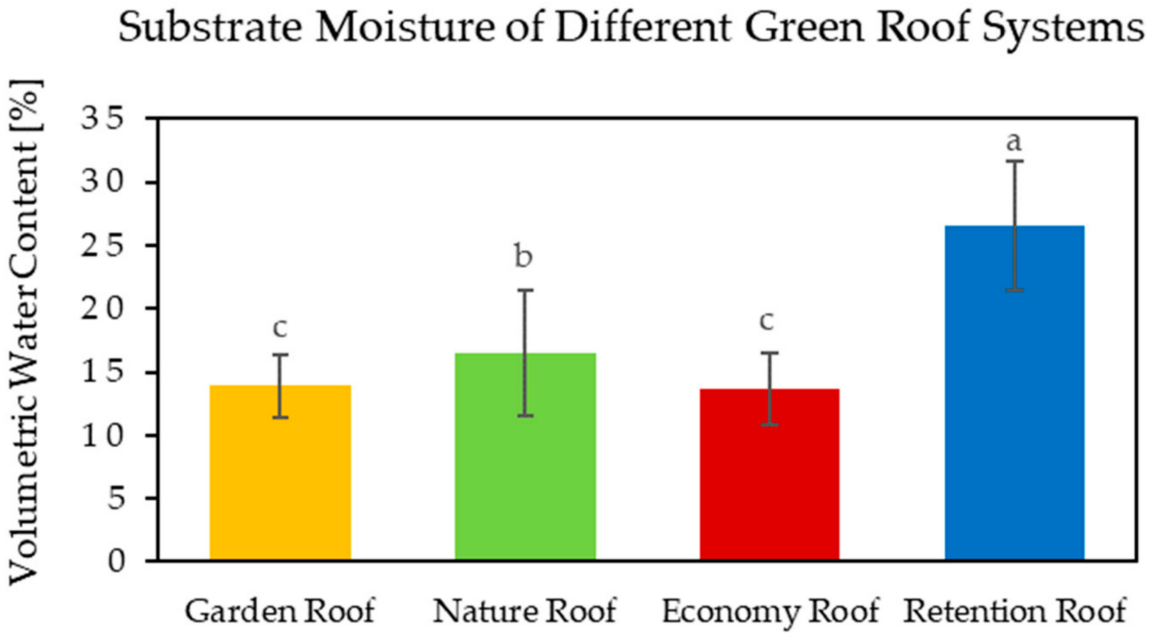


Figure 6. Average substrate moisture of the four different green roofs with means ± SD (n = 204 for *Garden Roof*; n = 205 for other roofs). Different letters above the whiskers indicate significant differences between means (Friedman Test $p < 0.01$).

Differences in the cover were largest until July; however, due to the frequent rain events and only moderately warm summer temperatures in 2021, the soil moisture of all roofs remained relatively stable throughout the entire measurement period. Despite the initially low cover of both *Retention Roof* and *Economy Roof*, the substrate moisture

did not strongly differ between the first and second half of the year. The *Retention Roof* had continuously high soil moisture, which shows that the water stored in the retention layer can effectively be returned to the substrate layer through the capillary fleece and the capillary bridges. This can be verified through comparison with the *Nature Roof*, which has the same system structure, except for the drainage layer, but lower soil moisture. Only when the water storage of the *Retention Roof* is completely empty, as in June, does the soil moisture drop. In April and May, the moisture values of the *Garden Roof* could be slightly overestimated, as it was watered twice in spring. Still, the soil moisture is generally low, which may be explained by the thicker substrate layer, in which the water is distributed more broadly. In the case of the *Economy Roof*, the substrate moisture is low because little water can be stored in the shallow substrate and drainage layer.

3.4. Evapotranspiration

Looking at the data for the whole measurement period, the highest evapotranspiration was measured in the summer months of June and July, while the spring and fall months had lower values (Figure 7). In the warmer period, differences between the roof systems can be observed. The *Retention* and *Garden Roof* showed the highest evapotranspiration rates of 4.88 mm d^{-1} and 4.77 mm d^{-1}, respectively; the *Nature Roof* had slightly lower values, with a peak of 3.34 mm d^{-1}, and the *Economy Roof* tended to have the lowest evapotranspiration, with only 2.67 mm d^{-1} in June.

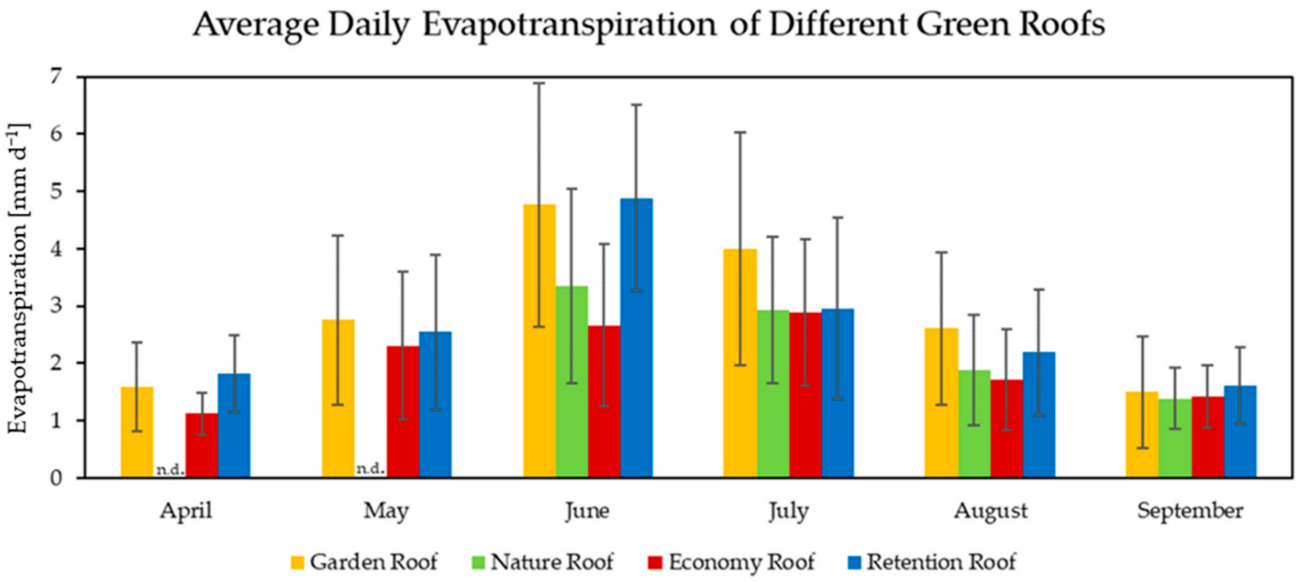


Figure 7. Average daily evapotranspiration of the four different green roofs with means ± SD from April to September 2021. October is not included here as data were only available for four days in that month.

The daily mean evapotranspiration over the entire measurement period was highest for the *Garden Roof*, with 2.62 ± 1.36 mm d^{-1} (Figure 8). The *Retention Roof* had an eva-potranspiration rate of 2.49 ± 1.19 mm d^{-1}. The *Nature Roof* came third, with 2.19 ± 0.90 mm d^{-1}, and the lowest evapotranspiration was measured for the *Economy Roof*, with 1.83 ± 0.82 mm d^{-1}. However, no significant differences were found between the first three roofs; only the *Economy Roof* had a significantly lower evapotranspiration rate.

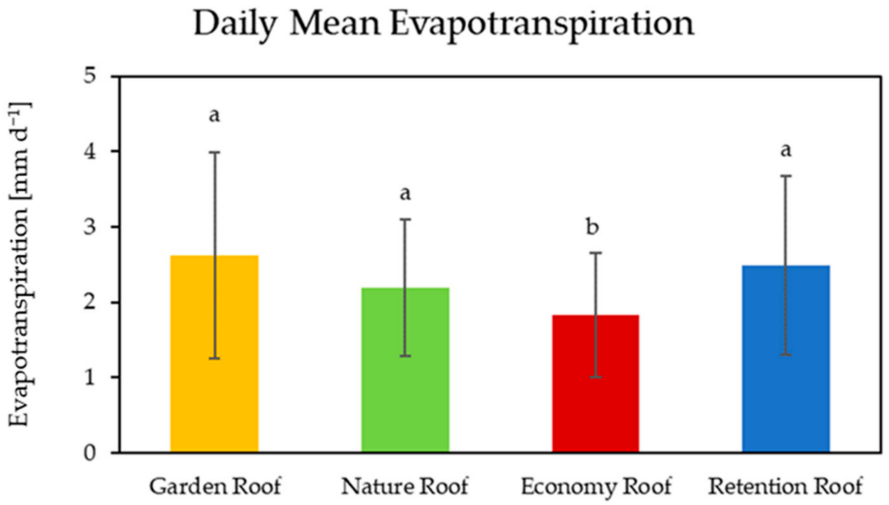


Figure 8. Average daily evapotranspiration of the four different green roofs with means ± SD (n = 121 for *Garden Roof*; n = 88 for *Nature Roof*, n = 134 for *Economy Roof* and n = 141 for *Retention Roof*). Different letters above the whiskers indicate significant differences between means (Friedman Test $p < 0.01$).

The total monthly evapotranspiration ranged from 33.7 mm for the *Economy Roof* in April to 146.4 mm for the *Retention Roof* in June (Table 2). During the entire measurement period, the *Garden Roof* achieved the highest total evapotranspiration of over 526 mm, the *Retention Roof* was close behind, with 488 mm, and the *Economy Roof* only reached 370 mm. Looking at the period from June to September to include the *Nature Roof* in the comparison, it can be noted that its evapotranspiration was higher than the *Economy Roof*, but lower than the *Retention Roof*.

Table 2. Total monthly evapotranspiration [mm] [1].

Month	Garden Roof	Nature Roof	Economy Roof	Retention Roof
April	47.7	n.d.	33.7	58.8
May	85.4	n.d.	102.8	78.8
June	143.2	100.3	80.0	146.4
July	123.8	91.0	89.4	91.8
August	80.8	58.2	53.2	68.0
September	45.1	41.7	42.6	48.5
Total (April–September)	526	n.d.	370	488
Total (June–September)	393	291	265	355

[1] All values are extrapolated to the full month to allow for comparison among the roof systems. October is not included here as data were only available for four days in that month.

The variation in the evapotranspiration rates between the different months likely arose from the fluctuations in air temperature and solar radiation: all green roof systems had their peak evapotranspiration rates in June and July, the months with the highest air temperatures and longest hours of sunshine (Appendix A, Figure A1), and thus with the highest available energy for potential evapotranspiration. However, the differences in evapotranspiration among the four roofs are most probably the result of the system components including the vegetation and their influence on the water availability. The *Retention* and the *Garden Roof* showed the highest evapotranspiration rates of all green roof systems, and these were the two setups with the greatest possible water storage: the *Retention Roof* has the largest storage volume, with a permanent water retention layer, from which water was able to migrate back into the substrate layer and produced a very high soil moisture content. The *Garden Roof* with 15 cm substrate and a drainage layer of 6 cm had the highest total setup, allowing a lot of water to remain in the system. Furthermore,

it was watered twice to keep the lawn vegetation alive. The evapotranspiration rates of the *Nature Roof* were much lower compared to *Retention* and *Garden Roof*. As the vegetation and substrate thickness of the *Nature Roof* are the same as in the *Retention Roof*, the thinner type of drainage layer appears to be responsible for the recorded difference in evapotranspiration. In the case of the *Economy Roof*, the low evapotranspiration rates can also be attributed to the shallow substrate and thin water-retention layer.

The observed trends in differences between the roofs for the single months are also reflected in the daily mean evapotranspiration over the entire measurement period. Here, it is important to note that the daily mean value of the *Nature Roof* may be slightly overestimated, as the evapotranspiration could not be calculated for April and May due to failure of the outflow sensor. Furthermore, to keep the grass vegetation alive, the *Garden Roof* was watered twice in spring, which also contributed to the high evapotranspiration rates.

When interpreting the data, it should be noted that the rain sensor failure in summer impairs the data quality. The rain that could not be recorded from mid-June to mid-August increased the weight of the roofs, so the calculated evapotranspiration resulted in negative values for rainy days. Therefore, 15 days in both June and July were excluded from the analysis. However, the slight rain events that occurred in the summer months led to an underestimation of the evapotranspiration, as the weight gain due to rain was not subtracted in that period.

Furthermore, it must be noted that the evapotranspiration is always composed of the water loss attributed to the transpiration of the plants, but also of the evaporation from the substrate. When considering that many *Sedum* species are facultative CAM-plants, which are able to close their stomata under water stress during hot and dry summer days [38,39], the evapotranspiration measured on the *Retention* and *Economy Roof* with a high share of succulent plants may also result from the evaporation of the substrate.

3.5. Variable Importance in Projection (VIP) Scores

The VIP-scores of the partial least square (PLS) regression provide insight into which factors are the key variables in determining the dependent variable, i.e., the evapotranspiration rate. In this context, variables with VIP-values above 0.8 are generally considered important [40]. The short-wave solar radiation, relative humidity and precipitation play a major role in consistently determining the evapotranspiration across all roof systems (Figure 9a–d). Additionalyl, the wind speed and the long-wave radiation are relevant in three out of four roof systems. However, some values also vary among the roofs or take a different order, which shows that the systems behave slightly differently: the evapotranspiration on the *Garden Roof* is mainly determined by the incoming solar radiation, the relative humidity and the leaf temperature (Figure 9a). On the *Nature Roof*, the precipitation reaches the highest score, followed by the short-wave radiation and the relative humidity (Figure 9b). The *Economy Roof* has short-wave radiation, relative humidity and soil moisture as the most important variables (Figure 9c), while the three highest scores of the *Retention Roof* are the relative humidity, short-wave radiation and soil heat flux (Figure 9d).

When the evapotranspiration is not measured directly via scales, an approximation is often obtained using the Penman–Monteith equation [41]. The main input parameters for the equation are the solar radiation, air temperature, relative humidity and the wind speed, which points out their relevance for the evapotranspiration process: the higher the solar radiation, air temperature and wind speed, and the lower the relative humidity, the higher the evapotranspiration rate [42].

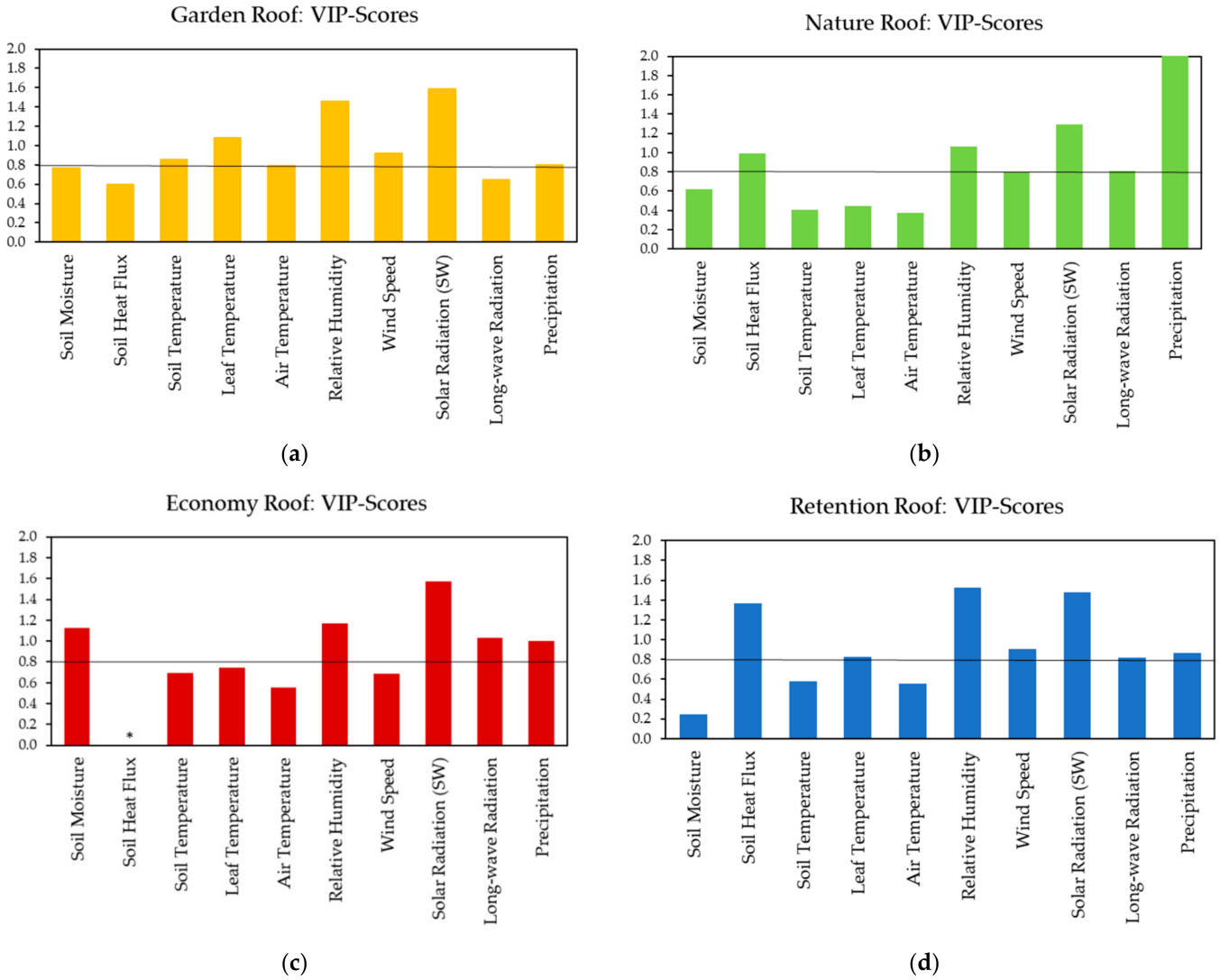


Figure 9. VIP-Scores resulting from the PLS-regression of the different green roof systems. (**a**) 7 components, evapotranspiration explained: 85.38%, CVadjusted: 0.2538; (**b**) 4 components, evapotranspiration explained: 62.40%, CVadjusted: 0.2992; (**c**) 5 components, evapotranspiration explained: 75.42%, CVadjusted: 0.1807 (**d**) 5 components, evapotranspiration explained: 74.50%, CVadjusted: 0.2128. * Due to sensor failure, the soil heat flux variable did not produce enough values to be included in the regression for the *Economy Roof*.

The three parameters of solar radiation, relative humidity and wind speed were also highly relevant for determination of the green roof evapotranspiration. The air temperature received relatively low VIP scores, possibly because the VIP scores were calculated based on the time in which all sensors were functioning, excluding the warm weather period from mid-June to mid-August. Besides, air temperature, short-wave and long-wave radiation are subject to collinearity. The high scores for both short-wave and long-wave radiation in the case of the *Nature*, *Economy* and *Retention Roof* may, therefore, have affected the distribution among the three variables, causing lower scores for air temperature. As the substrate moisture is mainly affected by rain events, these two variables may also have been affected by collinearity. None of the variables were excluded from the regression by choice, as is sometimes done to revise a model [43]. All variables were considered relevant and the exclusion of single variables resulted in a lower percentage of explained evapotranspiration.

A possible explanation for the difference in substrate moisture scores between the *Economy* and *Retention Roof* may be the water availability in these systems. The *Retention*

Roof had a continuously high substrate moisture. and thus plays no important role in determining the evapotranspiration. In the case of the *Economy Roof*, where the substrate moisture is rather low, a change in moisture can strongly affect the evapotranspiration, resulting in a higher score.

Leaf temperature received high scores for the *Garden* and *Retention Roof*; however, it is important to note that the temperature sensor was regularly repositioned among different species, which may have affected the relationship with the evapotranspiration rate.

Overall, it is important to consider that a few factors that influence the evapotranspiration rate could not be incorporated into the regression due to differences in the measurement intervals. These include the vegetation cover, the PAI, the season and the two irrigation events for the *Garden Roof*.

3.6. Substrate Temperature and Air Temperature at Vegetation Level

The substrate temperature and air temperature at the vegetation level were compared between an average day of the spring month, April, and a typical day in the warm summer month, June. In both months, the greatest substrate temperature differences were observed in the afternoon at around 3 p.m., when the green roofs reached their peak substrate temperatures. The *Economy Roof* was the warmest, at around 18 °C in spring and 30 °C in summer, and the *Nature Roof* was the second warmest in both months (Figure 10a,b). In April, the *Garden* and *Retention Roof* had a very similar temperature profile and reached around 13 °C, in June; however, the *Retention Roof* had the coldest substrate temperature at noon, with only 22 °C, while both the *Garden* and *Nature Roof* reached 26 °C. At night, the *Garden*, *Nature* and *Retention Roof* showed very similar temperatures and were about 3 °C warmer compared to the *Economy Roof*. Overall, the temperature amplitude was smallest for the *Retention Roof*.

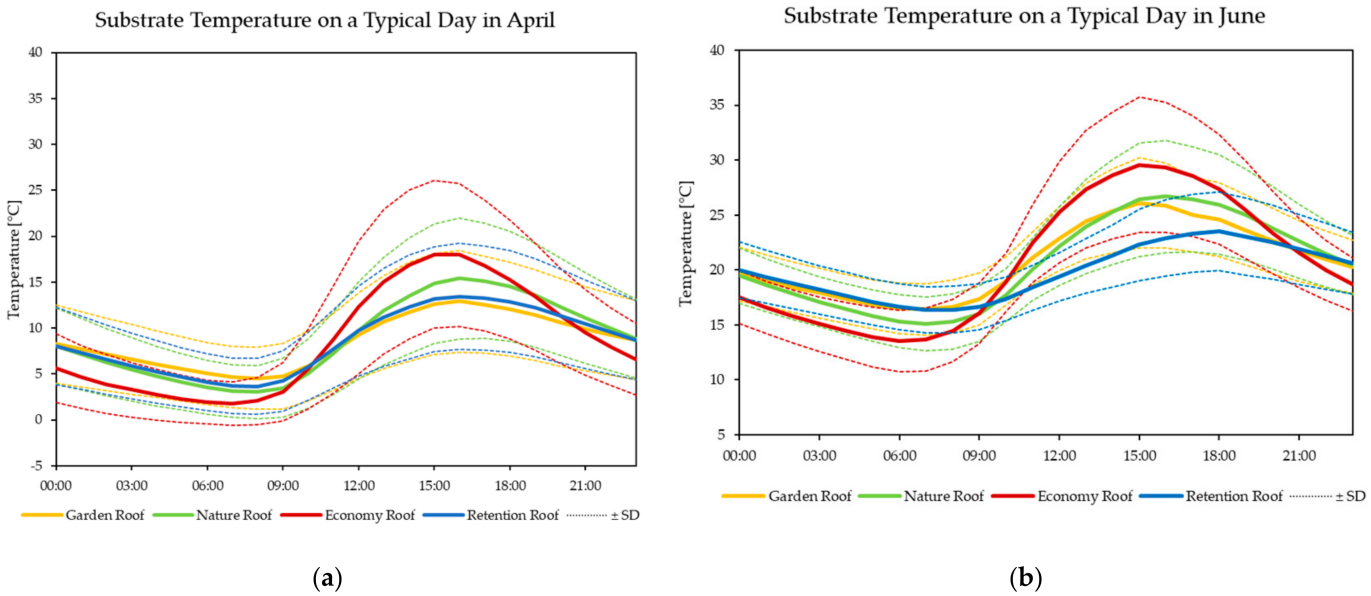


Figure 10. Substrate temperatures on an average day of the four different green roofs in: (**a**) April; (**b**) June. For each single day in April and June, the raw data were aggregated to 24-hourly means. Shown are means ± SD for each hour of 30 days in April and June, respectively (n = 30).

When looking at the air temperatures at the vegetation level, the largest differences were measured at daytime: in April, the *Economy Roof* had the lowest air temperature at noon, while the *Retention*, *Garden* and *Nature Roof* were 2–3 °C warmer (Figure 11a). In June, the *Economy Roof* turned out to be the warmest, at nearly 30 °C at midday, while the *Garden* and *Nature Roof* both reached around 28 °C (Figure 11b). The air temperature

above the *Retention Roof* was the coolest, with only 26 °C at noon; however it reached its maximum of 27 °C two hours later. In the afternoon, the *Garden Roof* was up to 2.5 °C cooler than *Nature* and *Retention Roof*, and up to 4.5 °C lower than the *Economy Roof*.

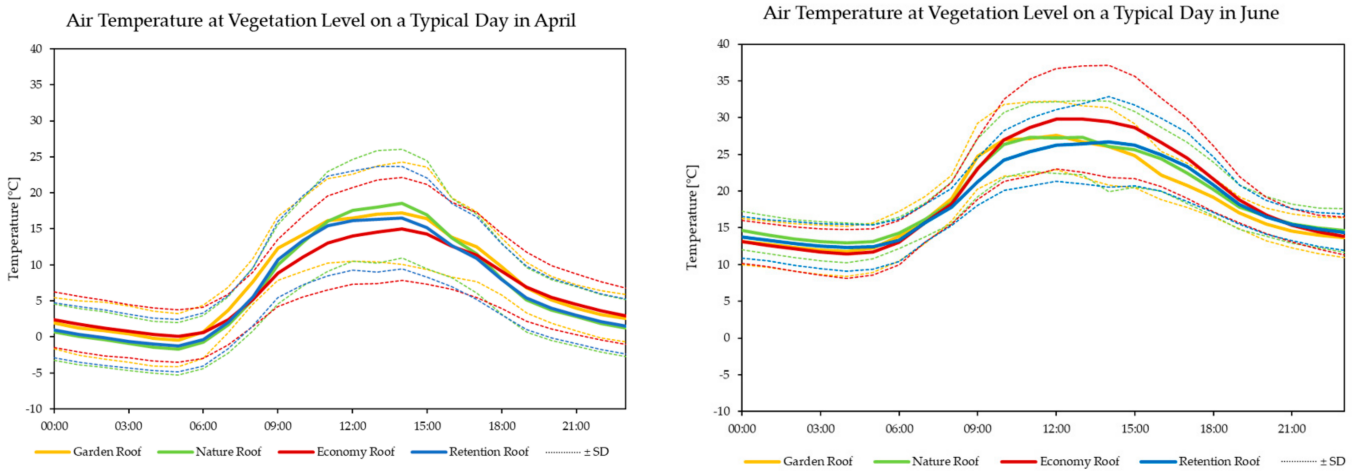


Figure 11. Air temperatures at vegetation level on an average day for the four different green roofs in: (**a**) April; (**b**) June. For each single day in April and June, the raw data were aggregated to 24-hourly means. Shown are means ± SD for each hour of 30 days in April and June, respectively (n = 30).

The small substrate temperature amplitude of the *Retention Roof* may be related to the higher soil moisture and the high specific heat capacity of water: a water-saturated substrate requires more energy to warm up and takes longer to cool down than a dry substrate. Conversely, the *Economy Roof*, with the thinner and drier substrate layer, has a lower specific heat capacity and, therefore, a larger temperature amplitude. This phenomenon can also explain the difference in peaks between the air temperature and substrate temperature: the higher the specific heat capacity, the longer the substrate needs to heat up and adapt to the ambient temperature. Among all roofs, the *Retention Roof*, with the highest soil moisture, reached its peak substrate temperature last.

In April, the air temperatures must be interpreted with the vegetation cover in mind: Both the *Economy Roof* and the *Retention Roof* had a much lower cover than the *Garden* and *Nature Roof*. As substrate can heat up quickly in the sun, the differences at around midday may have primarily been caused by the variation in cover. In June, however, the lowest air temperatures mainly occur above the roofs with highest evapotranspiration rate, namely, the *Garden* and *Retention Roof*. This indicates that the evaporative cooling effect may contribute to the differences in air temperature between the roofs. Nonetheless, the *Economy Roof* still had a lower vegetation cover, and the exposed substrate may have also led to increased air temperatures. It should also be considered that the sensors were attached to leaves of different plant species, and some might have been exposed to the sun while others were shaded. In June, the position of the sensors was changed once within each roof; thus, the data include two different leaf positions and may still be considered representative.

4. Discussion

4.1. Soil Moisture

The results did not show major differences in soil moisture between the period with a low and high plant area index (PAI). This is in line with the study by [44], in which no significant correlation was found between PAI and soil moisture for substrates with a low clay content.

When compared to roofs that receive additional irrigation, neither the *Garden Roof*, nor the *Economy Roof* reached comparable values: a study conducted in Utah, USA, assessed two irrigated miniature green roofs in terms of soil moisture and evapotranspiration [30]. Each roof had a soil thickness of 25 cm and one was covered with *Sedum* species, while the other was covered with grass. The soil moisture was reported to be 25–35% for the grass roof, and 20–40% for the *Sedum* roof for an entire year. Even though the sensors in the present study are placed several centimeters deeper in the substrate, where it would potentially be wetter, the *Garden* and *Economy Roof* only reached values of around 20%. However, the winter months with slightly higher precipitation are also not included in this study. On the other hand, the moisture values of the *Retention Roof* during summer are comparable with the irrigated *Sedum* roof from [30] and only drop during the driest and hottest days of June and September, while the overall summer average remains high. This is likely due to the additional water storage, from which water can migrate back into the substrate layer through capillary bridges, acting as a passive irrigation system. The high moisture values of the *Nature Roof* can be attributed to the thicker substrate and larger drainage and water storage layer compared to the *Economy Roof*.

4.2. Evapotranspiration

The relevance of sufficient plant-available water becomes particularly evident when comparing the results to studies assessing irrigated green roofs. For the summer average daily evapotranspiration, the previously mentioned study in Utah, USA, reports around 5 mm d^{-1} for the grass roof and approximately 3.5 mm d^{-1} for the *Sedum* roof [30]. Both the grass roof and the *Sedum* roof were irrigated, but neither contained a water storage layer. In the present study, the *Garden Roof* with lawn vegetation reached around 4.7 mm d^{-1} in June, a similar value to the irrigated grass roof in [30]. Although the *Garden Roof* has a thinner substrate layer than the grass roof and did not receive any irrigation in June, it contains a temporal water storage, which may have enabled the comparably high evapotranspiration rates. The *Economy Roof*, which can be considered equivalent to the *Sedum* roof by [30], reached only 2.67 mm d^{-1}. Here, the omission of irrigation that results in a lower substrate moisture, as well as the thinner substrate and drainage layer, are most likely responsible for the differences in evapotranspiration.

A study set in Toronto, Canada, measured an evapotranspiration rate of over 7 mm day^{-1} in July with a lysimeter containing an extensive green roof with a 20 cm substrate layer [45]. The high evapotranspiration rate is likely due to the regular irrigation and the situation in a slightly warmer climate compared to this study's site.

However, in the climate zone of the present study, high evapotranspiration rates have been recorded: a study conducted in northern Germany with a very similar experimental setup found that irrigation in summer can enhance the evapotranspiration rate to around 5 mm d^{-1} for extensive green roofs with 9–21 cm substrate [29]. Both the *Retention Roof* and the *Garden Roof* (with 10 and 15 cm substrate) reached evapotranspiration values close to 5 mm d^{-1} in June, and can be thus considered comparable to an irrigated green roof system.

4.3. Variable Importance in Projection (VIP) Scores

Due to the similar vegetation type, the *Garden* and *Economy Roof* are best suited to a comparison of the VIP-scores with the study conducted in Utah, USA, in which air temperature, soil moisture, solar radiation and relative humidity are named as the most influential variables [30]. In the present study, short-wave radiation and relative humidity were also among the most important variables, even though soil moisture had generally lower scores. Due to the close relationship between precipitation and soil moisture, it can be presumed that the results agree on the importance of plant-available water for the evapotranspiration process, which is manifested in the high scores for precipitation in this study and high soil moisture scores found by the authors of [30].

When looking at the different roof types, the authors of [30] found the solar radiation to be more relevant for the grass roof, while soil moisture was more important for the *Sedum* roof. These results correspond with the findings of this study, as soil moisture reached a much higher score for the *Economy Roof*, although the solar radiation is equally important for the *Economy* and *Garden Roof*. While the air temperature received high scores for both the grass and the *Sedum* roof in [30], this was only slightly important for the *Garden Roof*. This divergence may be due to the addition of long-wave radiation in the present study, which reached a high score in the case of the *Economy Roof* and may have led to a different distribution among the three variables of solar-radiation, long-wave radiation and air temperature.

Divergence from the VIP-scores reported by [30] may arise from the different study periods, as [30] used the data of a full year for the regression, while, in the present study, only the periods from April to the beginning of June and from mid-August to the beginning of October are included. Furthermore, the studies were conducted in different climate zones, namely a hot summer, sub-humid, continental climate in the case of [30], and a warm summer, humid continental climate in this study. The variables included in the regression also differed slightly between the studies, as soil heat flux, leaf temperature, soil temperature and long-wave radiation were included in this study, whereas the authors of [30] additionally included the air pressure and the surface soil moisture. These differences may be responsible for the varying distribution among the importance scores.

4.4. Substrate Temperature and Air Temperature at Vegetation Level

The results are in line with other studies observing that green roofs with shallower substrate layers exhibit greater temperature amplitudes during the day [46–48]. In [49], it was found that green roofs with higher substrate moisture also have lower substrate temperatures. Further, the evaporative cooling effect of green roofs was previously investigated, and model results have shown that irrigation can enhance the cooling effect [50]. However, the magnitude of the evapotranspiration and the resulting cooling effect generally varies due to the different green roof setups and study locations in different climate zones [29,30,45].

4.5. Limitations and Outlook

There are a few limitations to this study, mainly driven by the data quality. The period included in the analysis is rather short and does not represent an entire year. A number of sensors failed, and the lack of precipitation data limits the validity of the evapotranspiration rates during the summer months. Additionally, one of the scales showed strong variations, which may have been due to an insufficiently leveled setup. The smoothened hourly values, however, provided a good basis for the calculation of the evapotranspiration. The lysimeters used for measurements were relatively small; therefore, edge effects cannot be completely ruled out. Lastly, the experimental site was located at ground level, and the conditions are certainly different from an exposed roof top. However, the greening of underground structures such as car parks is also very common, and these roofs are often implemented as *Garden Roofs* at ground level.

At the experimental site, the data collection continues and, within a planned follow-up study, we aim to further investigate the underlying mechanisms of the differences among roofs, focusing on the contribution of the vegetation to the total evapotranspiration as well as using the long-term data to define the detailed physical and hydrological connections.

5. Conclusions

This study shows that both the *Garden* and the *Retention Roof* achieve very high evapotranspiration rates. The driving factors were identified as solar radiation and relative humidity, which are environmental variables that cannot be influenced. Additionally, the water availability in the form of rain and the resulting substrate moisture were shown to be highly relevant for the evapotranspiration. Even though rain is another environmental

factor that cannot be controlled, the results demonstrate that engineered solutions can regulate the substrate moisture. The system design of the *Retention Roof* with permanent water storage turned out to be highly effective at raising the moisture content through passive irrigation and creating high evapotranspiration rates. The *Garden Roof* with lawn vegetation and a thick substrate layer also stands out, with a high evapotranspiration and a very stable moisture content throughout the course of the year. In summer, both roofs exhibited lower substrate temperatures and had lower air temperatures at the vegetation level. Therefore, these two roof systems are most suitable for cities that aim to mitigate the urban heat island effect and restore the natural water cycle. Ultimately, the great differences between green roof systems require the inclusion of explicit information into city-scale models. Only when accurate results are available will urban planners be able to complete the decision-making processes and implement a blue—green infrastructure network that is optimized for heat mitigation and storm water management.

Author Contributions: Among the three authors, the work was divided according to the following categories: D.G. carried out the conceptualization, the methodology that involved the measurement concept, the identification of information to be analyzed and the selection of the manner of analysis, supervision, project administration and funding acquisition. M.M. did the writing and preparation of the original draft. J.J.K. was responsible for software and data curation. Validation and management of resources was carried out by D.G. and M.M. The investigation was performed by D.G. and J.J.K. Parts of the methodology, including the search for appropriate analyses, as well as the visualization and formal analysis, were realized by M.M. and J.J.K. The review and editing were carried out by D.G., J.J.K. and M.M. All authors have read and agreed to the published version of the manuscript.

Funding: The data were collected as part of the Project "Building physics design of urban surfaces for a sustainable quality of life and environment in cities" which is 60% funded by the Federal Ministry of Education and Research BMBF (Grant Number: 01LR1725Q). The remaining 40% was funded by Optigrün international AG.

Institutional Review Board Statement: Not applicable.

Informed Consent Statement: Not applicable.

Data Availability Statement: The raw data used for the analysis in this study can be handed out on request by contacting the corresponding author.

Acknowledgments: We kindly acknowledge the permission of Optigrün international AG to use the space for the experimental setup in the parking lot.

Conflicts of Interest: The authors declare that no conflict of interest occurred. The roof systems analyzed in this study are commercially available from Optigrün international AG; therefore, the funders had influence on the choice of systems to be assessed. The data were evaluated according to scientific standards, and the results are presented truthfully.

Appendix A

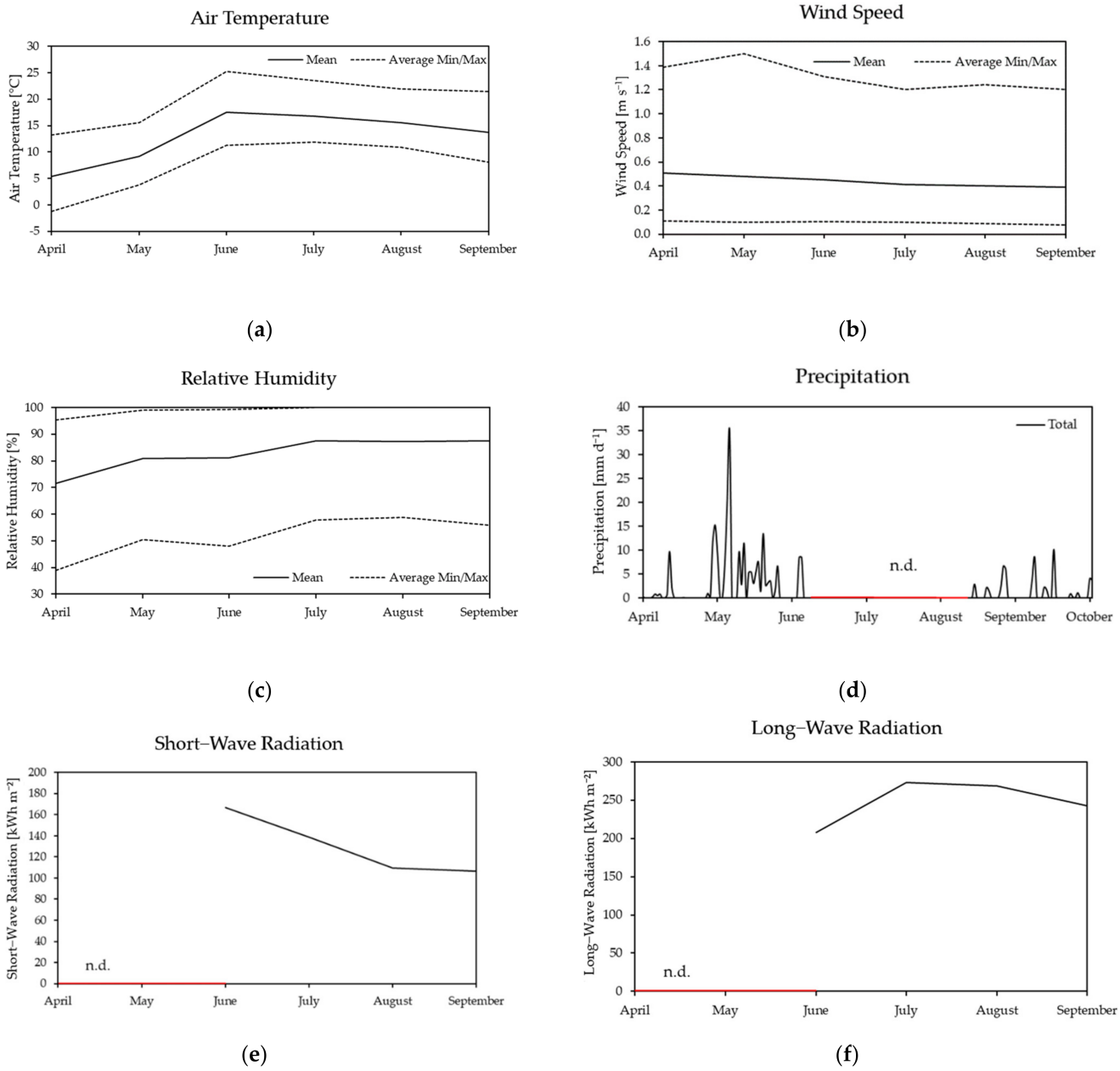


Figure A1. Weather during the study period from April to September 2021, shown as means, with average minimum and average maximum for: (**a**) air temperature; (**b**) wind speed; (**c**) relative humidity; weather during this period shown as average daily sums for: (**d**) precipitation; weather during this period shown as a monthly sum: (**e**) short-wave radiation; (**f**) long-wave radiation. October is not included here as data were only available for four days in that month.

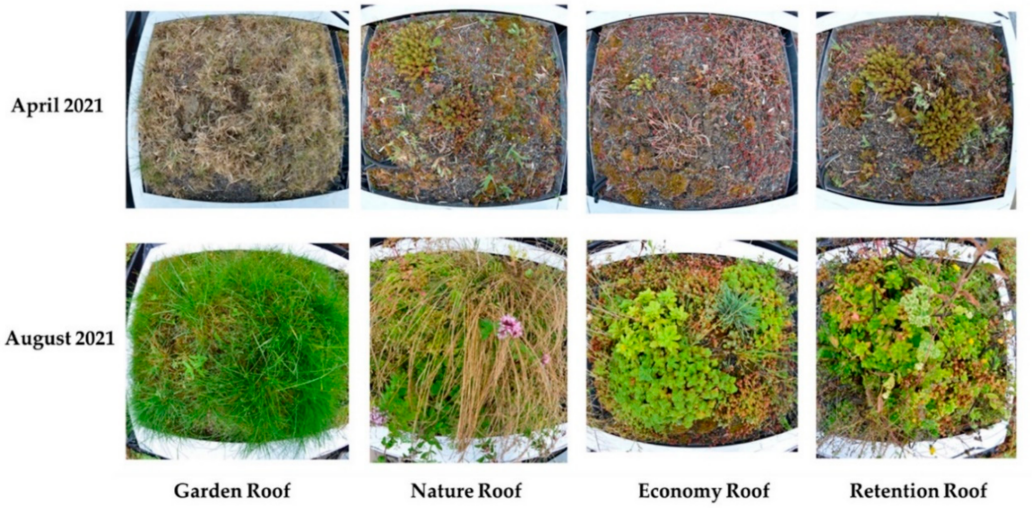


Figure A2. Exemplary photos of the four experimental roofs in April and August 2021.

References

1. Masson-Delmotte, V.; Zhai, P.; Pirani, A.; Connors, S.L.; Péan, C.; Berger, S.; Caud, N.; Chen, Y.; Goldfarb, L.; Gomis, M.I.; et al. Summary for Policymakers. In *Climate Change 2021: The Physical Science Basis. Contribution of Working Group I to the Sixth Assessment Report of the Intergovernmental Panel on Climate Change*; Cambridge University: Cambridge, UK, 2021.
2. Oke, T.R. The Energetic Basis of the Urban Heat Island. *Q. J. R. Meteorol. Soc.* **1982**, *108*, 1–24. [CrossRef]
3. Ward, K.; Lauf, S.; Kleinschmit, B.; Endlicher, W. Heat Waves and Urban Heat Islands in Europe: A Review of Relevant Drivers. *Sci. Total Environ.* **2016**, *569–570*, 527–539. [CrossRef]
4. Liu, W.; Engel, B.A.; Feng, Q. Modelling the Hydrological Responses of Green Roofs under Different Substrate Designs and Rainfall Characteristics Using a Simple Water Balance Model. *J. Hydrol.* **2021**, *602*, 126786. [CrossRef]
5. Hart, M.A.; Sailor, D.J. Quantifying the Influence of Land-Use and Surface Characteristics on Spatial Variability in the Urban Heat Island. *Theor. Appl. Climatol.* **2009**, *95*, 397–406. [CrossRef]
6. George, L.A.; Becker, W.G. Investigating the Urban Heat Island Effect with a Collaborative Inquiry Project. *J. Geosci. Educ.* **2003**, *51*, 237–243. [CrossRef]
7. Santamouris, M. Heat Island Research in Europe: The State of the Art. *Adv. Build. Energy Res.* **2007**, *1*, 123–150. [CrossRef]
8. Deutscher Wetterdienst. Available online: https://www.dwd.de/DE/klimaumwelt/klimaforschung/klimawirk/stadtpl/projekt_waermeinseln/sksm/sksm_node.html (accessed on 7 September 2021).
9. Kendrovski, V.; Baccini, M.; Martinez, G.; Wolf, T.; Paunovic, E.; Menne, B. Quantifying Projected Heat Mortality Impacts under 21st-Century Warming Conditions for Selected European Countries. *Int. J. Environ. Res. Public. Health* **2017**, *14*, 729. [CrossRef] [PubMed]
10. Krug, A.; Mücke, H.-G. Auswertung Hitze-Bezogener Indikatoren Als Orientierung Der Gesundheitlichen Belastung. *UMID Umw. Und Mensch-Inf.* **2018**, *2*, 70–74.
11. Christenson, E.; Elliott, M.; Banerjee, O.; Hamrick, L.; Bartram, J. Climate-Related Hazards: A Method for Global Assessment of Urban and Rural Population Exposure to Cyclones, Droughts, and Floods. *Int. J. Environ. Res. Public Health* **2014**, *11*, 2169–2192. [CrossRef] [PubMed]
12. Gabriel, K.M.A.; Endlicher, W.R. Urban and Rural Mortality Rates during Heat Waves in Berlin and Brandenburg, Germany. *Environ. Pollut.* **2011**, *159*, 2044–2050. [CrossRef]
13. United Nations: Department of Economic and Social Affairs, Population Division. *World Urbanization Prospects: The 2018 Revision*; United Nations: New York, NY, USA, 2019; ISBN 978-92-1-148319-2.
14. Manso, M.; Teotónio, I.; Silva, C.M.; Cruz, C.O. Green Roof and Green Wall Benefits and Costs: A Review of the Quantitative Evidence. *Renew. Sustain. Energy Rev.* **2021**, *135*, 110111. [CrossRef]
15. Krayenhoff, E.S.; Broadbent, A.M.; Zhao, L.; Georgescu, M.; Middel, A.; Voogt, J.A.; Martilli, A.; Sailor, D.J.; Erell, E. Cooling Hot Cities: A Systematic and Critical Review of the Numerical Modelling Literature. *Environ. Res. Lett.* **2021**, *16*, 053007. [CrossRef]
16. Mentens, J.; Raes, D.; Hermy, M. Green Roofs as a Tool for Solving the Rainwater Runoff Problem in the Urbanized 21st Century? *Landsc. Urban Plan.* **2006**, *77*, 217–226. [CrossRef]
17. Filazzola, A.; Shrestha, N.; MacIvor, J.S. The Contribution of Constructed Green Infrastructure to Urban Biodiversity: A Synthesis and Meta-analysis. *J. Appl. Ecol.* **2019**, *56*, 2131–2143. [CrossRef]
18. Ran, J.; Yang, Z.; Feng, Y.; Xiong, K.; Tang, M. Energy Performance Assessment and Optimization of Extensive Green Roofs in Different Climate Zones of China. *E3S Web Conf.* **2020**, *172*, 16003. [CrossRef]

19. Lee, K.E.; Williams, K.J.H.; Sargent, L.D.; Farrell, C.; Williams, N.S. Living Roof Preference Is Influenced by Plant Characteristics and Diversity. *Landsc. Urban Plan.* **2014**, *122*, 152–159. [CrossRef]
20. Lee, K.E.; Sargent, L.D.; Williams, N.S.G.; Williams, K.J.H. Linking Green Micro-Breaks with Mood and Performance: Mediating Roles of Coherence and Effort. *J. Environ. Psychol.* **2018**, *60*, 81–88. [CrossRef]
21. Versini, P.-A.; Gires, A.; Tchiguirinskaia, I.; Schertzer, D. Fractal Analysis of Green Roof Spatial Implementation in European Cities. *Urban For. Urban Green.* **2020**, *49*, 126629. [CrossRef]
22. Lomba-Fernández, C.; Hernantes, J.; Labaka, L. Labaka Guide for Climate-Resilient Cities: An Urban Critical Infrastructures Approach. *Sustainability* **2019**, *11*, 4727. [CrossRef]
23. Yang, J.; Wang, Z.-H. Physical Parameterization and Sensitivity of Urban Hydrological Models: Application to Green Roof Systems. *Build. Environ.* **2014**, *75*, 250–263. [CrossRef]
24. Balany, F.; Ng, A.W.; Muttil, N.; Muthukumaran, S.; Wong, M.S. Green Infrastructure as an Urban Heat Island Mitigation Strategy—A Review. *Water* **2020**, *12*, 3577. [CrossRef]
25. Vijayaraghavan, K. Green Roofs: A Critical Review on the Role of Components, Benefits, Limitations and Trends. *Renew. Sustain. Energy Rev.* **2016**, *57*, 740–752. [CrossRef]
26. Peng, L.; Jim, C. Green-Roof Effects on Neighborhood Microclimate and Human Thermal Sensation. *Energies* **2013**, *6*, 598–618. [CrossRef]
27. Morakinyo, T.E.; Dahanayake, K.W.D.; Kalani, C.; Ng, E.; Chow, C.L. Temperature and Cooling Demand Reduction by Green-Roof Types in Different Climates and Urban Densities: A Co-Simulation Parametric Study. *Energy Build.* **2017**, *145*, 226–237. [CrossRef]
28. Cascone, S.; Coma, J.; Gagliano, A.; Pérez, G. The Evapotranspiration Process in Green Roofs: A Review. *Build. Environ.* **2019**, *147*, 337–355. [CrossRef]
29. Kaiser, D.; Köhler, M.; Schmidt, M.; Wolff, F. Increasing Evapotranspiration on Extensive Green Roofs by Changing Substrate Depths, Construction, and Additional Irrigation. *Buildings* **2019**, *9*, 173. [CrossRef]
30. Feng, Y.; Burian, S.; Pardyjak, E. Observation and Estimation of Evapotranspiration from an Irrigated Green Roof in a Rain-Scarce Environment. *Water* **2018**, *10*, 262. [CrossRef]
31. Wang, C.; Wang, Z.-H.; Kaloush, K.E.; Shacat, J. Perceptions of Urban Heat Island Mitigation and Implementation Strategies: Survey and Gap Analysis. *Sustain. Cities Soc.* **2021**, *66*, 102687. [CrossRef]
32. Beck, H.E.; Zimmermann, N.E.; McVicar, T.R.; Vergopolan, N.; Berg, A.; Wood, E.F. Present and Future Köppen-Geiger Climate Classification Maps at 1-Km Resolution. *Sci. Data* **2018**, *5*, 180214. [CrossRef]
33. Wetterdienst.De. Available online: https://www.wetterdienst.de/Deutschlandwetter/Krauchenwies/Klima/ (accessed on 15 October 2021).
34. *Dachbegrünungsrichtlinien—Richtlinien Für Die Planung, Bau Und Instandhaltung von Dachbegrünungen*; Landschaftsbau, F.L. (Ed.) Landschaftsentwicklung Landschaftsbau e.V: Bonn, Germany, 2018.
35. RStudio Team. *RStudio Desktop*; RStudio: Boston, MA, USA, 2020.
36. R Core Team. *R: A Language and Environment for Statistical Computing*; R Foundation for Statistical Computing: Vienna, Austria, 2020.
37. Kessler, W. *Multivariate Datenanalyse: Für die Pharma-, Bio- und Prozessanalytik ein Lehrbuch*; Wiley-VCH: Weinheim, Germany, 2008; ISBN 978-3-527-31262-7.
38. Wai, C.M.; Weise, S.E.; Ozersky, P.; Mockler, T.C.; Michael, T.P.; VanBuren, R. Time of Day and Network Reprogramming during Drought Induced CAM Photosynthesis in Sedum Album. *PLoS Genet.* **2019**, *15*, e1008209. [CrossRef] [PubMed]
39. Lee, H.S.J.; Griffiths, H. Induction and Repression of CAM in *Sedum Telephium* L. in Response to Photoperiod and Water Stress. *J. Exp. Bot.* **1987**, *38*, 834–841. [CrossRef]
40. Wold, S. PLS for Multivariate Linear Modeling. In *Chemometric Methods in Molecular Design*; Van de Waterbeemd, H., Ed.; Wiley-VCH Verlag GmbH & Co. KGaA: Weinheim, Germany, 1994; ISBN 3-527-3004-9.
41. Cai, J.; Liu, Y.; Lei, T.; Pereira, L.S. Estimating Reference Evapotranspiration with the FAO Penman–Monteith Equation Using Daily Weather Forecast Messages. *Agric. For. Meteorol.* **2007**, *145*, 22–35. [CrossRef]
42. Allen, R.G.; Pereira, L.S.; Raes, D.; Smith, M. *Crop Evapotranspiration-Guidelines for Computing Crop Water Requirements*; FAO Irrigation and Drainage Paper; repr.; Food and Agriculture Organization of the United Nations: Rome, Italy, 2000; ISBN 978-92-5-104219-9.
43. Mehmood, T.; Sæbø, S.; Liland, K.H. Comparison of Variable Selection Methods in Partial Least Squares Regression. *J. Chemom.* **2020**, *34*, e3226. [CrossRef]
44. Liu, L.; Zhang, R.; Zuo, Z. The Relationship between Soil Moisture and LAI in Different Types of Soil in Central Eastern China. *J. Hydrometeorol.* **2016**, *17*, 2733–2742. [CrossRef]
45. Jahanfar, A.; Drake, J.; Gharabaghi, B.; Sleep, B. An Experimental and Modeling Study of Evapotranspiration from Integrated Green Roof Photovoltaic Systems. *Ecol. Eng.* **2020**, *152*, 105767. [CrossRef]
46. Reyes, R.; Bustamante, W.; Gironás, J.; Pastén, P.A.; Rojas, V.; Suárez, F.; Vera, S.; Victorero, F.; Bonilla, C.A. Effect of Substrate Depth and Roof Layers on Green Roof Temperature and Water Requirements in a Semi-Arid Climate. *Ecol. Eng.* **2016**, *97*, 624–632. [CrossRef]
47. Eksi, M.; Rowe, D.B.; Wichman, I.S.; Andresen, J.A. Effect of Substrate Depth, Vegetation Type, and Season on Green Roof Thermal Properties. *Energy Build.* **2017**, *145*, 174–187. [CrossRef]

48. Pianella, A.; Aye, L.; Chen, Z.; Williams, N. Substrate Depth, Vegetation and Irrigation Affect Green Roof Thermal Performance in a Mediterranean Type Climate. *Sustainability* **2017**, *9*, 1451. [CrossRef]
49. Jim, C.Y.; Peng, L.L.H. Substrate Moisture Effect on Water Balance and Thermal Regime of a Tropical Extensive Green Roof. *Ecol. Eng.* **2012**, *47*, 9–23. [CrossRef]
50. Heusinger, J.; Sailor, D.J.; Weber, S. Modeling the Reduction of Urban Excess Heat by Green Roofs with Respect to Different Irrigation Scenarios. *Build. Environ.* **2018**, *131*, 174–183. [CrossRef]

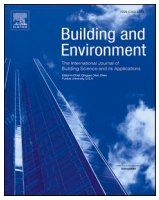
Building and Environment 269 (2025) 112356



Contents lists available at ScienceDirect

Building and Environment

journal homepage: www.elsevier.com/locate/buildenv





Green roof performance monitoring: Insights on physical properties of 4 extensive green roof types after 2 years of microclimatic measurements

Dominik Gößner *, Maria Kunle, Milena Mohri

Optigrün international AG, Am Birkenstock 15-19, 72505 Krauchenwies Göggingen, Germany

ARTICLE INFO

Keywords:
Green roof system
Blue-green infrastructure
Building microclimate
Urban heat island

ABSTRACT

Green infrastructure elements like green roofs provide a range of ecosystem services to urban areas. Although shallow extensive green roofs contribute less to stormwater retention and microclimatic improvement than other green roof types, they remain the most widely used system in European market. This study aims to establish a basis for optimizing green roof designs by thoroughly examining the differences in the physical characteristics of the roofs as well as their environmental impacts and performances in relation to their properties. Two years of microclimatic monitoring on four green roofs revealed distinctly different behaviors regarding evapotranspiration, substrate moisture, substrate temperature, ground-level air temperature, and heat flux. The performances in evapotranspiration and cooling of ground-level air temperature in summer were clearly related to substrate thickness and water storage capacity of the roofs. Furthermore, differences in rainwater interception and stomatal conductance were quantified among various plant species. The results highlight that green roofs with thick substrates or large water storage capacities, combined with highly transpiring and densely growing plant species are most likely to deliver the ecosystem services needed in cities. The collected data also proofs to be essential for high-precision modeling of green roofs' microclimatic effects in the context of urban planning.

1. Introduction

Taking into consideration the current development of climate change, especially in densely populated urban areas, the use of green infrastructure elements to mitigate negative impacts of the changing environment is a promising approach. Green roofs, which are one of the most common green infrastructure applications in cities and frequent subjects of scientific studies, show high potential for microclimate improvement and the restoration of the natural water cycle [5,33,34,39,42,54].

Even though the positive effects of green roofs are widely acknowledged [33], there is still a lack of understanding of green roofs as complex systems whose properties are influenced by the physical characteristics of their layers and their reactions to environmental influences. Especially when considering the variety of marketed green roof systems, most studies are limited either to differentiations only between extensive and intensive green roofs [44,53] or purely theoretical approaches using model simulations [30,35]. The few studies that compare different green roof systems specifically focus on either stormwater retention or on the building insulation potential [25,50,61]. There is no study linking green roof microclimatic effects to the respective green roof characteristics based on comprehensive energy and water household measurements taken over an extended period of time.

The aim of the present study is to gain an in-depth understanding of the dynamics within green roof systems bringing together energetic, water-related, and plant physiological aspects. and to provide a data basis for green roof simulations. As many building modeling tools are not able to accurately integrate green roofs (Jovanović et al. 2019), a better understanding of green roofs is essential for optimizing green infrastructure solutions and for meeting the current challenges in urban areas.

In order to capture the diverse physical properties and effects of green roof systems as well as their interactions with the environment in a holistic way, the study has the following objectives:

a) Compiling the physical properties of four different green roof systems

Considering the great diversity of existing green roof systems and their distinct influences on the microclimate [16], the physical properties should be studied in greater detail, summarized, and compared. From the data collected in this study, we expect to see relevant differences in the physical characteristics of the green roofs throughout all

* Corresponding author at: Optigrün international AG, Am Birkenstock 15-19, 72505 Krauchenwies Göggingen, Germany.
E-mail address: d.goessner@optigruen.de (D. Gößner).

https://doi.org/10.1016/j.buildenv.2024.112356
Received 24 July 2024; Received in revised form 8 November 2024; Accepted 26 November 2024
Available online 27 November 2024
0360-1323/© 2024 Elsevier Ltd. All rights are reserved, including those for text and data mining, AI training, and similar technologies.

seasons.

More specifically, we predict lower air temperatures at vegetation level, lower substrate temperature, and higher evapotranspiration rates in roof systems with greater water storage capacity and higher soil moisture. In addition, heat flux - the rate of heat transfer through a surface such as a green roof - and substrate moisture are likely to be more stable in green roof systems with thicker substrate layers.

b) Assessing the driving factors of the physical characteristics regarding the interactions among the observed parameters as well as their interaction with environmental factors

Green roofs as semi-natural systems are influenced by the characteristics of the components they are built from and also react to and interact with the surrounding environment. To gain a solid understanding of the green roof system as a complex system and draw accurate conclusions, the assessment requires a large dataset of both green roof systems and climatic factors.

As we predict differences among the green roofs regarding their physical properties, we assume that the systems also react differently to environmental influences. In particular, the roofs with the thickest substrate layer and the largest water storage capacity are expected to be more stable systems, less affected by variations in the surrounding air temperature, incoming radiation, or wind speed. Consequently, the regression coefficients should generally be smaller compared to the green roof system with the shallowest substrate layer and lowest water storage capacity.

c) Developing green roof design strategies to optimize their performance in microclimate regulation and stormwater retention

The findings on differences among green roof systems alongside the assessment of influencing environmental factors offer insights for refining green roof design, which can then be applied in urban planning. The emphasis lies on flood mitigation through stormwater retention and the reduction of the urban heat island effect during summer, which are common challenges in densely populated urban areas.

2. Materials and methods

2.1. Experimental design description

2.1.1. Microclimatic measurements

The research was conducted in the south of Germany, in Göggingen-Krauchenwies (48°0′20.27916″ N and 9°12′5.33952″ E) at an elevation of 623 meters above sea level. This location falls within the warm temperature, fully humid warm summer climate classification [31]. The setup encompassed four ground-level experimental green roofs, each designed as a lysimeter with a surface area of 0.5 m^2. A surrounding green roof was built to minimize potential edge effects in the experimental setup (**Figure S1**, supplementary material). Each green roof was equipped with sensors for leaf and air temperatures at the vegetation level, substrate temperature, substrate moisture content, heat flux, outflow and weight. Additionally, a weather station recorded precipitation, air temperature and relative, wind speed, incoming shortwave solar irradiance and incoming longwave radiation. Details on sensor models and manufacturers can be found in the supplementary material **Table S1**. The data was collected at an interval of 5 minutes, resulting in a dataset comprising 2 full years (April 1st 2021 to March 31st 2023). The roof systems are distributed by Optigrün international AG and contain various roof layers (Fig. 1). All experimental green roofs were fertilized with a slow-release fertilizer (Opticote, Optigrün international AG) at the beginning of the study period and were weeded approximately once per month in summertime to preserve the intended vegetation. Furthermore, the Garden roof with lawn species was watered occasionally, which is typical for maintaining this type of green roof. All roofs drain freely except the Retention roof, where the drainage hole is positioned at 3 cm height. Further information on the positioning of the sensors can be found in the supplementary material (**Figure S2**).

2.1.2. Focus: Stomatal conductance measurements

Stomatal conductance, the inverse of stomatal resistance, measures the rate of gas exchange between plant leaves and the surrounding air and reflects the loss of water vapor through leaves (Monteith, Szeicz, and Waggoner 1965). In the context of green roofs, it can be considered an indicator of the plants' water consumption and ability to cool the environment. On the experimental roofs, the stomatal conductance was

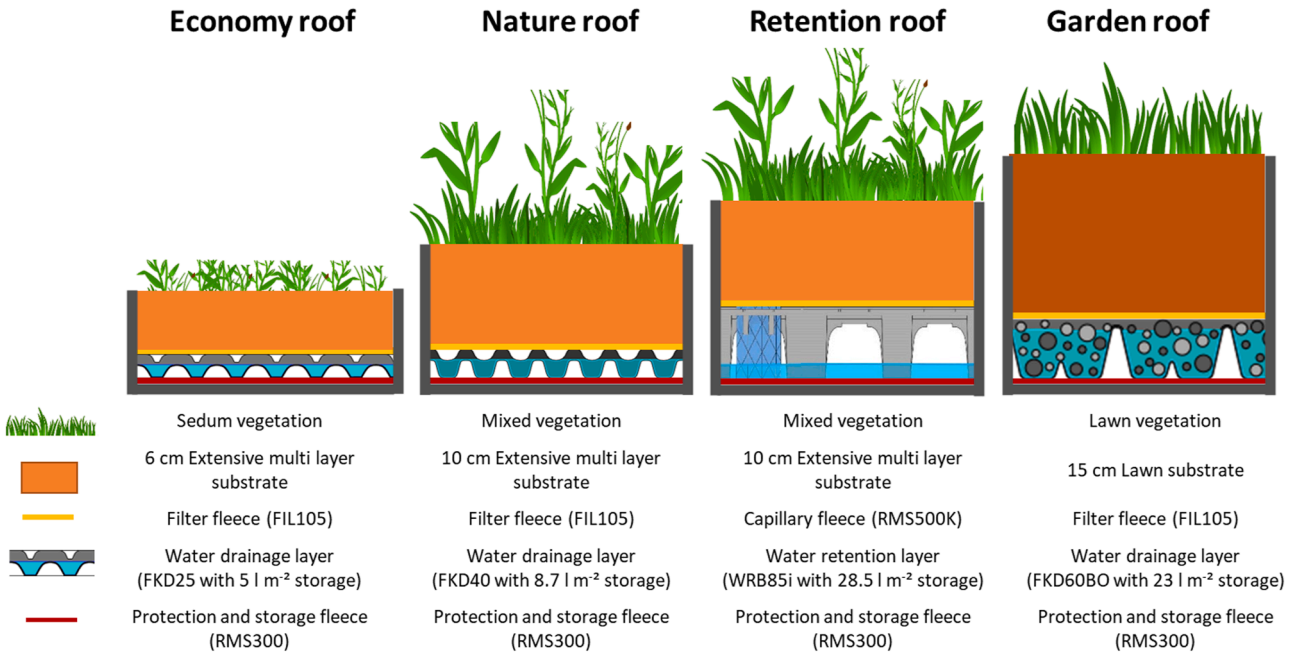


Fig. 1. Overview of the green roof types.

measured occasionally in September 2021, June 2022 and October 2022 under warm and clear weather conditions. The Garden roof contained *Festuca ovina*, the Economy roof was composed of *Sedum* species (*Sedum kamtschaticum* and *Sedum spurium*) and the Nature and Retention roof contained mainly *Sedum* species and herbs (*Sedum kamtschaticum, Sedum spurium,* and *Origanum vulgare*). These plant species were part of the original plant mix applied on the green roofs showed a high plant-cover. For all days combined, there were 72 observations in total for the Garden and Economy roof and 69 for the Nature and Retention roof.

Stomatal conductance measurements were performed on a single mature leaf from each adult plant, with the location on the leaf selected randomly, provided it was sufficiently large to accommodate proper placement of the porometer sensor. A steady-state Leaf Porometer (SC-1 Leaf Porometer, METER Group Inc.) was employed for the measurements, following calibration in accordance with the manufacturer's recommended technique. In total, 282 measurements of stomatal conductance were recorded.

2.1.3. Focus: Interception measurements

The interception capacity quantifies the amount of rainfall retained on the surface of a plant's above-ground biomass. A vegetation cover with high interception capacity can therefore improve a green roof system's water retention capability. The assessment of interception capacity was based on Dunkerley and Booth [9] with minor adjustments to adapt to the smaller scale of our experiment. Ten low-growing perennials including herbaceous species and subshrubs commonly utilized for green roof installations were assessed. The initial preselection was based on a list of low-growing perennials suitable for green roofs and developed through years of practical experience, the final selection was determined by the availability at the nearest plant nursery. Of each species, three replicates were selected. To determine the interception capacity, a 10 × 10 cm frame was used to define the area of each plant's aboveground biomass and excess aboveground biomass was trimmed. Then, the plant was cut just above the substrate, weighed and placed in floral foam blocks to mimic the natural arrangement. Each plant was irrigated with 500 ml water for 30 seconds using a rainfall-tip nozzle. After two minutes, the plants were re-weighed to determine the interception capacity based on the weight difference that was then extrapolated to 1 m^2 and averaged for each plant species. Additionally, the plant area index (the ratio of plant aboveground biomass to the substrate surface) was recorded using a digital camera (Nikon D3200) with a fisheye lens (Walimex pro, Studioexpress Vertriebs GmbH) and calculated in the image analysis software CAN-EYE (INRAE).

2.2. Data processing

The data within the hours in which maintenance activities, such as weeding, sensor replacements, or outflow sensor cleaning, were performed at the experimental setup were excluded from the dataset. Furthermore, on days when the Garden roof was irrigated, the weight data was set to 'Not Available' (NA) for the entire days, as the weight is used in the calculation of the evapotranspiration.

Upon careful scrutiny of the raw data, the following lower and upper limits were established to exclude outliers: Substrate temperature at the Garden, Nature, and Retention roof -10 to +45 °C, at the Economy roof -10 to +55 °C; heat flux at the Garden, Nature, and Retention roof -16 to +50 W m^{-2}, at the Economy roof -30 to +60 W m^{-2}; shortwave solar irradiance 0 to 1250 W m^{-2}; air temperature at vegetation level at the Nature, and Retention roof -10 to +50 °C, at the Garden and Economy roof -10 to +60 °C; leaf temperature at the Nature, Economy, and Retention roof -20 to+ 55 °C, at the Garden roof -20 to +65 °C; air temperature -10 to +40 °C; relative air humidity 0 to 100 %; substrate moisture 0 to 100 %; rainfall 0 to 9 mm; wind speed 0 to 3 m s^{-1}. Values outside of these ranges may have caused distortions in the data.

During periods of malfunctioning of sensors as well as during times of maintenance of the experimental fields, outlying data points that were substantially deviating from the overall trends at specific time points, were considered as obvious outliers and assigned a value of NA. Furthermore, due to malfunctioning of the rain sensor during snowfall, rainfall values were recovered from the German Meteorological Service open-source data (DWD Climate Data Center [10], n.d.]. Those smoothed hourly precipitation values were used, when at least one of the outflow sensors indicated water discharge within an hour following the rainfall observation.

On days with a net outflow of water that resulted in negative calculated evapotranspiration values, the evapotranspiration was set to 0 mm. To prepare and handle the data obtained from the lysimeter at both hourly and daily intervals, we applied a smoothing technique by computing the hourly and daily averages or sums for all measurements.

2.3. Calculations and statistical analyses

2.3.1. Calculation of vapor pressure deficit

The vapor pressure deficit (VPD) is the difference between the actual moisture in the air and the maximum amount of water the air can hold. As VPD increases, plant leaves lose more water vapor, leading to higher transpiration but also to potential water stress. In the context of green roofs, VPD therefore impacts the vegetative cooling effect. From a plant physiological perspective, Gates et al. [13] defines the VPD as the difference between the vapor pressure inside the plant's leaves (VP_{plant}) and the actual vapor pressure of the air (VP_{air}) and refers to Gates, Zolnier, and Buxton [13] for the calculation of VP_{plant} and VP_{air} as:

$$VP_{plant} = \frac{610.7 \times 10 \times exp^{\left(\frac{7.5 \times T_L}{273.3+T_L}\right)}}{1000} \quad (1)$$

and

$$VP_{air} = \frac{610.7 \times 10 \times exp^{\left(\frac{7.5 \times T_A}{273.3+T_A}\right)}}{1000} \times \frac{RH}{100} \quad (2)$$

where, T_L is the leaf temperature in degrees Celsius, T_A represents air temperature in degrees Celsius, and RH corresponds to relative air humidity as a percentage. Eq. 1 calculates the maximum water vapor pressure in the plant's leaf at the given leaf temperature, while Eq. 2 reflects the actual air vapor pressure based on the air temperature and the relative humidity.

2.3.2. Determination of evapotranspiration

The evapotranspiration of the experimental roofs was calculated using the smoothed hourly weight and outflow of each of the setups, and precipitation. Eq. (3) represents the formula for daily evapotranspiration:

$$Evapotranspiration = Weight_{00:00} - Weight_{24:00} - Outflow + Precipitation \quad (3)$$

Due to possible malfunctioning of outflow sensors during intense rain events, evapotranspiration was not calculated for days with rainfall above 2 mm.

2.3.3. Stomatal activity

We applied a logarithmic transformation to stomatal conductance measurements by taking the logarithm of each individual measurement, log10(x), where x represents the stomatal conductance value. This transformation was chosen to normalize the data and reduce skewness, as the original data exhibited a right-skewed distribution. To validate our measurements, the stomatal resistance was calculated based on the environmental conditions using the formula of Tabares-Velasco and Srebric [59]:

$$r_s = \frac{r_{\text{stomatal.min}}}{LAI} \times f_{\text{solar}} \times f_{\text{VPD}} \times f_{\text{VWC}} \times f_{\text{temperature}} \quad (4)$$

Where:

$$f_{\text{solar}} = 1 + exp^{(-0.034 \times (R_{sh} - 3.5))} \quad (5)$$

$$f_{\text{VWC}} = \begin{cases} 1 & \text{VWC} > 0.7 \times \text{VWC}_{fc} \\ \frac{0.70 \times \text{VWC}_{fc} - \text{VWC}_{wp}}{\text{VWC} - \text{VWC}_{wp}} & \text{VWC}_{wp} < \text{VWC} < 0.7 \times \text{VWC}_{fc} \\ 1000 & \text{VWC}_{wp} > \text{VWC} \end{cases} \quad (6)$$

$$f_{\text{VPD}} = \frac{1}{1 - 0.41 \times \ln(e_{s,\ \text{plants}} - e_a)} \quad (7)$$

$$f_{temperature} = \frac{1}{1 - 0.0016 \times (35 - (T_{\text{plants}} - 273.15))^2} \quad (8)$$

In these equations, r_s represents stomatal resistance to mass transfer, $r_{\text{stomatal.min}}$ corresponds to the minimum stomatal resistance to mass transfer, R_{sh} stands for incoming shortwave solar irradiance, VWC_{fc} is the substrate volumetric water content under field conditions, VWC_{wp} represents the substrate volumetric water content at the wilting point, $e_{s,\ \text{plants}}$ corresponds to the vapor pressure of the air in contact with plants in kPa, e_a represents the vapor pressure of the air in kPa, and T_{plants} stands for the average temperature of the plants in K. The values of VWC_{wp} were determined based on Aslam et al. [2]; Shedd, Dukes, and Miller [52] and Veihmeyer and Hendrickson [62] and were adjusted to account for potential underestimation of substrate moisture content in our observations, resulting in a value of 10 % for *F. ovina* and 5 % for the other species. $r_{\text{stomatal.min}}$ values were obtained from Tabares-Velasco and Srebric [59], with specific values as follows: 500 s m^{-1} for *Sedum* species, 50 s m^{-1} for *F. ovina*, 100 s m^{-1} for *O. vulgare*. $e_{s,\ \text{plants}}$ was calculated using the Tetens equation [46]:

$$e_s = 0.61078 \times exp^{\left(\frac{17.27 \times T}{T + 237.3}\right)} \quad (9)$$

Where T represents the temperature of air surrounding the leaves. e_a was calculated similarly, though here, T is the air temperature obtained from an on-site meteorological station. Furthermore, in our calculations, we employed the plant area index (PAI) instead of the traditional leaf area index (LAI). This decision was based on the limitations of the software, which allowed only for the calculation of the PAI. While for trees the PAI can be much larger due to the presence of woody stems and branches, for low-growing herbaceous plants the PAI and LAI are similar [29].

We converted our measured stomatal conductance values to stomatal resistance to be able to relate it to the stomatal resistance calculated with the formula of Tabares-Velasco and Srebric [59], using the following formula:

$$g_w\left(\frac{m}{s}\right) = \frac{g_w\left(\frac{mol}{m^2 s}\right)}{44.6 \frac{mol}{m^3} \times \left[\frac{273}{273+T}\right] \times \left[\frac{P}{101.3}\right]} \quad (10)$$

where the result, g_w, is the stomatal resistance in m s^{-1}, g_w as input is the stomatal conductance in mol m^{-2} s^{-1}, T is the air temperature in °C and P is the atmospheric pressure in kPa.

2.4. Statistical analysis

All statistical analyses were performed using R, version 4.2.2 (R [43]). A p-value of less than 0.05 was considered statistically significant across the entire analysis. Multiple linear regression models were employed to analyze the microclimatic variables separately for each green roof system. In order to quantify the strength and significance of correlations, the Pearson's correlation coefficients were computed. Multiple linear regression was selected as a simple model for assessing primary trends in relationships. Particularly for the modeling of evapotranspiration, studies show that linear regressions are a suitable model approach [27,51]. Although nonlinear models like genetic programming demonstrate a slightly higher performance in evapotranspiration estimation, the multiple linear regression also achieve reliable results without a significant lower accuracy [15]. Significant differences in stomatal conductance across plant species were assessed using ANOVA with Tukey's HSD post hoc test. For differences among the roof types, a repeated measures ANOVA using a single daily average value with a subsequent post hoc Tukey's test was used. To comprehensively examine seasonal variations, the data collected over the two-year period were categorized into four distinct seasons: spring (March to May), summer (June to August), fall (September to November), and winter (December to February).

3. Results and discussion

3.1. Air temperature at vegetation level

3.1.1. Differences among the green roofs

The air temperatures at vegetation level around early afternoon differ quite strongly in the summer months among the roofs (see Fig. 2). The highest mean was measured above the Economy roof in July with 32.12 (±7.52) °C. Above the Retention roof, the temperature was lowest with only 27.35 (±5.09) °C. Thus, the difference in mean temperature in July between the coolest and the warmest roof was just over 4.5 °C.

When summarizing the data for the entire summer season for 14:00, the differences in air temperature at vegetation level among the roofs remain visible: The Economy roof has the warmest mean temperature with 30.56 (± 8.15) °C, while the Retention and Nature roof were the coolest with 26.36 (± 5.75) °C and 26.67 (± 6.22) °C respectively. The Garden roof represented a middle ground between those extremes: in summer months mean air temperature at vegetation level at 14:00 was 28.58 (± 7.52) °C. In the winter months all roofs had similar mean values and differed only by 1–2 °C, with the Economy roof being almost always the warmest.

3.1.2. Driving factors of the air temperature at vegetation level

Overall, the shortwave solar irradiance clearly has the greatest influence on the air temperature at vegetation level (see Fig. 3), particularly for the Garden roof ($\beta = 19.05$, SE = 0.33, $p < 0.001$), and the least impact on the Retention roof ($\beta = 10.35$, SE = 0.22, $p < 0.001$). The substrate temperature also correlates positively with the air temperature at vegetation level across all roofs, while substrate moisture shows a slight negative correlation. All other variables are only partly significant or do not show a uniform pattern.

3.1.3. Discussion of the findings

Shortwave solar irradiance, wind speed, as well as air and surface temperature are commonly used for the calculation of heat fluxes on green roofs [18]. Heat flux is decisive for the calculation of air temperature at vegetation level [59] Even though heat flux did not show a clear correlation in the present study, shortwave solar irradiance and substrate temperature were found to be influencing the air temperature at vegetation level. The air temperature of the weather station was not included in the model due to the collinearity with shortwave solar irradiance. Yet, in general the findings regarding the driving factors of air temperature at vegetation level are in line with the present calculation methods. No other publications comparing air temperature of different green roof types and assessing its determinants were found. The cooling effect from the Retention roof with high water availability can vary due to differences in substrate thickness or study locations in

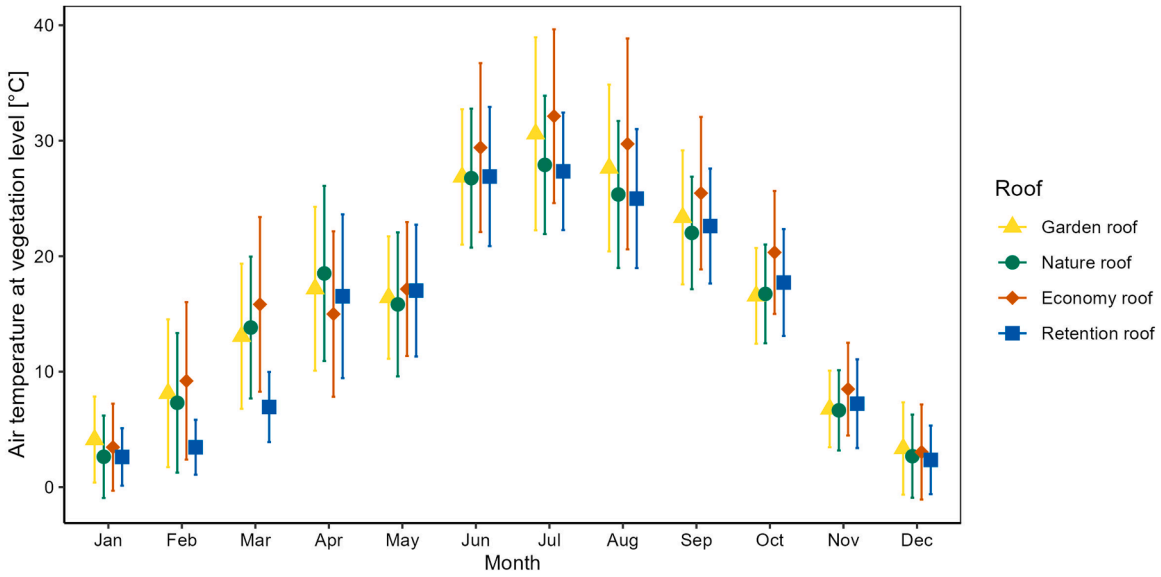


Fig. 2. Mean air temperatures at vegetation level (±SD) at 14:00 for different green roof types. Each mean represents the average of all 14:00 temperature readings collected throughout the corresponding month.

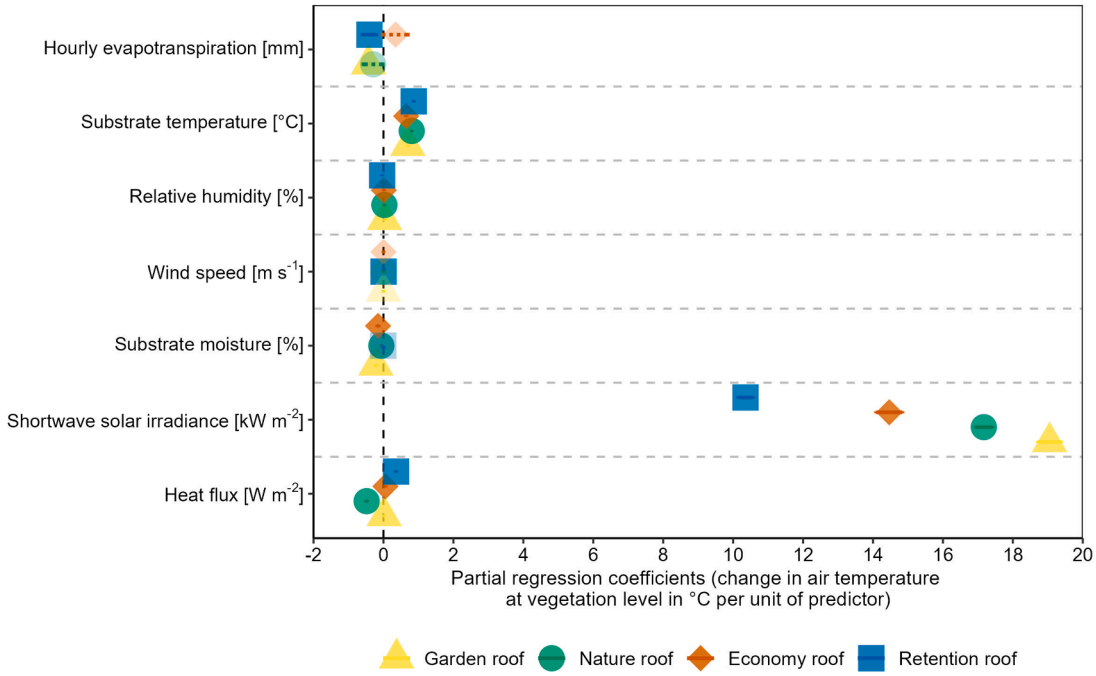


Fig. 3. Partial regression coefficients (±SE) for air temperature at vegetation level for different green roof types, analyzed on an hourly basis. Fully colored circles indicate statistically significant effects ($p < 0.05$), while semi-transparent circles represent non-significant effects.

different climate zones [12,20,25]. Previous studies and modeling results showed that irrigation can enhance the evaporative cooling effect [7,17].

Overall, the results show that the choice of roof type affects the surrounding microclimate, particularly in summer. Shallow green roofs with low water storage capacities exhibit higher air temperatures, which are influenced not only by direct sunlight but also by the substrate temperature. These results support the assumption, that the roof system with a larger water storage capacity show lower air temperatures at vegetation level. The second expectation, that shallower roofs are more strongly influenced by environmental factors, cannot be uniformly observed.

3.2. Focus: stomatal conductance

3.2.1. Differences among the plant species

The stomatal conductance was substantially different among the four measured species (see Fig. 4). Stomatal conductance measurements for *F. ovina* revealed a consistent range of values throughout the observation period. The conductance for *F. ovina* ranged from 81.4 to 636.9 with an average of 344.5 mmol m^{-2} s^{-1} (SD = 112.6). Stomatal conductance of *O. vulgare* exhibited a fluctuating pattern, with values ranging from 130.9 to 891.3 mmol m^{-2} s^{-1} with an average of 491.3 mmol m^{-2} s^{-1} (SD = 173.7). Stomatal conductance measurements for *S. kamtschaticum* were relatively stable with a range of 23.9 to 344.8 mmol m^{-2} s^{-1} with an average of 143.0 mmol m^{-2} s^{-1} (SD = 77.0). The stomatal conductance

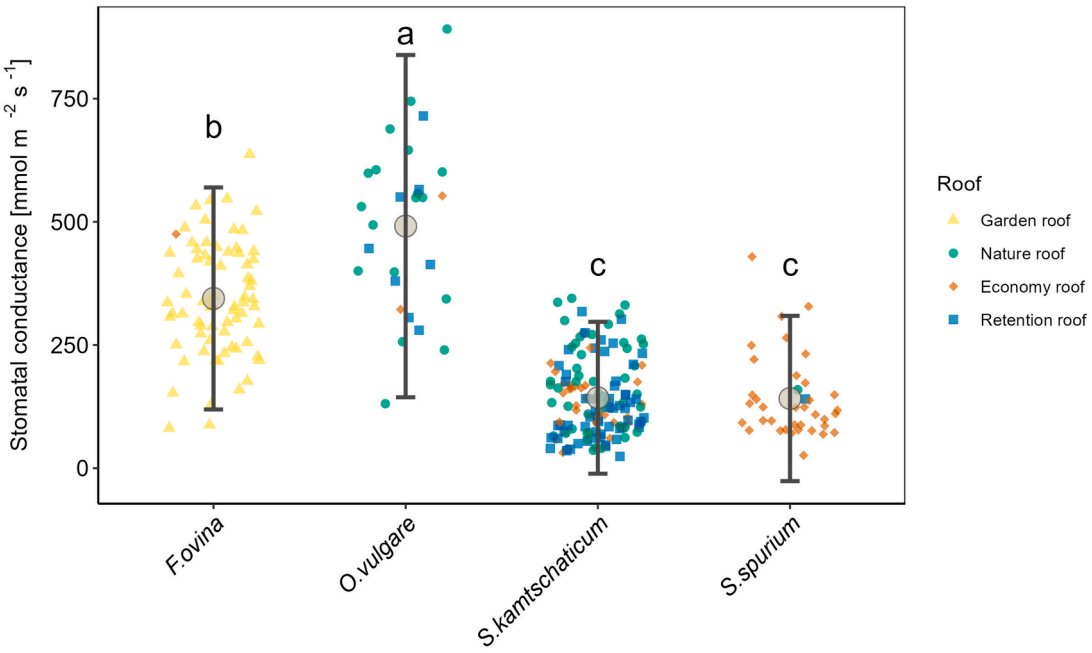


Fig. 4. Mean stomatal conductance (±SD) by species. Means with no letters in common are significantly different with $p < 0.05$.

in *S. spurium* was more varied, with values spanning from 26.1 to 429.2 mmol m^{-2} s^{-1} with an average of 141.5 mmol m^{-2} s^{-1} (SD = 83.9). The Tukey HSD post hoc test revealed that *O. vulgare* had significantly higher stomatal conductance values than *F. ovina*, while for both *Sedum* species the values were significantly lower than those of *O. vulgare* and *F. ovina*.

3.2.2. *Driving factors of stomatal conductance*

The model incorporating the stomatal conductance data of all plant species was statistically significant with heat flux being the only significant predictor variable. The heat flux exhibited a positive impact on stomatal conductance, with a 1 kW m^{-2} increase in heat flux leading to a small (2.4 %) but still, statistically significant ($p < 0.001$) increase in stomatal conductance (see Fig. 5).

The linear models developed for *S. kamtschaticum, S. spurium* and *O. vulgare* did not show any statistically significant impacts of the considered environmental factors. For *F. ovina*, substrate moisture, vapor pressure deficit and shortwave solar irradiance had a significant impact on stomatal conductance. A 1 % elevation in substrate moisture content corresponded to a 5.08 % augmentation in stomatal conductance ($p = 0.03$). The impact of shortwave solar irradiance was smaller, with an increase in the stomatal conductance of 0.05 % for every additional 1 kW m^{-2} ($p = 0.03$). Regarding the vapor pressure deficit, a 1 kPa increase caused a 27.34 % reduction in the stomatal conductance ($p = 0.03$).

The correlation between measured stomatal conductance and calculated stomatal conductance in *F. ovina* was significant ($\beta = -0.12$, SE = 0.04, $p < 0.01$), while for the remaining two species, the correlation was not significant. Nonetheless, the collective analysis across all species demonstrated a notable positive correlation ($\beta = 0.39$, SE = 0.07, $p < 0.001$), as depicted in Fig. 6. These findings highlight the varied

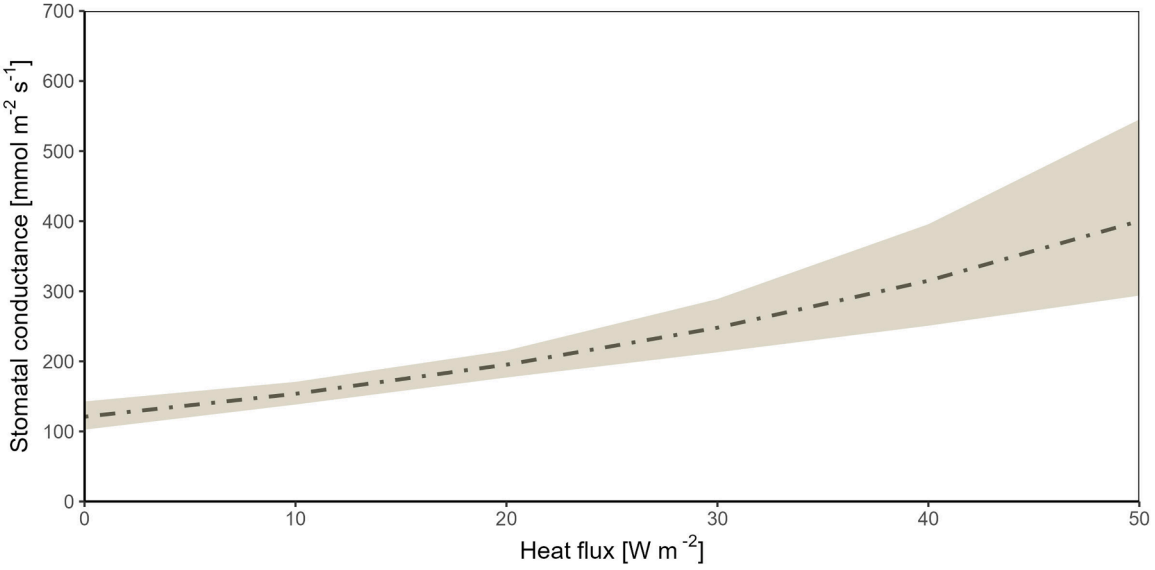


Fig. 5. Correlation between stomatal conductance and heat flux based on a fitted regression model. The shaded area represents the 95% confidence interval. The model across all plant species is statistically significant with F(5, 178) = 12.57, $p < 0.001$, R-square = 0.24.

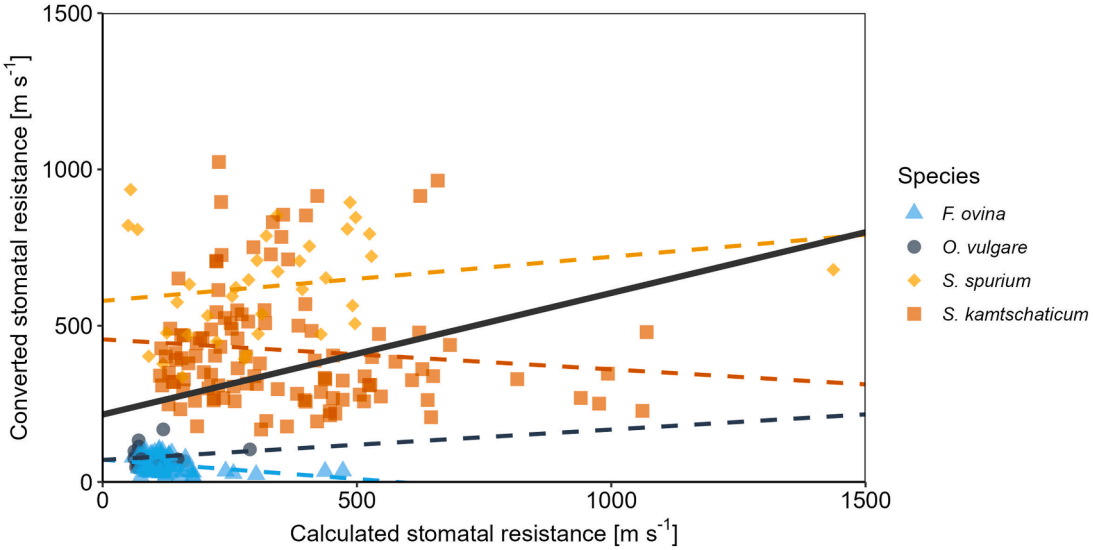


Fig. 6. Correlation between the measured (and then converted) stomatal resistance with the calculated stomatal resistance based on the calculations in Tabares-Velasco and Srebric [59] for the respective species (dashed regression lines) and across all species (solid regression line). R^2 values are *F. ovina*: 0.10, *O. vulgare*: -0.04, *S. spurium*: 0.01, *S. kamtschaticum*: 0.01, all species: 0.11.

stomatal responses among different plant species, with a positive correlation apparent when considering the combined dataset.

3.2.3. Discussion of the findings

The stomatal conductance measurements are in line with those from other authors: Baraldi et al. [4] measured 190 mmol m^{-2} s^{-1} for *Sedum spectabile* with a LI-COR 6400 photosynthesis measurement system. Tan et al. [61] measured the stomatal conductance of *Cyathula prostrata* of 50–700 mmol m^{-2} s^{-1} , using a Decagon SC-1 leaf porometer which is consistent with the present measurements for *O. vulgare*. Further, the converted stomatal resistance values of *S. spurium* are in line with the findings of *S. spurium* from Arriola-Cepeda, Vera, and Albornoz [1] who measured between 266 s m^{-1} and 973 s m^{-1} for this species, also with a Decagon SC-1 leaf porometer.

However, these values are substantially higher than 50–300 s m^{-1}, calculated by Sailor [49] as typical for green roofs, as well as 500–700 s m^{-1}, measured by Tabares-Velasco and Srebric [58] for succulents *Delosperma nubigenum* and *S. spurium.* This shows that stomatal resistance values based on theoretical models deviate from those measured directly. Consequently, there is a need for further research aiming to find the reason for these discrepancies.

The correlations found for *F. ovina* are in line with the findings of a variety of literature sources: Multiple stomatal conductance models confirm its enhancement by rising vapor pressure deficit [3,21,32,37,38,47,59] this interdependence was also measured by Kitano, Eguchi, and Matsui [28]

The positive correlation between substrate moisture and stomatal conductance is also often assumed in the above mentioned stomatal conductance models and was also measured by Tabares Velasco [57]. Regarding the effect on heat flux in the model across all species, no comparable studies were found. Yet, the positive link between stomatal conductance and vapor pressure deficit revealed by Tabares-Velasco and Srebric [59] supports the observed correlation of heat flux and stomatal conductance on green roofs. Vapor pressure deficit, a general indicator calculated based on air temperature as a proxy for heat flux, helps explain this relationship. As the above mentioned literature mainly focused on model set-up and validation, the exact correlation between the stomatal conductance and its driving factors were not assessed.

Despite the fact that the measurements of the stomatal resistance are similar to those of Tabares-Velasco and Srebric [59], the use of his suggested formula did not match our measurements. This shows that a suitable model for multiple green roof and plant types has yet to be found, since the model from Tabares-Velasco and Srebric [59] was only validated with a so called „cold-plate“ apparatus with only one plant type (*Delosperma nubigenum*) under laboratory conditions. The mismatch of the minimum stomatal resistance of this plant type measured by Tabares-Velasco and Srebric [58] with the values for *Sedum* species in the present study indicates that the use of only one plant type for the model creation may be the main reason for the model not being suitable for other plants and green roof types.

The differences in stomatal conductance among the plant species indicate the complexity of the physiological processes and though the measurements are mostly in line with other sources of relevant literature, it was not possible to apply the theoretical concept with the use of formulas.

3.3. Evapotranspiration

3.3.1. Differences among the green roofs

The seasonal evapotranspiration means for all roofs decreased from summer to winter in the order summer > spring > fall > winter. In summer, both the Garden and the Retention roof with 3.63 ± 0.20 and 3.60 ± 0.13 mm day^{-1} had distinctly higher evapotranspiration rates than the Nature and Economy roof with 2.56 ± 0.13 and 2.16 ± 0.13 mm day^{-1}. In spring, the Retention and Garden roof showed very similar seasonal means (1.83 ± 0.13 and 1.81 ± 0.13 mm day^{-1}), while the Economy roof had similar evapotranspiration rates to the Nature roof (1.46 ± 0.10 and 1.44 ± 0.14 mm day^{-1}). In fall, the seasonal means ranged between 0.64 and 0.93 mm day^{-1}, while in winter, the evapotranspiration rates were even lower, between 0.26 and 0.58 mm day^{-1}.

When looking at monthly averages, the highest evapotranspiration rate was recorded in July 2021 for the Garden roof (5.50 mm day^{-1}), the Nature roof (3.87 mm day^{-1}) and the Economy roof (3.78 mm day^{-1}). The Retention roof reached the highest average evapotranspiration in June 2021 with 5.28 mm day^{-1}. Looking at single days, the highest daily evapotranspiration values were recorded for the Retention roof with 6.79 mm day^{-1} on June 17th 2021 as well as the Garden roof with 6.75 mm day^{-1} on June 14, 2021. The Nature roof reached its maximum of 5.74 mm day^{-1} on June 13, 2021 and the Economy roof showed the peak of 4.85 mm day^{-1} on July 2, 2021.

The overall daily mean evapotranspiration within the 24-month study period was highest on the Garden roof (2.12 ± 0.10 mm day^{-1}),

followed by the Retention roof (1.72 ± 0.07 mm day^{-1}), Nature roof (1.31 ± 0.06 mm day^{-1}) and Economy roof (1.27 ± 0.05 mm day^{-1}).

3.3.2. Evapotranspiration in drought periods

Evapotranspiration rates during droughts, especially with high air temperatures, revealed interesting patterns. Fig. 7 illustrates how the Nature and Economy roof undergo a gradual reduction in evapotranspiration during a 10-day drought with high air temperatures. In contrast, the Garden and Retention roof experienced first a rise in evapotranspiration rate. After 5 days when the air temperature reached its maximum, the Garden roof dropped from 4.72 to only 1.68 mm day^{-1}. Contrarily, the Retention roof aligned its evapotranspiration pattern with air temperature. When the air temperature reached a daily average of 23.9°C, the evapotranspiration rate for this green roof type increased from 3.82 to 5.07 mm day^{-1}.

3.3.3. Driving factors of the evapotranspiration

The linear regression model identifies vapor pressure deficit as the most significant factor influencing evapotranspiration, although the effect differed between the roofs (see Fig. 8). For the Retention roof, a 1 kPa increase in the vapor pressure deficit resulted in a 0.07 mm day^{-1} increase in evapotranspiration. In contrast to that, the Nature and Economy roof both showed a significant negative relationship with the vapor pressure deficit, a reduction in evapotranspiration of 0.08 and 0.16 mm day^{-1} due to an increase in vapor pressure deficit of 1 kPa. Apart from that, the shortwave solar irradiance was significant across all four roofs: A 1 kW m^{-2} increase in mean shortwave solar irradiance received within an hour corresponded to a significant increase in evapotranspiration ranging from 0.04 to 0.07 mm day^{-1} (Retention and Economy roof). Substrate moisture and leaf temperature had positive effects on the evapotranspiration rate for all roofs: The increase in substrate moisture by 1 % led to an increase in evapotranspiration between 0.05 and 0.25 mm day^{-1} (Nature and Economy roof).

3.3.4. Discussion of the findings

Evapotranspiration values from other authors measured under a similar climate with similar non-irrigated green roof build-ups are scarce. Takebayashi and Moriyama [60] found a maximum evapotranspiration of 6.9 mm day^{-1} in Japan for a lawn green roof with a substrate thickness of 21 cm, similar to the Garden roof. The measurement was conducted in a 0.95 × 1.6 m roof sample by examining the water content ratio. Their maximum value is in line with the present measurement of 6.75 mm day^{-1}. A study conducted in northern Germany with a very similar experimental setup found that irrigation in summer can enhance the daily evapotranspiration rate to around 5 mm d^{-1} for extensive green roofs with 9 to 21 cm substrate [25]. Both the Retention roof and the Garden roof (with 10 and 15 cm substrate) reached evapotranspiration values of 6.79 and 6.75 mm d^{-1}, respectively, and thus can be considered comparable to an irrigated green roof system.

A decrease in evapotranspiration rate caused by a decline in substrate moisture was also observed by Djedjig et al. [8], who recorded the minimum evapotranspiration at 10 % substrate moisture. Voyde et al. [63] mentioned a rapid water loss through evaporation after watering, but this water loss gradually decreased as available water was reduced until the plants stopped transpiration.

Regarding the design of green roofs in water-scarce urban environments, a high water storage is beneficial, as the substrate moisture and thus the evapotranspiration rate will stay high as long as water is available.

The findings, that vapor pressure deficit together with shortwave solar irradiance and substrate moisture are the most important factors for evaporation, are generally in line with other studies: The most important factors for evapotranspiration were found to be substrate moisture [23] and solar irradiance [6,24,32,32,41,56,59] Vapor pressure deficit was indirectly mentioned by Jim and Tsang [24] as they came to the conclusion that apart from solar irradiance low relative humidity also had an important impact.

All in all, the evapotranspiration rates differ substantially among the roof types and particularly the observations during a summer drought made it clear, that a high water storage capacity allows the green roof to maintain high evapotranspiration rates, supporting our expectation related to the first study objective. The results of driving factors further support that substrate moisture is not a decisive factor in evapotranspiration rates of the Retention roof, as the roof generally has a high substrate moisture. Though the shallowest roof often exhibited the highest regression coefficient, this trend is not consistent throughout all environmental factors. Thus, in the case of evapotranspiration, the assumption about thicker green roof systems being more stable, cannot be confirmed.

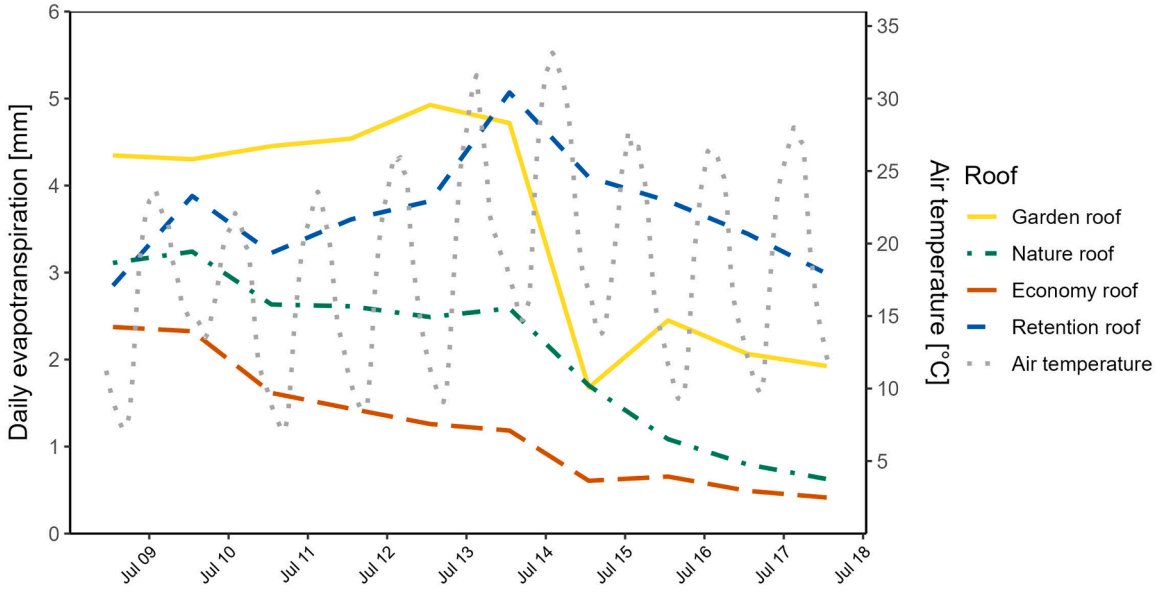


Fig. 7. Mean daily evapotranspiration of four different green roof systems during a summer drought.

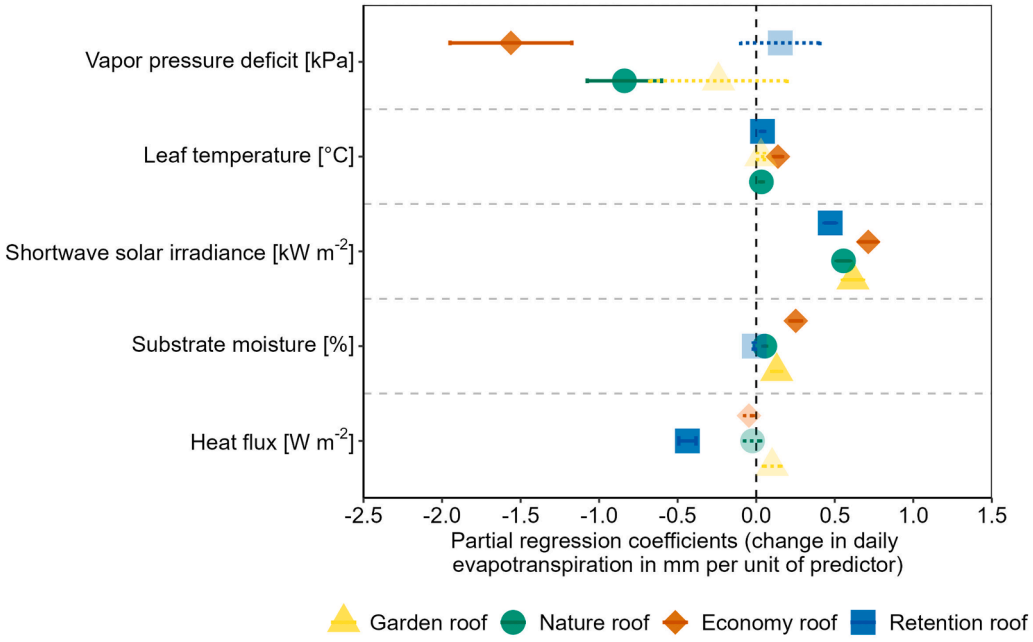


Fig. 8. Partial regression coefficients (± SE) for evapotranspiration for different green roof types, analyzed on a daily basis. Fully colored circles indicate statistically significant effects ($p < 0.05$), while semi-transparent circles represent non-significant effects.

3.4. Focus: Interception

3.4.1. Differences among the plant species

Significant differences in interception capacity were observed among the various plant species, as illustrated in Fig. 9. *S. chamaecyparissus* (a small shrub) showed the highest interception value, exceeding 1.5 l m^{-2}, while *O. vulgare* (herbaceous) displayed the lowest interception capacity, approximately at 0.3 l m^{-2}. The model results show the PAI strongly influences the interception capacity and that plants with a high PAI tend to have a greater interception capacity ($\beta = 0.356$, SE = 0.05, $p < 0.001$, $R^2 = 0.91$).

Based on our data, the empiric formula 11 ($R^2 = 0.76$) describes the relationship between the PAI and the interception capacity (S) for a PAI > 1.

$$S = -0.33 + 0.44 \times PAI \quad (11)$$

3.4.2. Discussion of the findings

Only few studies assessed the interception capacity of plants: Kemp, Hadley, and Blanuša [26] measured values of *S. spurium* of 0.3 and 0.6 l m^{-2} with a LAI between 1 and 2. Smets et al. [55] measured 4.22 ± 1.83 l m^{-2} for L. *angustifolia*. The measurement of *S. kamtschaticum* of 0.372 l m^{-2} and a PAI of 1.23 is in line with the above mentioned studies, while the results for L. *angustifolia* are substantially lower. This difference is most likely due to variations in how the calculations were conducted. In the study by Smets et al. [55], the interception capacity was based on the canopy projection area, which thus leads to the assumption of a plant cover of 100 %, while in the present study the plant cover was sometimes smaller. The measurements for green roof vegetation of over 1.5 l

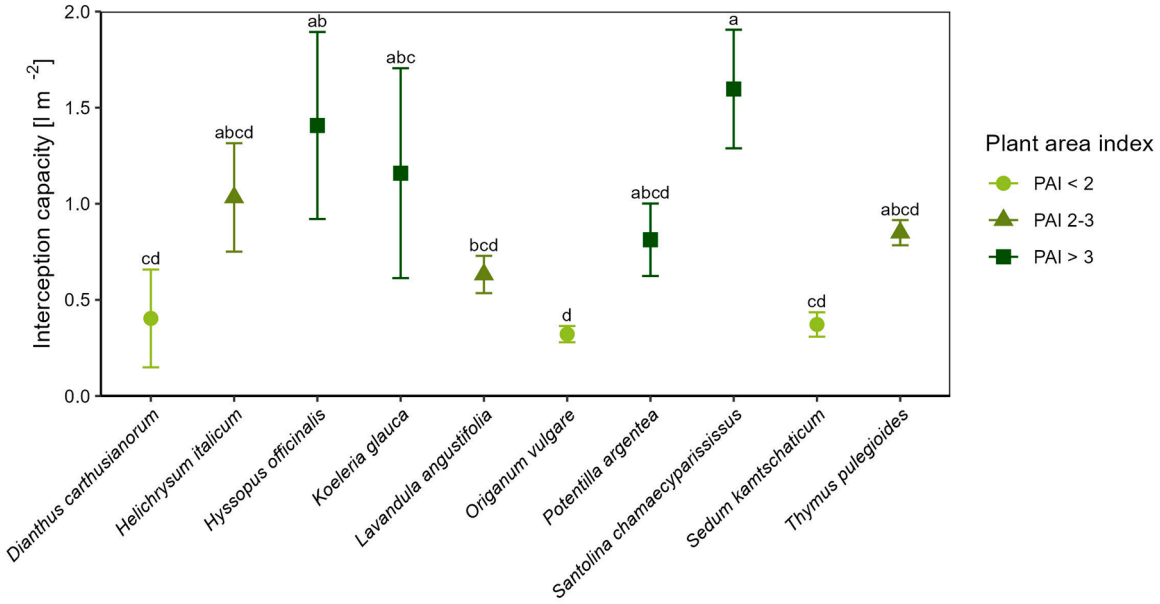


Fig. 9. Mean Interception capacity (±SD) by species. Means with no letters in common are significantly different with $p < 0.05$.

m^{-2} are more realistic, considering a green roof's vegetation does not always have a cover of 100 %.

Overall, the results show that the vegetation layer plays a relevant role in retaining smaller rain events and evaporation. Especially for modelling the energy and water balance of green roofs correctly, further research should be conducted to gain a better understanding of the interception capacities of different vegetations. Yet, for practical applications our findings indicate that choosing plant species with a high plant area index can help to increase direct rainwater evaporation from leaves and thereby to restore the natural water cycle on green roofs. Based on the PAI, the determined formula can be used for an estimation of the interception capacity of green roofs with a vegetation consisting of *Sedum* species or small shrubs. However, the results should be used with care, as the dataset is small and only includes 10 different plant species.

3.5. Heat flux

3.5.1. Differences among the green roofs

Throughout the monitoring period of two years, all green roof types exhibited distinct seasonal heat flux variations. The Retention roof was the only roof type that had solely negative seasonal heat flux means. They ranged between -0.46 and – 1.41 W m^{-2} with the lowest mean recorded in summer. The Nature and Economy roof showed positive means in spring (0.39 and 0.67 W m^{-2}), but only negative means in the other two seasons. Particularly in fall, the Economy roof had the lowest overall mean with -2.03 W m^{-2}, while in summer both Nature and Economy roof had shallower means of -0.18 and -0.38 W m^{-2}. In contrast, the Garden roof was the only roof type with positive mean heat fluxes in both spring and summer. Among all roof types, it also showed the highest overall means in these two seasons (1.64 and 1.99 W m^{-2} in spring and summer respectively). The standard errors of the reported means are all smaller than 0.06 W m^{-2}.

The daily patterns across the seasons also revealed notable differences among the roof types, especially concerning the daily peaks (see Fig. 10). During the spring season, peak values were recorded around the early afternoon between 12:00 and 15:00 and the Garden and Retention roof reached their maximum heat flux in this season. The Pearson's correlation coefficient between heat flux on various roofs and air temperature ranged from $r = 0.37$ to $r = 0.63$, indicating a strong positive linear relationship ($p < 0.001$).

In summer, the Garden and Economy roof exhibited the highest heat flux during the day, while the peak of the Economy roof shifted to the morning hours (10:00 to 11:00). The diurnal amplitude of heat flux was widest on July 3, 2022 for that roof system (−23.37 to 59.36 W m^{-2}). This suggests that the Economy and Garden roof absorb significant heat during the day and release it gradually through the night. The Pearson's

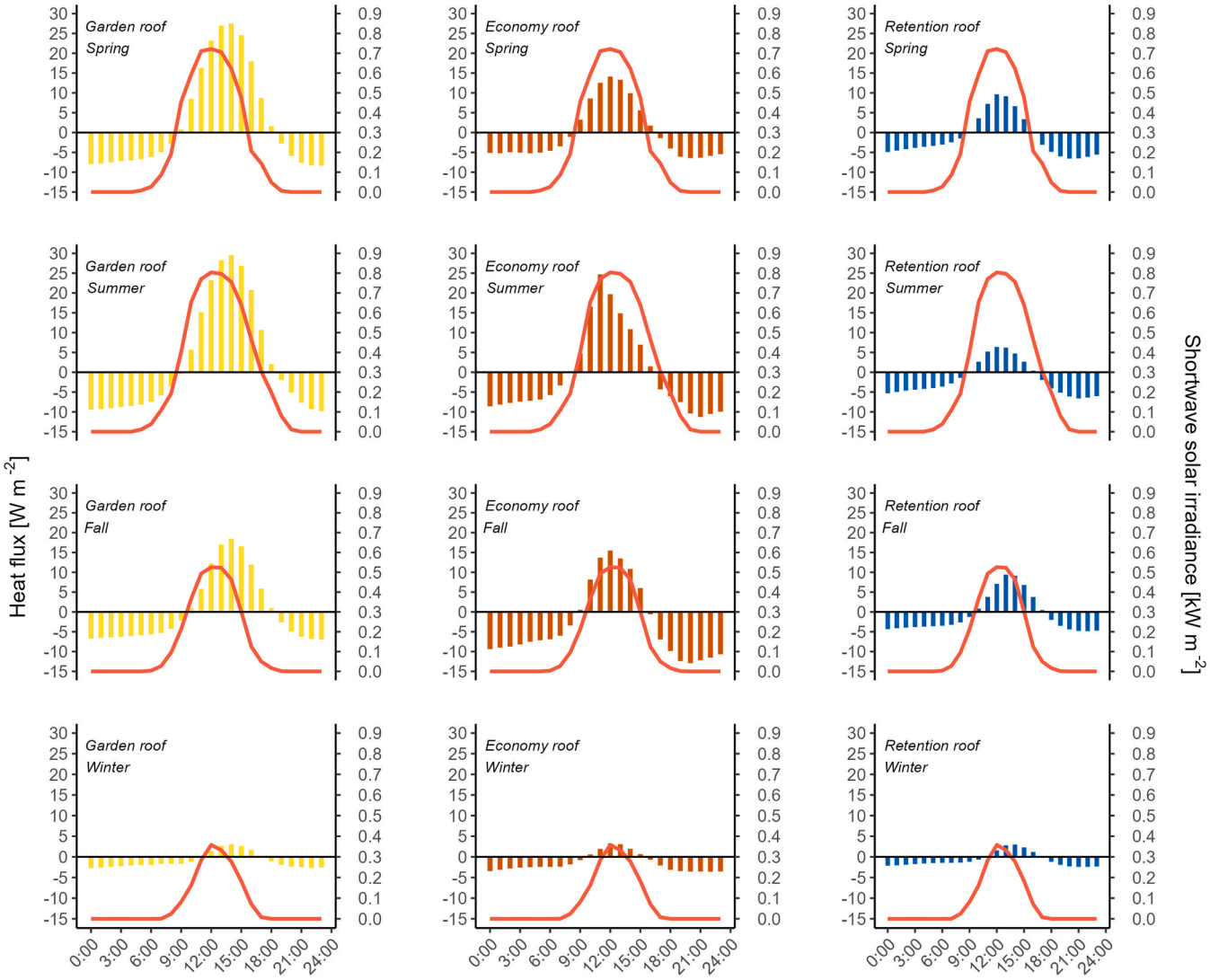


Fig. 10. Mean heat flux (blue bars) and incoming shortwave solar irradiance (red line) on sunny days (with shortwave solar irradiance > mean shortwave solar irradiance in the respective season) for different green roof types.

correlation coefficient between heat flux on various roofs and air temperature in summer months ranged from $r = 0.36$ to $r = 0.72$ ($p < 0.001$).

The Pearson's correlation coefficient between heat flux and air temperature in fall months ranged from $r = 0.41$ to $r = 0.58$ ($p < 0.001$). On September 4, 2022, the Economy roof exhibited a diurnal amplitude ranging from -17.62 to 31.51 W m^{-2}, indicating a reduction in heat absorption and dissipation during the season.

During the winter season the green roofs experienced the lowest heat flux values, in line with the reduced shortwave solar irradiance and colder temperatures. The Garden roof exhibited the widest range of diurnal amplitude on February 26, 2022, from −6.18 to 2.34 W m^{-2}, indicating minimal heat exchange during the colder months. The Pearson's correlation coefficient between heat flux on various roofs and air temperature in winter months was relatively low, ranging from $r = 0.11$ to $r = 0.29$ ($p < 0.001$).

3.5.2. Driving factors of the heat flux

Distinct significant negative heat flux dynamics emerged on the Economy roof in the context of PAI influence (see Fig. 11). Heat absorption negatively correlated with plant development and spatial expansion, as increased biomass coverage led to heightened heat dissipation (Economy roof: $\beta = -1.87$, SE = 0.85, $p < 0.05$). The correlation of heat flux with substrate temperature was statistically significant for both the Garden and Retention roof, showing negative correlations. Incoming longwave radiation had a significant positive influence on heat flux, even though the estimates were all smaller than 0.15 W m^{-2}. Regarding the effect of substrate moisture on heat flux, no significant correlation was found.

3.5.3. Discussion of the findings

Getter [14] examined the heat flux of a green roof setup, similar to the Economy roof with a drainage layer, a fleece, a minimum of 5 cm of substrate and mostly sedum vegetation, situated on an inverted (insulation) roof in Michigan, USA, during the different seasons. Under spring day conditions, they recorded a heat flux range of -6 to 2 W m^{-2} (Economy roof in the current study: −9 to 12 W m^{-2}). In summer the range in Getter [14] was from -4 to 6 W m^{-2} with a peak at 3 pm (Economy roof in the current study: −11 to 23 W m^{-2}).

Tabares-Velasco and Srebric [59] measured a range from -10 to 8 W m^{-2} for a green roof similar to an Economy roof on an insulated steel deck in Chicago, Illinois.

In comparison with the measurements of the above-mentioned authors, the amplitude of the present measured values is considerably higher. The heat flux in a lysimeter consisting of a relatively small metal case might not comparable to the setup of a standard roof and therefore the collected data may not serve for calculating the energy balance of buildings. However, it can be a useful parameter for the validation of an evapotranspiration model for different green roof setups.

Regarding the influence of the PAI on the heat flux, Getter [14] and Morau, Libelle, and Garde [36] found that the magnitude of the heat flux decreases when the LAI increases, which is in line with the present results. Getter [14] attributed this to the shading effect of the leaves.

The findings in Saadatian et al. [48] indicate that for the effect of substrate moisture on heat flux, dry substrate is generally a better insulator, because wet substrate increases the conductivity of the substrate. However, in summer conditions wet substrate can perform better in terms of cooling the building because due to evapotranspiration it acts as a passive cooler. Therefore, the correlation between heat flux and substrate moisture depends substantially on the present environmental conditions. While the cooling potential of a green roof with a wet substrate is high on a hot day, the correlation is weaker on a cold day, as the conductivity of the moist substrate leads to a higher heat flux magnitude. The findings by Getter [14] support this assumption. They observed an increase in heat flux as substrate moisture rises, although this pattern was not recorded consistently. Jim and He [22] found that only larger changes in substrate moisture led to a positive correlation with heat flux.

In general, the findings support the assumption that the heat flux reduced in thicker roof systems. However, the results also show that substrate thickness is not the only decisive factor, but is complemented by both the substrate temperature as well as the vegetation cover. Yet, due to the small size of the experimental roofs, the recorded heat flux values may not be representative, as demonstrated by comparisons with literature sources. Also, the influence of the environmental factors on the shallower roofs did not display higher regression coefficients.

3.6. Substrate temperature

3.6.1. Differences among the green roofs

The highest substrate temperature in the early afternoon (29.62 ± 5.73 °C) occurred in June on the Economy roof (see Fig. 12). At the same time, the Retention roof exhibited 8.5 °C less - only 21.15 (± 2.78) °C. In August, the difference between the daily warmest and coolest substrate

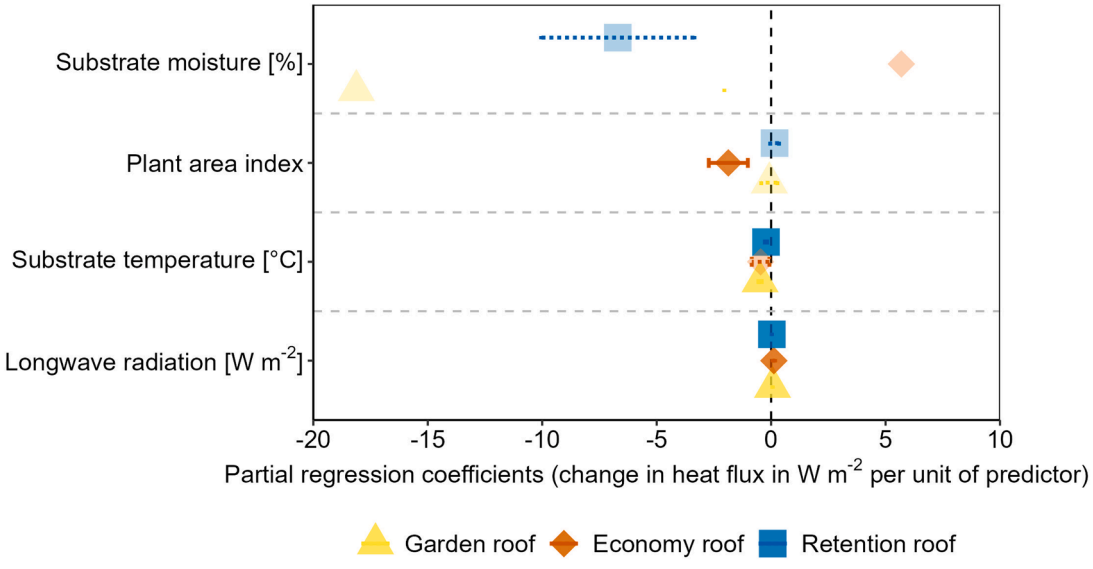


Fig. 11. Partial regression coefficients (±SE) for heat flux for different green roof types, analyzed on an hourly basis. Fully colored circles indicate statistically significant effects ($p < 0.05$), while semi-transparent circles represent non-significant effects.

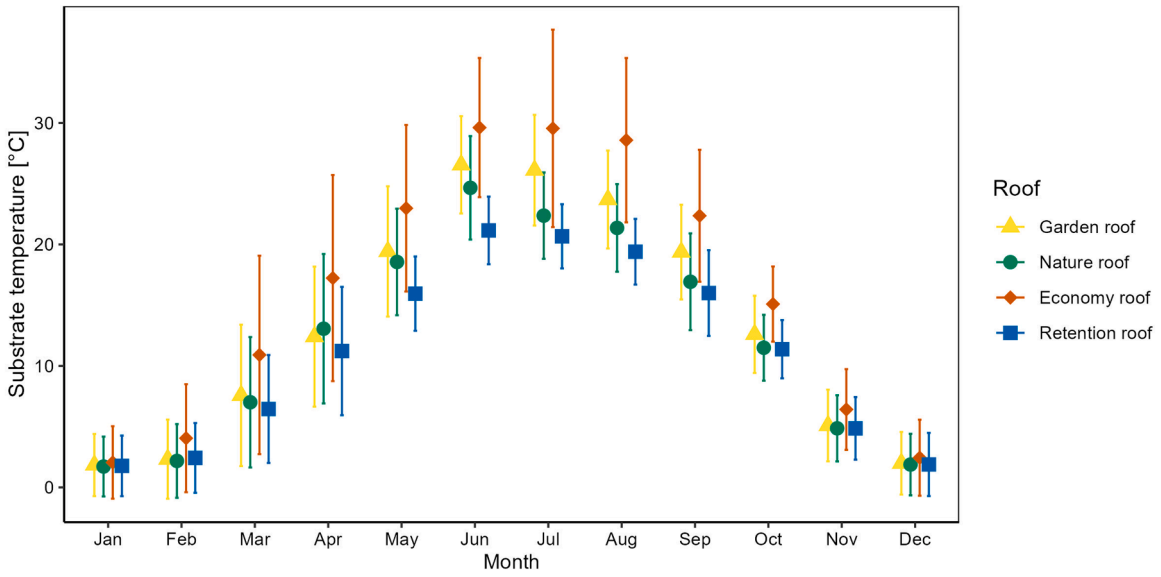


Fig. 12. Mean substrate temperatures (±SD) at 14:00 for different green roof types. Each mean represents the average of all 14:00 temperature readings collected throughout the corresponding month.

temperature was at its maximum with just over 9 °C difference between the Economy and Retention roof. While the differences during the summer months from May to September amounted to an average of 8 °C, in winter the substrate temperature was very similar among the roofs, with differences between the coolest and warmest mean temperature ranging from 0.3 to 1.9 °C.

3.6.2. *Driving factors of substrate temperature in dry and wet substrate conditions*

Regardless of substrate moisture conditions and the specific site under investigation, a clear negative correlation between substrate temperature and moisture was observed (see Fig. 13). This correlation was particularly high under dry conditions (< 10% substrate moisture), with all roof types except for the Retention roof exhibiting a more robust response to elevated moisture levels.

Under moist conditions, the negative correlation persisted but

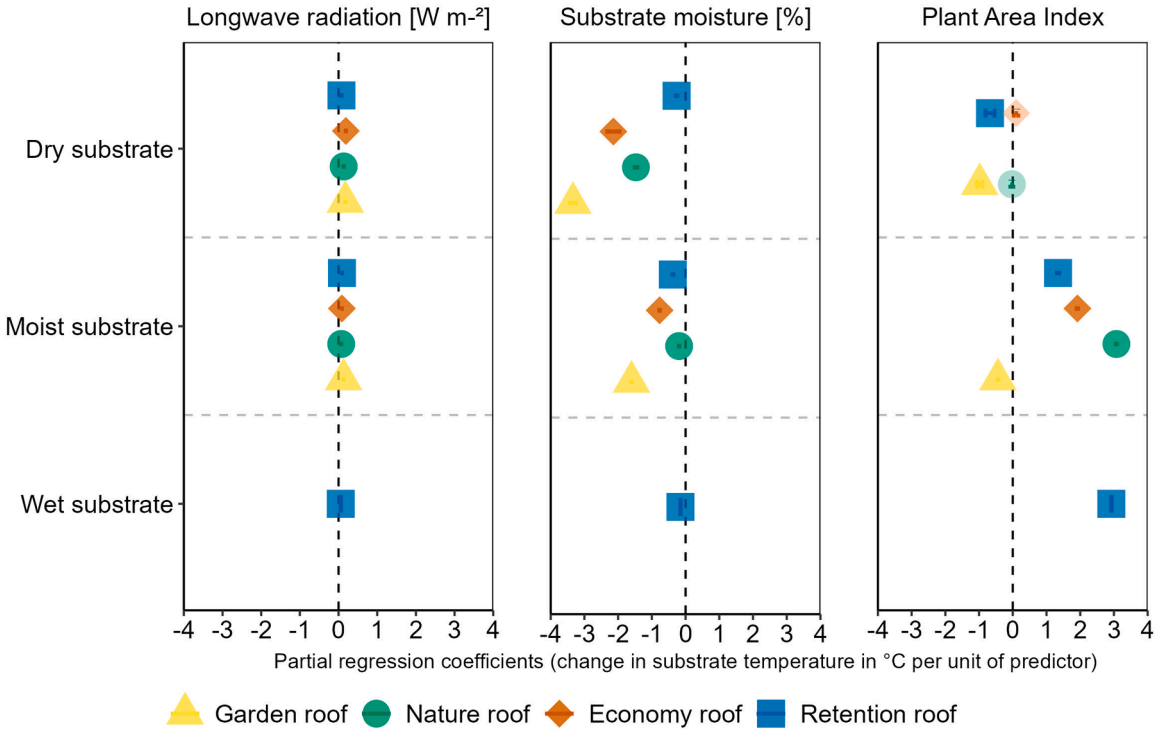


Fig. 13. Partial regression coefficients (±SE) for substrate temperature for different green roof types, based on 5-minute interval data. Fully colored circles indicate statistically significant effects ($p < 0.05$), while semi-transparent circles represent non-significant effects. Substrate moisture levels are categorized as follows: ≤ 10 % for dry substrate; ≥ 15 % for moist substrate on the Garden, Nature, and Economy roof; 15 %-25 % for moist substrate in the Retention roof, ≥ 25% for wet substrate on the Retention roof.

appeared weaker, with the exception of the Retention roof. In contrast, the Retention roof exhibited a cooling trend as moisture levels exceeded 25%, where each additional percentage point of water content was associated with a 0.15 °C decrease ($\beta = -0.15$, SE = 0.002, $p < 0.001$).

Incoming longwave radiation consistently resulted in substrate warming in all cases. In contrast to the other factors, the correlation between substrate temperature and PAI varied: Under dry conditions, the Garden and Retention roof exhibited a negative association. In moist and wet conditions, substrate temperature on all roofs, except for the Garden roof, tended to be warmer when densely covered with vegetation.

3.6.3. Discussion of the findings

The results match other studies that showed how green roofs with thinner substrate layers produce larger temperature amplitudes [11,40,45]. Jim and Peng [23] found that green roofs with a moister substrate also have cooler substrate temperatures. This is in line with our results, even though the data shows that the negative correlation between substrate temperature and substrate moisture is stronger for dry substrate.

To summarize, from spring to fall, the substrate temperature was always the lowest for the green roof system with higher water storage capacity and always the highest for the shallowest roof system, supporting the assumptions in the introduction. Important influencing factors include the plant area index and the substrate moisture, though their effect size differed depending on the substrate's moisture condition. However, no clear tendency was observed regarding the effect of environmental variables on shallow versus thicker roof systems. In general, substrate temperature plays an important role in the microclimate of a green roof.

3.7. Substrate moisture

3.7.1. Differences among the green roofs

Across the entire measurement period, the Retention roof showed the highest average substrate moisture with 33.05 (±8.23) %. In contrast, the substrate moisture of the Economy and Garden roof was substantially lower with 15.87 (±3.89) % and 15.90 (±2.84) % respectively. The Nature roof exhibited an average substrate moisture of 18.84 (±5.37) %.

For all roof types, the seasonal average substrate moisture was lowest in summer and highest during winter. Spring and fall means were very similar, differing by no more than 2 % for each roof. Looking at the monthly averages, all roofs showed the lowest substrate moisture in September 2021 with 11.27 %, 12.36 %, 12.45 % and 22.13 % for the Garden, Nature, Economy and Retention roof respectively. The highest monthly averages were recorded in February 2022 and March 2023 (18.82 %, 25.46 %, 21.13 % and 44.85 % for the Garden, Nature, Economy and Retention roof). The temporal variation in substrate moisture was largest for the Retention roof, measuring 38.70 (±4.55) % in winter and 25.65 (±3.8) % in summer, with a difference of over 13 %. The Garden roof, on the other hand, exhibited the most stable substrate moisture conditions with a difference of only 2.22 % between the daily averages in summer (14.79 % - lowest) and winter (17.01 % - highest). The differences between the highest and lowest seasonal means were 6.67 % and 5.41 % for the Nature and Economy roof.

3.7.2. Driving factors of substrate moisture

Amongst all variables, shortwave solar irradiance had the strongest impact on substrate moisture, even though the direction of the correlation differs among the green roof systems (see Fig. 14). While for the Garden, Economy and Nature roof substrate moisture was positively correlated to shortwave solar irradiance, for the Retention roof a negative correlation was observed. Likewise, the influence of evapotranspiration was not uniform among the roofs. While the substrate moisture of the Garden and Economy roof was positively correlated to substrate moisture, the Retention roof showed a negative correlation. Precipitation exhibited only significant correlations for the Nature and Retention roof - positive in both cases. Leaf temperature was negatively related to substrate moisture for all roofs. The remaining variables show mixed tendencies.

3.7.3. Discussion of the findings

Literature dealing with the substrate moisture content of green roofs

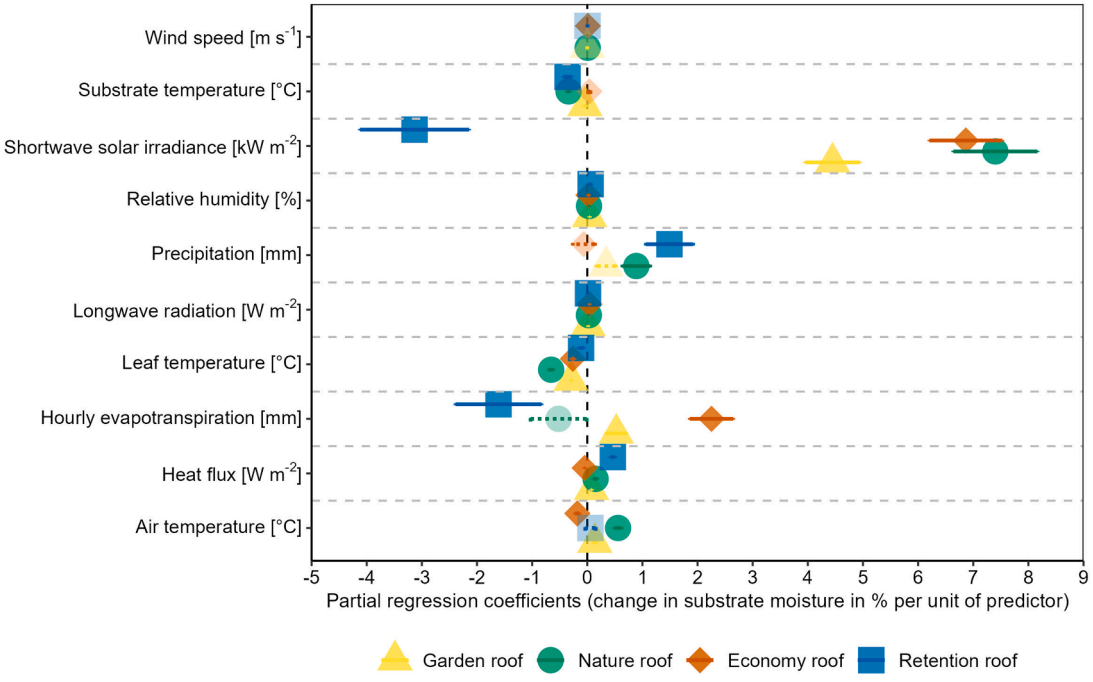


Fig. 14. Partial regression coefficients (±SE) for substrate moisture for different green roof types, analyzed on an hourly basis. Fully colored circles indicate statistically significant effects ($p < 0.05$), while semi-transparent circles represent non-significant effects.

mainly focuses on the thermal behavior of green roofs, but no study explicitly examined the mean substrate moisture of different seasons or roof systems, the substrate moisture in relation to the PAI or the incoming longwave radiation. Tan et al. [61] measured the substrate moisture of a 1 m^2 large and 35 cm thick green roof build-up with and without a retention layer, using a Decagon soil moisture measurement device. While the green roof with retention layer maintained a substrate moisture of around 35 %, the roof without retention layer measured only 22 %. During a hot and dry period of 9 days, the substrate moisture of the green roof with retention layer fell to 22 %, the other green roof to 5 %. On a 8.600 m^2 green roof in Berlin with a substrate thickness of 9 cm and no drainage layer, Heusinger and Weber [19] observed a maximum substrate moisture of 42.3 % throughout a period of 14 month. The mean substrate moisture during dry periods measured 10 %. Considering the above-mentioned range of measured substrate moistures, it can be concluded that the values in this study are plausible.

As the substrate moisture is a key parameter for the vitality of green roof vegetation, stable moisture conditions are important. Even though the roof with the thickest substrate layer showed the most stable moisture conditions, the roof system with the shallowest system did not have the least stable moisture conditions. Also, the regression coefficients were not uniformly higher for the shallower roof systems. Therefore, a more profound analysis is needed before confirming the hypothesis regarding substrate thickness and stability of substrate moisture. The analysis of the driving factors showed that a number of variables influence the substrate moisture, though the intensity of the effects varies among the green roof types. In general, the less a roof type is influenced by meteorological conditions such as air temperature, shortwave solar irradiance, rain or windspeed, the more stable and robust it is considered.

3.8. Relevance for urban sustainable planning

3.8.1. Implications of the findings for urban planners

As cooling the urban environment is one of the aims of urban greening, it is important to know how different types of green roofs perform regarding the cooling effect. The results on the physical properties of the green roof systems create a valuable decision basis. The measurements of stomatal conductance are of practical use when selecting plant species for a high cooling efficiency, though they also require an adequate water supply. Another aim of urban greening is retaining stormwater during extreme weather events. This study shows that interception capacity can serve as an important new factor to consider when selecting plants for green roofs. The data provide a decision basis for the vegetative cover, as some plant species demonstrated over 1.5 l m^{-2} of rainwater interception. Regarding the insulation of buildings, a green roof system with wet substrate is necessary for the evapotranspiration process and therefore supports the heat insulation in buildings, though in winter conditions, a wet substrate has a negative effect on the insulation. Green facades have similar effects (cooling, retaining rainwater on canopies, insulating) as the above mentioned. Regarding the cooling of the surrounding air, green facades can be even more beneficial in urban areas, though they are clearly more expensive than green roofs [33].

3.8.2. Practical design strategies for effective green roofs

Generally, the cooling effect of green roofs is present as long as substrate and plants have enough water available. Plant species with high stomatal conductance and large PAI enhance cooling in summer, but also have an accordingly high water demand. A green roof with a high water storage capacity leading to a high substrate moisture allows for high evapotranspiration rates and efficient cooling, though in case it falls dry, also tends to heat up. The key factor for constructing a highly effective green roof is therefore to find a balance between water availability and water usage of plants and substrate evaporation. This means that, regardless of the climate zone, green roofs should preferably include a large water storage layer similar to the Retention roof in order to enhance the water storage capacity and the cooling effect. Plant selection must be considered separately for each climate zone and building site. Based on the results, a general recommendation to urban planners and policy makers is to promote the installation of green roofs with large water storage capacities. A large water storage capacity can be considered the most efficient way to benefit from the positive effects of green roofs.

3.9. Opportunities and limitations

While this study benefits from a long measurement period and numerous variables, several limitations must be considered. These include the small size of the green roofs that may have caused edge effects, although they were mitigated by a surrounding green roof construction. Yet, the results were comparable to other studies assessing larger green roofs for all variables except for the heat flux measurements which may have been influenced by the metallic construction. However, for all other variables, there is no indication that the small green roof size compromised the measurements. Most data gaps fell within the moderate seasons, but the missing precipitation data during the first summer was problematic. We recovered data from the nearest weather station, but potential impacts of missing data cannot be entirely excluded. Outliers were carefully removed to maintain a reliable dataset without excluding valid extreme points. However, models should be interpreted carefully, as not all model diagnostics were ideal. Although normal distribution was mostly achieved, linear relationships and homogeneous residual variance were not always present. Thus, significant results with small effect sizes should be viewed cautiously, and the focus should remain on general trends. Partial collinearity among temperature variables (e.g., solar irradiance, air temperature) posed challenges, but we included only one variable per model when possible.

Despite these limitations, the study produced highly interesting and relevant results that contribute to the research of green roofs and green infrastructure. For studies with a similar setup, we recommend the inclusion of a control roof and the more profound analysis of direct and indirect influences on variables that include also potential time lags. Assessing the same roof types in different climate zones would further provide helpful insights, as it is possible that the green roofs behave differently in other climatic conditions such as tropical or more arid climates.

4. Conclusion

This study revealed that physical behavior and therefore also the environmental effects can vary significantly between the different green roof types. The driving factors for physical properties also differ in direction and strength between the roofs, revealing a high complexity within these urban green infrastructure elements. In terms of modeling the physical behavior of green roofs, the study shows the effects as well as the direction and strength of driving factors in relation to different setups. Due to the large number of recorded variables, the analyzed dataset gives a more holistic view than most other studies. Overall, this study provides valuable insights for green roof modeling approaches and sustainable urban planning. For future research, the modelling of stomatal conductance and interception capacity of green roof plants as well as the and the determination of the matching native or non-native plant species for vital and biodiverse green roofs would be of high practical use. Lastly, the assessment of the long-term performance of green roofs under different climate change scenarios would support evidence-based strategies for a climate-resilient urban development.

Funding

The data was collected as part of a research Project funded to 60 % by the Federal Ministry of Education and Research BMBF (Grant Number:

01LR1725Q). The remaining 40% was funded by Optigrün international AG.

CRediT authorship contribution statement

Dominik Gößner: Writing – review & editing, Project administration, Funding acquisition, Conceptualization, Investigation, Methodology, Validation, Supervision, Resources, Writing – original draft. **Maria Kunle:** Writing – review & editing, Project administration, Data curation, Formal analysis, Investigation, Methodology, Visualization, Software. **Milena Mohri:** Writing – review & editing, Project administration, Formal analysis, Investigation, Methodology, Visualization, Software, Writing – original draft.

Declaration of competing interest

The authors declare that they have no known competing financial interests or personal relationships that could have appeared to influence the work reported in this paper.

Supplementary materials

Supplementary material associated with this article can be found, in the online version, at doi:10.1016/j.buildenv.2024.112356.

Data availability

Data will be made available on request.

References

[1] Rocío Arriola-Cepeda, Sergio Vera, Francisco Albornoz, Experimental study on the stomatal resistance of green roof vegetation of semiarid climates for building energy simulations. Healthy, Intelligent and Resilient Buildings and Urban Environments, International Association of Building Physics (IABP), 2018, pp. 535–540, https://doi.org/10.14305/ibpc.2018.gb-2.01.
[2] Mehtab Muhammad Aslam, Joseph K. Karanja, Ian C. Dodd, Muhammad Waseem, Xu Weifeng, Rhizosheath: an adaptive root trait to improve plant tolerance to phosphorus and water deficits? Plant Cell Environ. 45 (10) (2022) 2861–2874, https://doi.org/10.1111/pce.14395.
[3] Roni Avissar, R.A Pielke, The impact of plant Stomatal control on Mesoscale atmospheric circulations, Agric. For. Meteorol. 54 (2–4) (1991) 353–372, https://doi.org/10.1016/0168-1923(91)90013-G.
[4] Rita Baraldi, Luisa Neri, Federica Costa, Osvaldo Facini, Francesca Rapparini, Giulia Carriero, Ecophysiological and Micromorphological characterization of green roof vegetation for urban mitigation, Urban. For. Urban. Green. 37 (January) (2019) 24–32, https://doi.org/10.1016/j.ufug.2018.03.002.
[5] Umberto. Berardi, The outdoor microclimate benefits and energy saving resulting from green roofs retrofits, Energy Build. 121 (June) (2016) 217–229, https://doi.org/10.1016/j.enbuild.2016.03.021.
[6] Stefano Cascone, Julià Coma, Antonio Gagliano, Gabriel Pérez, The evapotranspiration process in green roofs: a review, Build. Environ. 147 (January) (2019) 337–355, https://doi.org/10.1016/j.buildenv.2018.10.024.
[7] Dirk Cirkel, Bernard Voortman, Thijs van Veen, Ruud Bartholomeus, Evaporation from (Blue-)Green roofs: assessing the benefits of a storage and capillary irrigation system based on measurements and modeling, Water. (Basel) 10 (9) (2018) 1253, https://doi.org/10.3390/w10091253.
[8] Rabah Djedjig, Salah-Eddine Ouldboukhitine, Rafik Belarbi, Emmanuel Bozonnet, Development and validation of a coupled heat and mass transfer model for green roofs, Int. Commun. Heat Mass Transf. 39 (6) (2012) 752–761, https://doi.org/10.1016/j.icheatmasstransfer.2012.03.024.
[9] D.L. Dunkerley, T.L. Booth, Plant canopy interception of rainfall and its significance in a banded landscape, arid western New South Wales, Australia, Water. Resour. Res. 35 (5) (1999) 1581–1586, https://doi.org/10.1029/1999WR900003.
[10] DWD Climate Data Center (CDC). n.d. "5-Minütige Stationsmessungen Des Niederschlages Für Deutschland, Version V24.3." Accessed July 17, 2023. https://opendata.dwd.de/climate_environment/CDC/observations_germany/climate/5_minutes/precipitation/recent.
[11] Mert Eksi, D.Bradley Rowe, Indrek S. Wichman, Jeff A. Andresen, Effect of substrate depth, vegetation type, and season on green roof thermal properties, Energy Build. 145 (June) (2017) 174–187, https://doi.org/10.1016/j.enbuild.2017.04.017.
[12] Youcan Feng, Steven Burian, Eric Pardyjak, Observation and estimation of evapotranspiration from an irrigated green roof in a rain-scarce environment, Water. (Basel) 10 (3) (2018) 262, https://doi.org/10.3390/w10030262.
[13] R.S. Gates, S. Zolnier, J. Buxton, Vapor pressure deficit control strategies for plant production, IFAC Proc. Vol. 31 (12) (1998) 271–276, https://doi.org/10.1016/S1474-6670(17)36076-7.
[14] Kristin L. Getter, Seasonal heat flux properties of an extensive green roof in a Midwestern U.S. Climate.", Energy Build. (2011).
[15] Mustafa Goodarzi, Saeid Eslamian, Performance evaluation of linear and nonlinear models for the estimation of reference evapotranspiration, Int. J. Hydrol. Sci. Technol. 8 (1) (2018) 1, https://doi.org/10.1504/IJHST.2018.088651.
[16] Dominik Gößner, Milena Mohri, Justine Jasmin Krespach, Evapotranspiration measurements and assessment of driving factors: a comparison of different green roof systems during summer in Germany, Land. (Basel) 10 (12) (2021) 1334, https://doi.org/10.3390/land10121334.
[17] Jannik Heusinger, David J. Sailor, Stephan Weber, Modeling the reduction of urban excess heat by green roofs with respect to different irrigation scenarios, Build. Environ. 131 (March) (2018) 174–183, https://doi.org/10.1016/j.buildenv.2018.01.003.
[18] Jannik Heusinger, Stephan Weber, Comparative microclimate and dewfall measurements at an urban green roof versus bitumen roof, Build. Environ. 92 (October) (2015) 713–723, https://doi.org/10.1016/j.buildenv.2015.06.002.
[19] Jannik Heusinger, Stephan Weber, Surface energy balance of an extensive green roof as quantified by full year eddy-covariance measurements, Sci. Total Environ. 577 (January) (2017) 220–230, https://doi.org/10.1016/j.scitotenv.2016.10.168.
[20] Ali Jahanfar, Jennifer Drake, Bahram Gharabaghi, Brent Sleep, An experimental and modeling study of evapotranspiration from integrated green roof photovoltaic systems, Ecol. Eng. 152 (June) (2020) 105767, https://doi.org/10.1016/j.ecoleng.2020.105767.
[21] P.G. Jarvis, The interpretation of the variations in leaf water potential and stomatal conductance found in canopies in the field, Philos. Trans. R. Soc. Lond. B, Biol. Sci. 273 (927) (1976) 593–610, https://doi.org/10.1098/rstb.1976.0035.
[22] C Y Jim, Hongming He, Coupling heat flux dynamics with meteorological conditions in the green roof ecosystem, Ecol. Eng. (2010).
[23] C.Y. Jim, Lilliana L.H. Peng, Substrate moisture effect on water balance and thermal regime of a tropical extensive green roof, Ecol. Eng. 47 (October) (2012) 9–23, https://doi.org/10.1016/j.ecoleng.2012.06.020.
[24] C.Y. Jim, S.W. Tsang, Modeling the heat diffusion process in the abiotic layers of green roofs, Energy Build. 43 (6) (2011) 1341–1350, https://doi.org/10.1016/j.enbuild.2011.01.012.
[25] Daniel Kaiser, Manfred Köhler, Marco Schmidt, Fiona Wolff, Increasing evapotranspiration on extensive green roofs by changing substrate depths, construction, and additional irrigation, Buildings 9 (7) (2019) 173, https://doi.org/10.3390/buildings9070173.
[26] S. Kemp, P. Hadley, T. Blanuša, The influence of plant type on green roof rainfall retention, Urban. Ecosyst. 22 (2) (2019) 355–366, https://doi.org/10.1007/s11252-018-0822-2.
[27] Neda Khanmohammadi, Hossein Rezaie, Majid Montaseri, Javad Behmanesh, The application of multiple linear regression method in reference evapotranspiration trend calculation, Stochastic Environ. Res. Risk Assess. 32 (3) (2018) 661–673, https://doi.org/10.1007/s00477-017-1378-z.
[28] Masaharu Kitano, Hiromi Eguchi, Tsuyoshi Matsui, Analysis of heat balance of leaf with reference to stomatal responses to environmental factors, Biotron Institute (1983).
[29] Andreas Klingler, Andreas Schaumberger, Francesco Vuolo, László B. Kalmár, Erich M. Pötsch, Comparison of direct and indirect determination of leaf area index in permanent grassland, PFG – J. Photogram. Remote Sens. Geoinform. Sci. 88 (5) (2020) 369–378, https://doi.org/10.1007/s41064-020-00119-8.
[30] Jan Knappe, Manfred Van Afferden, Jan Friesen, GR2L: a robust dual-layer green roof water balance model to assess multifunctionality aspects under climate variability, Front. Clim. 5 (March) (2023) 1115595, https://doi.org/10.3389/fclim.2023.1115595.
[31] Markus Kottek, Jürgen Grieser, Christoph Beck, Bruno Rudolf, Franz Rubel, World map of the Köppen-Geiger climate classification updated, Meteorologische Zeitschrift 15 (3) (2006) 259–263, https://doi.org/10.1127/0941-2948/2006/0130.
[32] Louis S.H. Lee, C.Y. Jim, Thermal-cooling performance of subtropical green roof with deep substrate and woodland vegetation, Ecol. Eng. 119 (August) (2018) 8–18, https://doi.org/10.1016/j.ecoleng.2018.05.014.
[33] Maria Manso, Inês Teotónio, Cristina Matos Silva, Carlos Oliveira Cruz, Green roof and green wall benefits and costs: a review of the quantitative evidence, Renew. Sustain. Energy Rev. 135 (January) (2021) 110111, https://doi.org/10.1016/j.rser.2020.110111.
[34] Jeroen Mentens, Dirk Raes, Martin Hermy, Green roofs as a tool for solving the rainwater runoff problem in the urbanized 21st century? Landsc. Urban. Plan. 77 (3) (2006) 217–226, https://doi.org/10.1016/j.landurbplan.2005.02.010.
[35] Tobi Eniolu Morakinyo, K.W.D.Kalani.C. Dahanayake, Edward Ng, Cheuk Lun Chow, Temperature and cooling demand reduction by green-roof types in different climates and urban densities: a Co-simulation parametric study, Energy Build. 145 (June) (2017) 226–237, https://doi.org/10.1016/j.enbuild.2017.03.066.
[36] Dominique Morau, Teddy Libelle, François Garde, Performance evaluation of green roof for thermal protection of buildings in reunion Island, Energy Procedia 14 (2012) 1008–1016, https://doi.org/10.1016/j.egypro.2011.12.1047.
[37] J. Noilhan, S. Planton, A simple parameterization of land surface processes for meteorological models, Mon. Weather. Rev. 117 (3) (1989) 536–549, https://doi.org/10.1175/1520-0493(1989)117<0536:ASPOLS>2.0.CO;2.

[38] K. Ogle, J.F. Reynolds, Desert dogma revisited: coupling of stomatal conductance and photosynthesis in the desert shrub, *Larrea Tridentata*, Plant Cell Environ. 25 (7) (2002) 909–921, https://doi.org/10.1046/j.1365-3040.2002.00876.x.
[39] Anna Palla, Ilaria Gnecco, Luca Lanza, Hydrologic restoration in the urban environment using green roofs, Water. (Basel) 2 (2) (2010) 140–154, https://doi.org/10.3390/w2020140.
[40] Andrea Pianella, Lu Aye, Zhengdong Chen, Nicholas Williams, Substrate depth, vegetation and irrigation affect green roof thermal performance in a mediterranean type climate, Sustainability. 9 (8) (2017) 1451, https://doi.org/10.3390/su9081451.
[41] Menghao Qin, George Walton, Rafik Belarbi, Francis Allard, Simulation of whole building coupled Hygrothermal-airflow transfer in different climates, Energy Convers. Manage 52 (2) (2011) 1470–1478, https://doi.org/10.1016/j.enconman.2010.10.010.
[42] Emanuele Quaranta, Ciril Arkar, Cristina Branquinho, Elena Cristiano, Ricardo Cruz De Carvalho, Michal Dohnal, Ilaria Gnecco, et al., A daily time-Step hydrological-energy-biomass model to estimate green roof performances across europe to support planning and policies, Urban. For. Urban. Green. 93 (March) (2024) 128211, https://doi.org/10.1016/j.ufug.2024.128211.
[43] R Core Team, R: A Language and Environment for Statistical Computing, R Foundation for Statistical Computing, Vienna, Austria, 2023. https://www.R-project.org/.
[44] M. Razzaghmanesh, S. Beecham, The hydrological behaviour of extensive and intensive green roofs in a dry climate, Sci. Total Environ. 499 (November) (2014) 284–296, https://doi.org/10.1016/j.scitotenv.2014.08.046.
[45] Rodolfo Reyes, Waldo Bustamante, Jorge Gironás, Pablo A. Pastén, Victoria Rojas, Francisco Suárez, Sergio Vera, Felipe Victorero, Carlos A. Bonilla, Effect of substrate depth and roof layers on green roof temperature and water requirements in a semi-arid climate, Ecol. Eng. 97 (December) (2016) 624–632, https://doi.org/10.1016/j.ecoleng.2016.10.025.
[46] R.C. Rodgers, G.E. Hill, Equations for vapour pressure versus temperature: derivation and use of the antoine equation on a hand-held programmable calculator, Br. J. Anaesth. 50 (5) (1978) 415–424, https://doi.org/10.1093/bja/50.5.415.
[47] R.J. Ronda, H.A.R. De Bruin, A.A.M. Holtslag, Representation of the canopy conductance in modeling the surface energy budget for low vegetation, J. Appl. Meteorol. 40 (8) (2001) 1431–1444, https://doi.org/10.1175/1520-0450(2001)040<1431:ROTCCI>2.0.CO;2.
[48] Omidreza Saadatian, K. Sopian, E. Salleh, C.H. Lim, Safa Riffat, Elham Saadatian, Arash Toudeshki, M.Y. Sulaiman, A review of energy aspects of green roofs, Renew. Sustain. Energy Rev. 23 (July) (2013) 155–168, https://doi.org/10.1016/j.rser.2013.02.022.
[49] D.J. Sailor, A green roof model for building energy simulation programs, Energy Build. 40 (8) (2008) 1466–1478, https://doi.org/10.1016/j.enbuild.2008.02.001.
[50] Bernhard Scharf, Irene Zluwa, Case study investigation of the building physical properties of seven different green roof systems, Energy Build. 151 (September) (2017) 564–573, https://doi.org/10.1016/j.enbuild.2017.06.050.
[51] Saeed Sharafi, Mehdi Mohammadi Ghaleni, Evaluation of multivariate linear regression for reference evapotranspiration modeling in different climates of Iran, Theor. Appl. Climatol. 143 (3–4) (2021) 1409–1423, https://doi.org/10.1007/s00704-020-03473-0.
[52] Mary Shedd, Michael D. Dukes, Grady L. Miller, Effect of irrigation control on St. Augustinegrass quality and root growth, Proc. Florida State Hortic. Soc. 121 (2008) 340–345.
[53] Cristina M. Silva, M.Glória Gomes, Marcelo Silva, Green roofs energy performance in mediterranean climate, Energy Build. 116 (March) (2016) 318–325, https://doi.org/10.1016/j.enbuild.2016.01.012.
[54] Lauren Smalls-Mantey, Franco Montalto, The seasonal microclimate trends of a large scale extensive green Roof, Build. Environ. 197 (June) (2021) 107792, https://doi.org/10.1016/j.buildenv.2021.107792.
[55] V. Smets, W. Akkermans, B. Verbeiren, M. Hermy, B. Somers, Ex-Situ estimation of interception storage capacity of small urban plant species, J. Hydrol. (Amst) 572 (May) (2019) 869–883, https://doi.org/10.1016/j.jhydrol.2019.03.047.
[56] T. Susca, S.R. Gaffin, G.R. Dell'Osso, Positive effects of vegetation: urban heat island and green roofs, Environ. Pollut. 159 (8–9) (2011) 2119–2126, https://doi.org/10.1016/j.envpol.2011.03.007.
[57] Tabares Velasco, Paulo Cesar, Predictive Heat and Mass Transfer Model of Plant-Based Roofing Materials for Assessment of Energy Savings, Pennsylvania State University, 2009. Dissertation.
[58] Paulo Cesar Tabares-Velasco, Jelena Srebric, Experimental quantification of heat and mass transfer process through vegetated roof samples in a new laboratory setup, Int. J. Heat. Mass Transf. 54 (25–26) (2011) 5149–5162, https://doi.org/10.1016/j.ijheatmasstransfer.2011.08.034.
[59] Paulo Cesar Tabares-Velasco, Jelena Srebric, A heat transfer model for assessment of plant based roofing systems in summer conditions, Build. Environ. 49 (March) (2012) 310–323, https://doi.org/10.1016/j.buildenv.2011.07.019.
[60] Hideki Takebayashi, Masakazu Moriyama, Surface heat budget on green roof and high reflection roof for mitigation of urban heat island, Build. Environ. 42 (8) (2007) 2971–2979, https://doi.org/10.1016/j.buildenv.2006.06.017.
[61] Chun Liang Tan, Puay Yok Tan, Nyuk Hien Wong, Hiroyuki Takasuna, Tadashi Kudo, Yuichi Takemasa, Chin Voon Jesslyn Lim, Hui Xuan Valerie Chua, Impact of soil and water retention characteristics on green roof thermal performance, Energy Build. 152 (October) (2017) 830–842, https://doi.org/10.1016/j.enbuild.2017.01.011.
[62] F.J. Veihmeyer, A.H. Hendrickson, Soil moisture at permanent wilting of plants, Plant Physiol. 3 (3) (1928) 355–357, https://doi.org/10.1104/pp.3.3.355.
[63] Emily Voyde, Elizabeth Fassman, Robyn Simcock, Julia Wells, Quantifying evapotranspiration rates for New Zealand green roofs, J. Hydrol. Eng. 15 (6) (2010) 395–403, https://doi.org/10.1061/(ASCE)HE.1943-5584.0000141.

urban science

MDPI

Article

Year-Round Modeling of Evaporation and Substrate Temperature of Two Distinct Green Roof Systems

Dominik Gößner

Department of Environmentally Sound Urban and Infrastructure Planning, HafenCity University Hamburg, 20457 Hamburg, Germany; dominik.goessner@hotmail.de

Abstract

This paper presents a novel model for the year-round simulation of evapotranspiration (ET) and substrate temperature on two fundamentally different extensive green roof types: a conventional drainage-based "Economy Roof" and a retention-optimized "Retention Roof" featuring capillary water redistribution. The main scope is to bridge the gap in urban climate adaptation by providing a modeling tool that captures both hydrological and thermal functions of green roofs throughout all seasons, notably including periods with dormancy and low vegetation activity. A key novelty is the explicit and empirically validated integration of core physical processes—water storage layer coupling, explicit rainfall interception, and vegetation cover dynamics—with the latter strongly controlled by plant area index (PAI). The PAI, here quantified as the plant surface area per unit ground area using digital image analysis, directly determines interception capacity and vegetative transpiration rates within the model. This process-based representation enables a more realistic simulation of seasonal fluctuations and physiological plant responses, a feature often neglected in previous green roof models. The model, which can be fully executed without high computational power, was validated against comprehensive field measurements from a temperate climate, showing high predictive accuracy (R^2 = 0.87 and percentage bias = −1% for ET on the Retention Roof; R^2 = 0.91 and percentage bias = −8% for substrate temperature on the Economy Roof). Notably, the layer-specific coupling of vegetation, substrate, and water storage advances ecological realism compared to prior approaches. The results illustrate the model's practical applicability for urban planners and researchers, offering a user-friendly and transparent tool for integrated assessments of green infrastructure within the context of climate-resilient city design.

Keywords: green roof; Retention Roof; blue-green roof; green roof modeling; evapotranspiration modeling; substrate temperature modeling

check for updates

Academic Editor: Aya Hagishima

Received: 5 August 2025
Revised: 7 September 2025
Accepted: 17 September 2025
Published: 30 September 2025

Citation: Gößner, D. Year-Round Modeling of Evaporation and Substrate Temperature of Two Distinct Green Roof Systems. *Urban Sci.* **2025**, *9*, 396. https://doi.org/10.3390/urbansci9100396

Copyright: © 2025 by the author. Licensee MDPI, Basel, Switzerland. This article is an open access article distributed under the terms and conditions of the Creative Commons Attribution (CC BY) license (https://creativecommons.org/licenses/by/4.0/).

1. Introduction

Urbanization and climate change have intensified the frequency and severity of flooding and heat events in cities. This development is largely driven by increased impervious surfaces and altered cycles of hydrology and energy. As a consequence, cities are increasingly affected by stormwater overload, elevated energy demands, and growing risks to public health during extreme weather events. Green roofs have emerged as nature-based solutions that mitigate these adverse impacts by enhancing stormwater retention, improving local microclimates, and reducing building energy demands, among other co-benefits [1–4].

In particular, retention-type green roofs—systems with enhanced water storage capacity—are now frequently implemented as stormwater management tools at both

building and district scales. They are supposed to not only retain rainfall during extreme weather events but also to support aesthetic integrity and maintain healthy vegetation during summer months for continued cooling benefits [5,6]. Given that the use of potable water for irrigation is often limited or prohibited, understanding and predicting a green roof's water consumption and cooling performance is essential for optimal design and function. From an urban planning perspective, the most important ecosystem services of green roofs are attractive appearance [4,6,7], cooling effect [8,9], increased urban biodiversity [10,11], and delaying runoff during precipitation events [12,13].

The hydrodynamic calculation of runoff delay is well documented in the literature [14–16] and one key input variable for these simulations is substrate moisture at the onset of a rain event, which strongly depends on evapotranspiration rates during prior dry periods. Similarly, evapotranspiration plays a decisive role in the thermal behavior of the roof by promoting latent heat loss, while substrate temperature governs sensible heat exchange between roof surfaces and the surrounding air. These two parameters—evapotranspiration and substrate temperature—therefore represent the most relevant calculable variables for evaluating both the hydrological performance and urban cooling capacity of green roofs. Their accurate prediction is essential to quantify retention capacity, guide irrigation strategies, and evaluate energy saving potential for green infrastructure planning [8,17–19].

Nevertheless, a review of existing modeling approaches reveals several persistent research gaps in the simulation of substrate temperature and evapotranspiration on green roofs. The summary in Table 1 presents a comparative analysis of eleven models which calculated both evapotranspiration and substrate temperature and were published between 1998 and 2021, highlighting the state of current modeling efforts. They have been reviewed regarding the calculation (Ca) and validation (Va) of soil moisture, stomatal resistance, interaction with drainage/retention layer, plant area index (PAI—the ratio of plant aboveground biomass to the substrate surface)/soil cover fraction (SCF—the ratio of plant cover of a measurement area), and interception, the simulation of which are important for a comprehensive model [20–22]. As well as regarding the validated ability to simulate a full year, having evapotranspiration measurements for result validation and no need for numeric solvers are necessary characteristics for a reliable and easy to use model, without the need of extensive computational power. While many studies address some of these aspects, no model provides a simulation with all the mentioned key parameters and characteristics.

One clear shortcoming across much of the existing literature is the limited validation of key variables, particularly interception, stomatal resistance, and the interaction between substrate and drainage or retention layers. While evapotranspiration is a central component of most models, only two (Takebayashi and Moriyama, 2007 [23]; Tabares-Velasco et al., 2012 [24]) include validation.

A second limitation is the underrepresentation of validated biophysical plant processes. Validated seasonal variation in plant parameters such as PAI and SCF, which are crucial for accurate modeling of evapotranspiration [25], remain largely underrepresented. Notable exceptions include the models by Tabares-Velasco et al. [25], de Munck et al. [26], and Decruz [27].

Overall, model usability remains a concern. Several modeling frameworks, especially those rooted in hydrodynamic or hygrothermal simulation, require extensive computational resources or the application of specialized software packages. Although these can provide high-resolution results, they are often impractical for implementation in daily use software for planners, engineers, or policymakers aiming to assess green roof scenarios in everyday applications. Models suitable for annual simulation with minimal computational effort are notably lacking in the reviewed literature.

Perhaps the most consistent omission among existing studies is the neglect of drainage and retention layer interactions. In many commercially available green roofs today, water flow is not limited to vertical percolation within the substrate. Lateral flows, capillary upward fluxes, and water storage in sub-layers significantly affect evapotranspiration dynamics and substrate thermal properties [20,22,28], yet none of the reviewed models explicitly represent this hydraulic coupling, limiting their capacity to capture the behavior of retention-optimized green roofs. In modern multilayered systems, this shortcoming becomes increasingly relevant for both hydrological and thermal modeling.

Finally, none of the models attempt full-year simulation with empirical validation against evapotranspiration. Instead, many studies focus on single seasons (typically summer) or isolated events, reducing the models' ecological realism and generalizability.

Table 1. Overview of models with calculation of evapotranspiration and substrate temperature comparing specific characteristics and key model parameters.

Author(s)	Year	Soil Moisture		Stomatal Resistance		Interaction with Drainage/ Retention Layer	PAI/SCF		Interception		Full Year Simulation	Validation With Evapotranspiration Data	No Numeric Solvers Needed
		Ca	Va	Ca	Va	Ca	Ca	Va	Ca	Va			
Palomo del Barrio Q	1998	✔	✘	✔	✘	✘	✘	✘	✘	✘	✘	✘	✘
Alexandri & Jones [23]	2007	✔	✔	✔	✔	✘	✔	✘	✘	✘	✘	✘	✘
Takebayashi & Moriyama [23]	2007	✘	✘	✔	✘	✘	✘	✘	✘	✘	✘	✔	✘
Sailor [8]	2008	✔	✘	✔	✘	✘	✔	✘	✘	✘	✔	✘	✘
Ouldboukhitine et al. [29]	2011	✔	✘	✔	✘	✘	✔	✘	✘	✘	✘	✘	✘
Tabares-Velasco et al. [25]	2012	✘	✘	✔	✔	✘	✔	✔	✘	✘	✘	✔	✔
Djedjig et al. [30]	2012	✔	✔	✔	✘	✘	✔	✘	✘	✘	✘	✘	✘
de Munck et al. [26]	2013	✔	✔	✔	✘	✘	✔	✔	✔	✘	✘	✘	✔
Decruz [27]	2016	✔	✔	✔	✘	✘	✔	✔	✔	✘	✘	✘	✘
Tian et al. [31]	2017	✔	✘	✔	✘	✘	✔	✘	✘	✘	✘	✘	✘
Hong et al. [32]	2021	✘	✘	✔	✘	✘	✘	✘	✘	✘	✘	✘	✘

Abbreviations: Ca means calculated. Va means validated. ✘ means parameter not included. ✔ means parameter included.

In summary, while notable progress has been made in individual aspects of green roof modeling, Table 1 illustrates that gaps remain in integrated, validated, and practically usable simulations of evapotranspiration and substrate temperature. Addressing these gaps—particularly the incorporation of vegetation dynamics, interception calculation, full-year applicability and drainage layer interaction—remains a key challenge and motivation for the development of more comprehensive models, such as the one proposed in the present study.

The overarching goals of this study are as follows:

1. To model the two most essential variables—evapotranspiration and substrate temperature—with a high degree of accuracy, as they are fundamental for the prediction of the water use and energy performance of green roofs under changing weather conditions.
2. To ensure usability and practicality, the model is designed to be applied with easily accessible input data, without requiring high computational resources, making it widely usable.
3. To improve model accuracy by addressing key research gaps, specifically
   - include interception calculation
   - capture seasonal variation in PAI and SCF

- simulate and validate a full year
- include hydraulic coupling with drainage and retention layer

To achieve these aims, existing approaches are combined and refined into a model for green roof evapotranspiration and temperature, which is tested across representative green roof types. All simulations in this study were run using Microsoft Excel (Version 16.78 for Mac) to underscore its practical applicability without the need for advanced programming or simulation tools.

2. Materials and Methods

2.1. Study Site and Experimental Setup

For validation of the model, measurement data from the whole year of 2022 for two different green roof types, the so-called Economy Roof and Retention Roof, was used. The Economy Roof with its four layers (protection fleece, drainage mat, filter fleece, and substrate) is the most common standard build-up for extensive green roofs, at least for the German market and its neighboring countries [33,34]. The Retention Roof differs from the Economy Roof in its use of a water retention layer instead of a drainage layer and a capillary connection from this layer to the substrate. The measurements were carried out in previous studies [22,28] in the south of Germany, in Krauchenwies-Göggingen (48°0′20.27916″ N and 9°12′5.33952″ E) at an elevation of 623 m above sea level. This location falls within a warm temperature, fully humid warm summer climate classification [35]. The setup encompassed the two green roofs, each placed in a lysimeter with a surface area of 0.5 m^2. As shown in Figure 1, the lysimeters were placed on a sealed surface. To minimize potential edge effects, e.g., an increased heat flux due to the sealed surface, a surrounding green roof was built for this experimental setup. Each green roof was equipped with sensors for leaf and air temperature at the vegetation level, substrate temperature, substrate moisture content, heat flux, outflow, and weight. Additionally, a weather station recorded precipitation, air temperature and relative humidity, wind speed, incoming shortwave solar irradiance, and incoming longwave radiation. A detailed list of the sensors, their location and their accuracy can be found in Table 2. The data was collected at intervals of 5 min, resulting in a dataset comprising 2 full years (1 April 2021 to 31 March 2023). The roof systems are distributed by Optigrün international AG, Krauchenwies-Göggingen, Germany and contain various roof layers (Figure 2). All experimental green roofs were fertilized with a slow-release fertilizer (Opticote, Optigrün international AG) at the beginning of the study period and were weeded approximately once per month in summertime to preserve the intended vegetation. The Economy Roof drains freely, while the discharge of the Retention Roof is restricted, as the drainage hole is positioned at 3 cm height. Further details about this research can be found in the corresponding publication by [28].

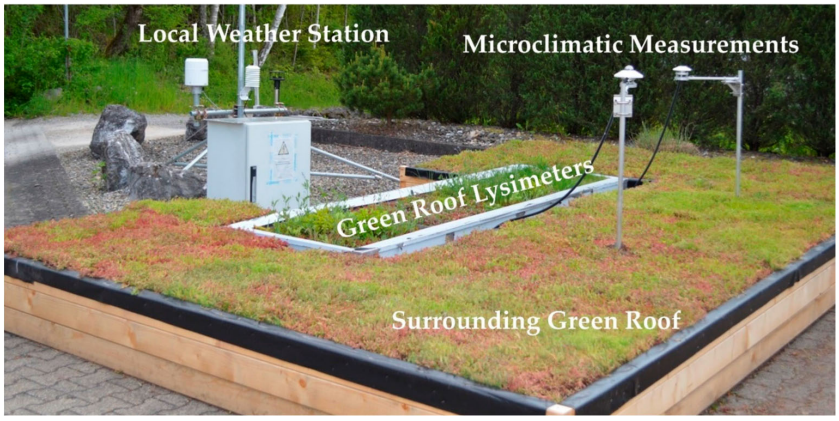


Figure 1. Measurement site in Göggingen-Krauchenwies, Germany [28].

Table 2. List of measured parameters, measurement devices used, approximate position of the sensors, and their accuracy.

Layer	Parameter	Measurement Device	Manufacturer	Accuracy
Atmospheric Layer	Precipitation	Rain[e]	LAMBRECHT meteo GmbH, Göttingen, Germany	±1 mm or ±1%
	Air Temperature	CS215 Temperature and Relative Humidity Probe	Campbell Scientific Inc., Logan, UT, USA	±0.3 °C (at 25 °C) ±0.4 °C (5° to 40 °C) ±0.9 °C (−40° to +70 °C)
	Relative Humidity	CS215 Temperature and Relative Humidity Probe	Campbell Scientific Inc., Logan, UT, USA	±2% (10% to 90% range) at 25 °C ±4% (0% to 100% range) at 25 °C
	Short-Wave Solar Radiation	CMP10 Pyranometer	Kipp & Zonen B.V., Delft, The Netherlands	Total zero offset: <±9 W m^{-2} Non-stability (change/year): <±0.5% Non-linearity (100 to 1000 W m^{-2}): <±0.2% Temperature response: <±1% (−10 °C to +40 °C)
	Long-Wave Radiation	CGR3 Pyrgeometer (facing the sky)	Kipp & Zonen B.V., Delft, The Netherlands	Non-stability (change/year): <1% Non-linearity: <1% Temperature Dependence of Sensitivity: <5% (−14 °F to +104 °F)
	Wind Speed	WindSonic4 Two-Dimensional Sonic Anemometer	Campbell Scientific Inc., Logan, UT, USA	±2% (at 12 m s^{-1})
Vegetation Layer	Leaf Temperature + Air Temperature	Leaf and Air Temperature Type LAT-B2, Broadleaf	ECOMATIK GmbH, Dachau, Germany	±0.2 °C
Substrate Layer	Volumetric Water Content	CS655 Soil Water Content Reflectometer	Campbell Scientific Inc., Logan, UT, USA	±1%
	Substrate Temperature	105E Temperature Probe	Campbell Scientific Inc., Logan, UT, USA	±0.5 °C
	Heat Flux	HFP01 Heat Flux Plate	Hukseflux Thermal Sensors B.V., Delft, The Netherlands	±3%
Total Setup	Weight	Scale 9392.16.140	Soehnle Industrial Solutions GmbH, Backnang, Germany	±15 g
	Outflow	Small Rain Gauge 100.054	Pronamic ApS, Ringkoebing, Denmark	±5%

The PAI, the SCF, and the interception capacity were also quantified. For the measurement of the vegetation cover and the PAI, triplicate photos were taken of each roof approximately once per week with a digital camera (D3200, Nikon, Düsseldorf, Germany and 8 mm/3.5 Fish-Eye II Lens Walimex pro, Studioexpress Vertriebs GmbH, Wiernsheim, Germany). The calculation of the vegetation cover and PAI was performed with the freeware CAN-EYE (INRAE, Paris, France).

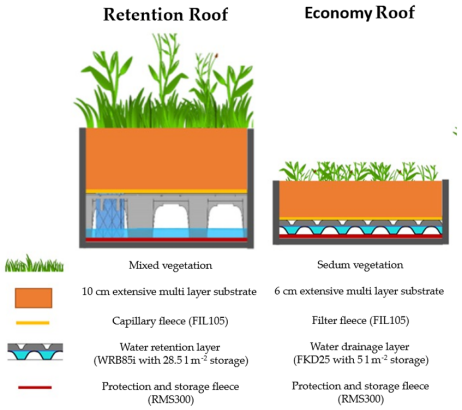


Figure 2. Build-up from Gößner et al. [28] of the two different green roof systems modeled in this study.

The interception capacity quantifies the amount of rainfall retained on the surface of a plant's above-ground biomass. Vegetation cover with high interception capacity can therefore improve a green roof system's water retention capability. The assessment of interception capacity was based on Dunkerley and Booth [36], with minor adjustments to adapt to the smaller scale of our experiment. Ten low-growing perennials including herbaceous species and subshrubs commonly utilized for green roof installations were assessed. The initial preselection was based on a list of low-growing perennials suitable for green roofs and developed through years of practical experience, the final selection was determined by the availability at the nearest plant nursery. Of each species, three replicates were selected. To determine the interception capacity, a 10 × 10 cm frame was used to define the area covered by each plant's aboveground biomass, and excess biomass outside this frame was trimmed. Then, the plant was cut just above the substrate, weighed, and placed in floral foam blocks to mimic the natural arrangement. Each plant was irrigated with 500 mL water for 30 s using a rainfall-tip nozzle. After two minutes, the plants were re-weighed to determine the interception capacity based on the weight difference, which was then extrapolated to 1 m^2 and averaged for each plant species.

The water retention layer of the Retention Roof leads, in comparison to the Economy Roof, to highly increased soil moisture (17.18% higher on average), lower temperatures (4.2° cooler air at vegetation level on average during summer), and increased evapotranspiration (0.45 mm day^{-1} more evaporation on average). These different effects of the two green roofs are attributed to their differences in technical build-up. An evapotranspiration and substrate temperature model for green roofs should be able to model both types of green roofs.

2.2. Green Roof Model

As forecasting evapotranspiration is one of the main objectives of the model, and stomatal behavior plays a crucial role in the transpiration process, a detailed approach was chosen using the Penman–Monteith equation, which includes a dynamic calculation of stomatal resistance. In contrast, the simulation of substrate moisture, substrate temperature, and the capillary connection between the retention layer and the substrate was implemented in a more straightforward manner to avoid the need for computationally complex numerical solvers. A summary of all equations and constants used in the model is provided in Appendix A.

Stomatal behavior directly regulates plant transpiration activity. Previous research has shown that stomatal responses—and, consequently, transpiration rates—can vary significantly depending on environmental conditions [28,37,38]. For this reason, the stomatal resistance function is considered a key element for controlling transpiration and is particu-

larly important for accurately computing the varying evapotranspiration rates associated with different green roof configurations.

The model requires the following meteorological input parameters: shortwave radiation, air temperature, precipitation, air humidity, and wind velocity. These parameters are freely available in Germany from a national network of weather stations. This data can be accessed via an open data server at the following link. User instructions are given in German and English: https://opendata.dwd.de/climate_environment/CDC/ (accessed on 26 August 2025).

2.2.1. Evaporation and Transpiration

In the model, interception and its evaporation is modeled explicitly, as a relevant part of small rain events can be retained at the plants' surface [39,40]. Consequently, the original Penman–Monteith equation is only used to quantify the potential plant transpiration (TR).

$$TR_p = \frac{1}{\lambda}\left[\frac{\Delta(R_n - G)}{\Delta + \gamma\left(1 + \frac{r_c}{r_a}\right)} + \frac{\frac{pc_p(e_s - e_a)}{r_a}}{\Delta + \gamma\left(1 + \frac{r_c}{r_a}\right)}\right] \quad (1)$$

where R_n is the net radiation (MJ m^{-2}), G is the soil heat flux (MJ m^{-2}), $(e_s - e_a)$ represents the vapour pressure deficit (kPa) of the air, p is the atmospheric density (kg m^{-3}), c_p is the specific heat capacity of the air (kJ kg^{-1} °C^{-1}) , γ is the psychrometric constant (kPa °C^{-1}), r_c is the stomatal resistance (s m^{-1}), and r_a is the aerodynamic resistance (s m^{-1}).

To determine the potential evaporation (E_p) for the interception storage, stomatal resistance restraint is eliminated from the Penman–Monteith equation [37].

$$E_p = \frac{1}{\lambda}\left[\frac{\Delta(R_n - G)}{\Delta + \gamma} + \frac{\frac{pc_p(e_s - e_a)}{r_a}}{\Delta + \gamma}\right] \quad (2)$$

In the model, stomatal resistance (r_c) determines the amount of transpiration as a function of solar radiation ($f(solar)$), air temperature ($f(temp)$), substrate water content ($f(VWC)$), and vapour pressure deficit ($f(VPD)$) [8]:

$$r_c = \frac{r_{cmin}}{0.5\ PAI} f(solar) f(VWC) f(VPD) f(temperature) \quad (3)$$

$$f(solar) = 1 + e^{-0.034(R_s - 3.5)} \quad (4)$$

$$f(VWC) = \begin{cases} 1 & \theta > 0.7\theta_{fk} \\ \frac{\theta_{fk} - \theta_{wp}}{\theta - \theta_{wp}} & \theta_{wp} < \theta < 0.7\theta_{fk} \\ 1000 & \theta_{wp} > \theta \end{cases} \quad (5)$$

$$f(VPD) = \frac{0.4}{1 - 0.41ln(e_s - e_a)} + 0.21 \quad (6)$$

$$f(temp) = \begin{cases} 1000 & T_a < 278.15 \\ \frac{1}{1 - 0.0006(18 - (T_a - 273.15))^2} & T_a \geq 278.15 \end{cases} \quad (7)$$

where r_{cmin} is the minimum stomatal resistance (s m^{-1}). The stomatal resistance varies between plant species. The lowest measured stomatal resistance for the prevailing plant (sedum spurium) on the Economy Roof was 336 s m^{-1}, and 168 s m^{-1} on the Retention Roof for sedum kamtschaticum [22].

The function of solar radiation has been suggested by Sailor [8], where R_s is the solar radiation (W m^{-2}). The function of the volumetric water content has been modified by

Tabares-Velasco [25]. θ is the volumetric water content (VWC in $m^3\ m^{-3}$), θ_{fk} is the VWC of the substrate at field capacity ($m^3\ m^{-3}$), and θ_{wp} is the VWC of the substrate at the wilting point ($m^3\ m^{-3}$). For the used substrate, θ_{wp} is 0.06 $m^3\ m^{-3}$ and θ_{fk} is 0.455 $m^3\ m^{-3}$. Both values were determined in the laboratory at TU Braunschweig. With a θ_{fk} value of greater than 0.35 $m^3\ m^{-3}$, the substrate meets the requirements of the FLL green roof guidelines [41].

For this study the function of vapor pressure deficit has been modified on an empirical basis, as the resulting restrain in transpiration was too high in relation to our measurements. Therefore, "+0.21" was added to the formula, which results, in general, in lower output values of the formula and thus increases the calculated evaporation.

e_s is the vapor pressure of the air at saturation (kPa) and e_a the actual vapor pressure (kPa).

The function of temperature is based on Tabares-Velasco et al. [25], referring to leaf temperature. The original function does not consider temperatures below 0 °C. Since one aim of this work is to minimize the required computational power, the heat transfer of the vegetated area, including plant surface temperatures, is not calculated for reasons of simplicity. Instead, the air temperature (T_a) was used as an input parameter (K). As the model should be capable of modeling a whole year, the temperature function was modified to enable a calculation that includes negative air temperatures.

As the above mentioned parameters can vary quickly during the day [38], a model with relatively small time steps is necessary. In this study, the time step was 5 min.

To obtain the actual evaporation and transpiration of the vegetation the approach of Muzylo [42] is used:

$$ET = E_i + TR \tag{8}$$

$$TR = \left(1 - \frac{C}{S_{max}}\right) TR_p \tag{9}$$

$$E_i = min\left(E_p, E_p \frac{C}{S_{max}}\right) \tag{10}$$

where the actual evapotranspiration (ET in mm) consists of the actual evaporation of the interception storage (E_i in mm) and the actual transpiration of the plants (TR in mm). C is the amount of intercepted rainfall (mm) and interception storage and S_{max} the maximum interception storage (mm).

As the green roof surface is normally not fully covered with vegetation, especially not the whole year, the bare substrate area is calculated separately from the plant covered area. Camillo and Gurney [43] suggested the following equation for describing the evaporation of the substrate (E_s in $kg\ m^{-2}\ s^{-1}$):

$$E_s = \frac{\rho_s - \rho_a}{r_a + r_s} \tag{11}$$

where p_s is the water vapour density of the substrate ($kg\ m^{-3}$) and p_a the water vapour density of the air ($kg\ m^{-3}$).

Based on their own measurements, Tabares-Velasco, 2009 [37], suggested the following formula for the substrate surface resistance (r_s):

$$r_s = 34.5 \left(\frac{\theta}{\theta_{fk}}\right)^{-3.3} \tag{12}$$

For calculating the radiation budgets, formulae from the Food and Agriculture Organization (FAO) are used [44], modified for the use of time steps smaller than 24 h.

2.2.2. PAI

Based on measurements of the PAI (−) development on the economy and Retention Roof build-ups over the period of two years [22], the following empirical descriptions are used:

$$PAI_e = 3sin0.0086J + 2 \quad (13)$$

$$PAI_r = 4.5sin0.0086J + 2 \quad (14)$$

where the index e stands for economy, r stands for Retention Roof, and J is the number of the day of the year (−).

Due to more available water and higher substrate thickness, the Retention Roof has denser vegetation (mean 5.04, SD 1.85) than the Economy Roof (mean 3.97, SD 0.87). The formula for the Economy Roof has a PBIAS of 7% and 9% for the Retention Roof, indicating a good model fit. However, the R^2 values of 0.37 (Economy Roof) and 0.31 (Retention Roof) show that PAI calculation is only an approximation, as the PAI is strongly dependent on the prevailing environmental conditions.

2.2.3. Interception

S_{max} is closely connected to PAI. According to the measured data, PAI strongly influences the interception capacity and plants with a high PAI tend to have a greater interception capacity ($\beta = 0.356$, SE = 0.05, $p < 0.001$, $R^2 = 0.91$). Based on this data the empirical formula 15 ($R^2 = 0.76$) describes the relationship between the PAI and S_{max} for a PAI > 1 [22].

$$S_{max} = -0.33 + 0.44PAI \quad (15)$$

The water balance of the interception of the plant area is described as

$$\int N\,dt\,SCF = \int E_i\,dt + \int D\,dt + \int_{t_1}^{t_2} dC \quad (16)$$

where the rainfall N (mm) on the vegetated area consists of the actual evaporation of the interception storage (E_i in mm), the discharge from the storage (D in mm), and the change in the interception storage (C in mm).

2.2.4. Soil Cover Fraction

During measurements in a two-year period from [22], the *SCF* of both green roof types remained relatively stable, with a median of 0.96 for the Retention Roof and 0.9 of the Economy Roof (Figure 3).

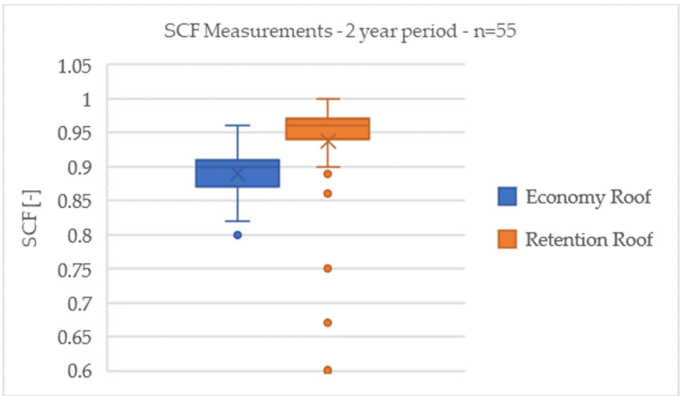


Figure 3. Box-plot measurements of SCF.

2.2.5. Substrate

For simulating the substrate water content the following simple approach was employed, by adding the amount of precipitation falling directly on the substrate ($N \times SFC_i$ in mm), the discharge from the interception storage (D in mm), and the substrate resaturation amount to the water content (I *in mm*) and subtracting the evaporation from the substrate surface (E_s in mm), the water consumption for plant transpiration (TR in mm), and the discharge when the substrate is saturated (θ_d in mm). As extensive green roofs with thin substrate thicknesses are modeled, the non-even distribution of the water content is neglected. h_{sub} is the substrate thickness (mm).

$$\theta = \frac{N \times SCF_i - E_s \times SCF_i - TR + D + I}{h_{sub}} - \theta_d \quad (17)$$

$$\theta_d = max(0; \theta - \theta_s) \quad (18)$$

The substrate temperature is determined using a simple heat transfer equation based on [45]. The non-even distribution of the water content is neglected.

$$T_s = \frac{G_{sub} + G_{plant}}{C_a \, h_{sub}} \quad (19)$$

where T_s is the substrate temperature (°C), G_{sub} the soil heat flux of the substrate (MJ m^{-2}), G_{plant} the soil heat flux of the plants (MJ m^{-2}), and C_a the volumetric heat capacity of the substrate (MJ m^{-3} K^{-1}). The basis for G_{sub} is R_{nsub} and for G_{plant}, R_n is reduced in dependency on the PAI.

2.2.6. Drainage and Substrate Resaturation

If the used drainage in the green roof has water storage, the water in this storage interacts with the substrate and the plants. Most water storages of green roofs have no capillary connection with the substrate. In this case the substrate gets moistened through water vapor processes. Some green roof types (Retention Roofs) though, have a capillary connection between water storage and substrate. In this case, the substrate gets saturated as long as there is water available [28]. Via the substrate resaturation velocity (i in mm period^{-1}) in combination with the maximum substrate resaturation value (θ_{Imax} in m^3 m^{-3}) the two processes can be simulated by choosing empirical values. According to our 2-year measurements of the Retention Roof, for θ_{Imax} the maximum value of a period from 2 days after the last precipition until the next precipitation but with water in the retention/drainage layer was 0.41 m^3 m^{-3}. For the Economy Roof, θ_{Imax} was 0.23 m^3 m^{-3}. Via a comparison between measurements and simulation, i was chosen in an iterative empirical way to match the measured substrate moisture behavior during periods without rain. For the Retention Roof, an i of 0.005 mm 5 min^{-1} was determined, and for the Economy Roof an i of 0.002 mm 5 min^{-1}.

$$I = \begin{cases} min(\int i \, dt \, , \, D_s) & i \geq (\theta_{Imax} - \theta) h_{sub} \\ min((\theta_{Imax} - \theta) h_{sub} \, , \, D_s) & i < (\theta_{Imax} - \theta) h_{sub} \\ 0 & \theta \geq \theta_{Imax} \end{cases} \quad (20)$$

The drainage storage (D_s in mm) itself receives water from the substrate when the substrate is oversaturated (q_s in mm) and loses water via discharge (q_d in mm) when the drainage storage is full and due to the substrate resaturation process (I).

$$D_s = max(q_s - I - q_d, 0) \quad (21)$$

$$q_d = max(D_s - D_{smax}, 0) \quad (22)$$

$$q_s = \theta_d h_{sub} \quad (23)$$

3. Results

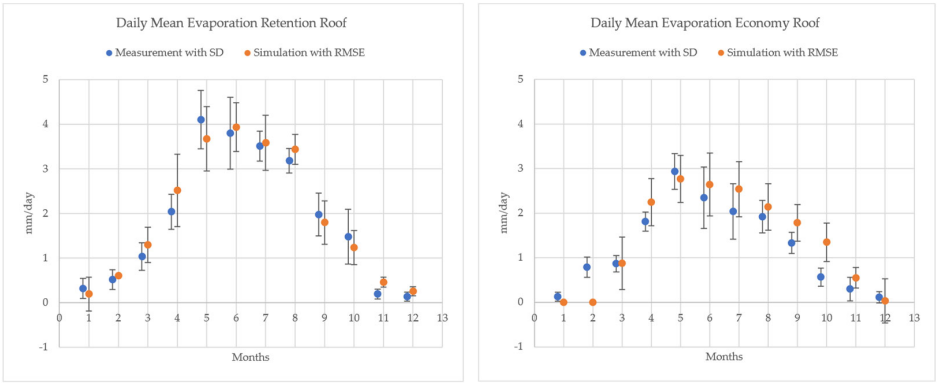
3.1. Evapotranspiration Modelling

The model's performance in predicting evapotranspiration (ET) was assessed seasonally and annually by comparing measured and simulated ET using R^2, root mean square error (RMSE), and percentage bias (PBIAS) as statistical indicators (Table 3).

Table 3. Evapotranspiration model performance based on coefficient of determination (R^2), root mean square error (RMSE), and percentage bias (PBIAS).

Models	Retention Roof			Economy Roof		
	R^2	RMSE	PBIAS (%)	R^2	RMSE	PBIAS (%)
Winter (December–March)	0.86	0.67	−2	0.58	1.30	13
Spring (April–May)	0.80	2.20	−12	0.85	1.42	8
Summer (June–August)	0.96	2.22	6	0.89	3.31	20
Autumn (September–November)	0.86	1.94	−6	0.90	1.79	78
Total year (January–December)	0.87	1.75	−1	0.77	2.20	22

Across the whole year, the Retention Roof model produced high predictive accuracy, with R^2 values ranging from 0.80 to 0.96 across all seasons. The annual PBIAS of just −1% indicates an excellent overall fit and minimal systematic error. Daily mean ET was captured well throughout the year, except in April and May, where minor underestimations occurred, and in October, where ET was slightly overestimated (Figure 4a).



(**a**) (**b**)

Figure 4. Daily mean evaporation from 1 January to 12 December for (**a**) the Retention Roof and (**b**) the Economy Roof.

In contrast, the Economy Roof model performed well in spring and summer for the Economy Roof ($R^2 > 0.80$) but showed a consistent overestimation of ET in autumn (especially in October) and underperformance in winter ($R^2 \approx 0.52$). The autumn overestimation is further confirmed by a PBIAS of 20% in those months, suggesting that senescence and reduced stomatal conductance in real plants may not be fully captured by the current parameterization. A pronounced seasonal trend is evident: the model tends to underestimate ET from January to May and overestimate it from June to December (Figure 4b). This behavior reflects an area where the model's stomatal resistance function may not fully align

with physiological adjustments of vegetation under variable irradiation, temperature, and substrate moisture combinations.

Despite structural and vegetative differences, both roofs showed good alignment in ET prediction during the active growing season, but the Retention Roof's capillary water supply and thicker substrate enabled significantly higher ET, particularly under dry spells and warm conditions. On average, Retention Roof ET was 0.45 mm day^{-1} higher, aligning with prior field studies by Gößner et al. [28] and Cirkel et al. [20].

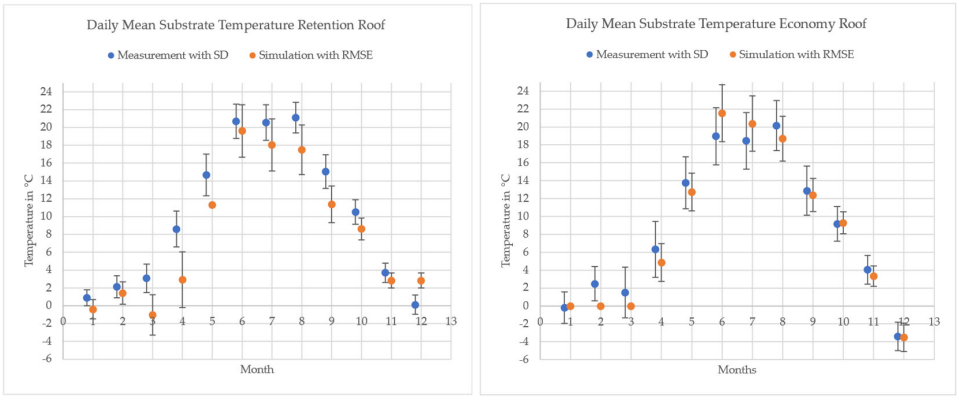
3.2. Substrate Temperature Modelling

Model accuracy in predicting substrate temperature varied clearly between roof types and seasons (Table 4).

Table 4. Substrate temperature model performance based on coefficient of determination (R^2), root mean square error (RMSE), and percentage bias (PBIAS).

Models	Retention Roof			Economy Roof		
	R2	RMSE	PBIAS (%)	R2	RMSE	PBIAS (%)
Winter (December–March)	0.43	3.82	−90	0.67	2.68	−41
Spring (April–May)	0.69	4.36	−7	0.88	4.40	−1
Summer (June–August)	0.42	5.75	−12	0.93	4.47	4
Autumn (September–November)	0.82	3.09	−21	0.92	2.82	−5
Total year (January–December)	0.83	4.33	−21	0.91	4.07	−8

For the Economy Roof, R^2 ranged from 0.88 to 0.92 for spring through autumn, with a PBIAS of −5 to −1%, demonstrating a strong model fit. However, winter predictions were not accurate, likely due to the absence of freeze–thaw physics in the model (PBIAS—41%). The monthly daily mean temperature values, however, showed a very good fit for the total year (Figure 5b). Regarding the winter months, this may be coincidental.



(a) (b)

Figure 5. Daily mean substrate temperature from 1 January to 12 December for (**a**) the Retention Roof and (**b**) the Economy Roof.

The model's performance decreased substantially for the Retention Roof, especially during high substrate moisture and winter periods. Here, R^2 dropped to 0.42. The monthly daily mean substrate temperatures were, apart from December, consistently underestimated (Figure 5a).

Looking at the measurement data over a period exceeding one month, Retention Roof substrate temperatures hovered just above 0 °C, suggesting frozen substrate, while the model, lacking phase-change functionality, simulated large daily amplitudes.

This deviation is a result of the simplified heat capacity calculation, which does not reflect the increased thermal inertia of wet or frozen substrates. Despite this, the model still demonstrated moderate predictive power during warm seasons (R^2 = 0.42–0.82; PBIAS = −7 to −21%).

4. Discussion

4.1. Evaluation of Model Performance Relative to Study Goals

This study aimed to (1) accurately simulate ET and substrate temperature, (2) ensure the model's year-round usability and low computational demand, and (3) improve model accuracy by addressing key research gaps. The degree to which each goal was achieved is discussed below.

4.1.1. Evapotranspiration

The model performed strongly in simulating daily mean ET, especially for the Retention Roof, which achieved seasonal regression coefficients of determination (R^2) between 0.80 and 0.96 and annual PBIAS of just −1%. The strong agreement between measured and modeled ET behavior highlights the value of including substrate–drainage interactions, which are absent from other green roof models, especially for Retention Roof systems. Notably, the Retention Roof yielded higher ET rates than the Economy Roof, consistent with observed patterns from Gößner et al. [28], where thicker substrates and water availability extended transpiration phases.

For the Economy Roof, the model showed good agreement in spring and summer ($R^2 > 0.80$) but had lower predictive power in winter ($R^2 \approx 0.52$) and significantly overestimated ET in autumn. This is likely due to the model's lack of adequate adjustment for seasonal vegetation senescence. In addition, the measured and simulated maximum daily temperatures during September (mean daily max.) and October (mean daily max.), lay 0.72 °C higher than the long-term medium from 2002 to 2024 for September and 0.86 °C higher for October (based on DWD data, see Section 2.2). These high temperatures support a high transpiration rate in the model. However, this does not correspond with the actual behavior of the plants. Comparing the daily mean measurements and the modeled daily mean for the whole year, the Economy Roof shows a tendency for underestimation of the evaporation from January till May and an overestimation from June to December. Consequently, setting the restraints for transpiration in the model higher will lead to a better fit for the model from June to December, but to a significantly larger underestimation for January till May. This also indicates that the actual plant behavior is not yet fully described by the formulae used.

4.1.2. Substrate Temperature

Substrate temperature modeling proved more robust for the freely draining Economy Roof, indicating that the simplified heat capacity formulation is most reliable under moderate moisture content. Under saturated conditions, particularly in the Retention Roof during late winter, the model significantly underestimated temperatures. Looking at the data, the underestimation intensifies when the substrate moisture content is above 30%. Beneath high moisture content, the model is also not accurate when freezing occurs. This could be observed on the Retention Roof particularly during cold periods (January–March), where substrate temperatures were measured at ~0–2 °C, while the model simulated stronger diurnal fluctuations due to lacking phase change thermal dynamics. During months without freezing, substrate temperature was well predicted for the Economy Roof, with R^2 ranging from 0.88 to 0.92 and PBIAS from −5 to −1%.

The constant underestimation when substrate moisture exceeded 30% suggests the need to establish a parameter for moisture-dependent thermal conductivity and heat capacity in future work—an approach not yet standard in most green roof models. To improve thermal prediction, future model extensions should take into account phase-change heat storage in wet substrates (e.g., via integration of freeze–thaw models), Moisture-dependent thermal conductivity, dynamic albedo shifts related to snow, or wet surface reflectance.

4.1.3. Year-Round Usability and Computational Efficiency

The model achieved full-year simulation with a 5 min resolution using Microsoft Excel, confirming its high practical usability and adaptability. This stands in contrast to many high-fidelity models often implemented in numerical solvers (e.g., HYDRUS-1D), which, while detailed, are not application friendly for planners and non-specialist stakeholders [26].

With no dependence on proprietary software or high-performance computing, this tool has a high suitability for integration in user software, with the ability to simulate both ET and substrate temperature jointly, including plant physiological effects.

4.1.4. Closing Knowledge Gaps in Process Representation

The most notable gap in previous models is the lack of comprehensive, year-round validation against measured ET data, with most studies either limited to summer periods or short events. By implementing continuous, multi-seasonal validation, the present model demonstrates robust year-round predictions especially for the Retention Roof, which achieved high R^2 values across all seasons. This full-year validation offers a more nuanced understanding of temporal dynamics and systematic biases—such as the observed seasonal underestimation and overestimation patterns—which would be obscured in single-season or event-based studies.

Another substantial innovation is the explicit integration of drainage and retention layer interactions. All mentioned existing models simplify water movement to vertical percolation, neglecting the significant roles of lateral flows, capillary interactions, and water storage in sub-layers. Here, the model simulates these hydraulic couplings using empirical resaturation rates and maximum storage values derived from measurement data. Including these dynamics was pivotal in accurately predicting ET during dry periods.

Furthermore, this study incorporates year-round measurements of PAI and SCF, allowing empirical representation of seasonal vegetation shifts and their direct impact on interception and ET capacity. Such detailed vegetation parameters have rarely been implemented in previous green roof models, resulting in improved simulation of plant physiological responses (as evidenced by the close PAI/interception correlation, $R^2 = 0.91$). Incorporating dynamic vegetation factors fills another gap, supporting recent findings on the importance of plant phenology for hydrological and thermal performance.

Another advancement is the integration of an explicit interception calculation within the model. Unlike most existing green roof models this model dynamically calculates interception based on measured PAI and soil cover fraction SCF. This allows for a realistic representation of rainfall intercepted by vegetation and substrate surfaces, a process that directly affects available water for ET and drainage. The integration of interception addresses a commonly overlooked process, thereby improving hydrological realism.

4.1.5. Comparative Model Performance in Literature Context

Compared to existing modeling studies, the performance of the presented model shows incremental improvements in some areas, particularly for ET on the Retention Roof,

but also highlights where performance remains comparable to earlier work, especially regarding substrate temperature and ET on the Economy Roof (Table 5).

Table 5. Model performance comparison.

	Substrate Temperature			Evapotranspiration	
	R^2	RMSE	PBIAS	R^2	PBIAS
Economy Roof	0.91	4.07	−8%	0.77	22%
Retention Roof	0.83	4.33	−21%	0.87	−1%
Sailor [8]		4.1			
Tabares [25]		1.8 to 2.0	−4 to −6%		−24% to 4%
Decruz [27]		1.1 to 2.4			
de Munck [26]	0.91	4.32			
Feng [46]				0.28–0.67	5 to 11%

For ET, the model achieves a strong correlation and low bias on the Retention Roof (R^2 = 0.87, PBIAS = –1%), reflecting a real advancement in terms of year-round accuracy and balanced hydrological prediction. This level of performance exceeds the models by Feng (PBIAS 5–11%, R^2 0.28–0.67) or Tabares (PBIAS –24% to +4%).

In contrast, the Economy Roof produces an R^2 of 0.77 and a PBIAS of 22%, suggesting a moderate overestimation and a performance level comparable to the existing models of Feng (PBIAS 5–11%, R^2 0.28–0.67) and Tabares (PBIAS –24% to +4%). While the incorporation of interception and layered retention processes represents a methodological improvement and a key reason for the good performance of the Retention Roof, these improvements did not translate into a clear overall gain in predictive accuracy.

For substrate temperature, the results are robust but not exceptional. The model achieves similar performance metrics to previously published approaches, particularly under warm and rather dry conditions. Comparable values reported by de Munck (R^2 = 0.91; RMSE ≈ 4.3) and Tabares (RMSE ~2.0, PBIAS –4 to –6%) place the current model of the economy roof within the upper performance range, but not significantly beyond it.

In summary, the presented model stands out mainly through its process completeness and transparency, with unique features such as integrated interception modeling, dynamic vegetation inputs, and explicit retention-layer coupling. These advances show the models realism and reproducibility. However, in terms of quantitative performance—particularly for substrate temperature and ET on more simplified roof types—it achieves results broadly in line with existing models. The clearest gain is observed in hydrological performance on retention-optimized systems.

4.2. Limitations and Recommendations

While the presented model achieves robust performance in the simulation of ET—particularly on the retention roof—several limitations remain that underline necessities for future refinement.

Most notably, substrate temperature simulations under freezing and water-saturated conditions showed reduced accuracy, especially for the Retention Roof during winter months. This underperformance highlights the need to expand the thermal module by incorporating moisture-dependent thermal conductivity and heat capacity, as well as freeze-thaw dynamics and latent heat storage. These processes are crucial for replicating thermal buffering and phase-change effects, which are currently oversimplified.

In addition, it seems that vegetation dormancy transitions, particularly in late autumn, are not yet fully captured.

The transferability and reproducibility of the presented model are subject to climatic and contextual limitations. First, all measurements and model validations were conducted at a single temperate, humid site in southern Germany, which is characterized by distinct seasonal dynamics and a relatively uniform distribution of precipitation throughout the year. This means that part of the model equations and parameters, including vegetation development (PAI) and interception are calibrated for climates with moderate winters, warm summers, and sufficient rainfall. In regions with fundamentally different climatic conditions—such as arid zones with pronounced droughts, subtropical climates with highly seasonal rainfall, or areas with persistent snow cover in winter—processes may behave differently and require re-calibration or adaptation. Furthermore, the model is based on two specific green roof systems (Economy Roof and Retention Roof) that use substrate types, thicknesses, and plant species commonly found in the German and central European market, particularly drought-tolerant Sedum species. In other regions, alternative plant communities or substrate assemblies with different water retention and heat storage properties may influence the magnitude and timing of both ET and temperature regulation. It is therefore essential to locally validate vegetation parameters and substrate hydrophysical properties before applying the model in new contexts. Additionally, the field experiment was carried out on relatively small lysimeter surfaces under controlled edge conditions in a peri-urban environment. Larger roof areas, more complex urban settings, or significant variations in exposure, shading, or wind regimes could alter the local microclimate and influence the performance of green roof systems beyond the bounds tested here. Consequently, the direct transfer of the model to other geographic and climatic contexts must proceed with caution. Site-specific adjustments and empirical validation are recommended to ensure reliable model performance and reproducibility under different environmental boundary conditions.

4.3. Practical Implications

A key strength of the presented model is its low computational demand, enabling year-round simulations without the need for proprietary software or numerical solvers. This makes it particularly suitable for integration into urban planning software, where quick assessments and scenario evaluations are often required within constrained time and resource environments.

The model demonstrates how a mechanistically informed, yet accessible tool could support the evaluation and design of green infrastructure under variable and evolving climate conditions.

Of particular relevance is its scalability for use in climate-resilient infrastructure planning, where green roofs are increasingly recognized as multifunctional assets for water retention, thermal regulation, and biodiversity enhancement. The year-round simulation capability addresses the research gap illustrated before.

By also capturing the ET process of Retention Roofs the model is well-positioned for inclusion in forward-looking planning frameworks such as DWA-A 102-1 from the German association of water management, which promotes the integration of green roofs into water-sensitive and heat-adaptive strategies at both building and urban scales [47]. Moreover, the empirical basis of the model should facilitate reproducibility and foster trust among practitioners and decision-makers.

5. Conclusions

This study developed and empirically validated a new model to simulate year-round evapotranspiration and substrate temperature for two fundamentally different extensive green roof types. The model demonstrates very high accuracy for evapotranspiration on

retention-optimized roofs, with an R^2 value of 0.87 and a PBIAS of –1%, and for substrate temperature on conventional roofs, with an R^2 of 0.91 and a PBIAS of –8%. Notable methodological advancements include the explicit integration of rainfall interception, dynamic modeling of plant canopies through PAI and SCF, and the simulation of water storage layer coupling—features that were absent in most prior models. Model performance proves robust across all seasons, and the approach can be implemented without relying on high computational power.

If incorporated into appropriate software tools, the model enables practitioners and planners to reliably predict the key hydrological and thermal functions of green roofs year-round, thereby supporting informed decisions in urban stormwater management and heat mitigation. Its low computational demand makes it especially applicable for routine planning and design in urban green infrastructure, corresponding to sector standards such as DWA-A 102-1.

Despite these strengths, some limitations remain: accuracy in substrate temperature simulation diminishes under freezing or fully saturated conditions, and estimates for evapotranspiration in conventional shallow roofs are less reliable during periods of plant dormancy. Consequently, further model improvements should aim to address freeze–thaw dynamics, moisture-dependent thermal properties, and vegetation dormancy and stress responses. In summary, the presented model closes key methodological gaps and is well suited for comprehensive assessment and design of green roofs in climate-resilient urban contexts. Future work should focus on extending its applicability to a broader range of climate zones and vegetation types, and on further refining the simulation of winter processes.

Funding: The data were collected as part of the Project "Building physics design of urban surfaces for a sustainable quality of life and environment in cities" which is 60% funded by the Federal Ministry of Education and Research BMBF (Grant Number: 01LR2022D). The remaining 40% was funded by Optigrün international AG.

Data Availability Statement: The raw data used for the analysis in this study can be provided on request by contacting the corresponding author.

Acknowledgments: We kindly acknowledge the permission of Optigrün international AG to use space for the experimental setup in the parking lot.

Conflicts of Interest: The author is an employee at the Optigrün international AG. The roof systems analyzed in this study are commercially available from Optigrün international AG, therefore, the funders had an influence on the choice of systems to be assessed. Still, all scientific standards were adhered to during the evaluation and processing of the data and the results are presented truthfully.

Abbreviations

The following abbreviations are used in this manuscript:

a_s	Angstrom parameter $[-]$
b	seasonal correction factor $[-]$
b_s	Angstrom parameter $[-]$
c	cloud cover $[-]$
C	interception storage [mm]
C_a	volumetric heat capacity air $\left[\text{MJ m}^{-3}\ \text{K}^{-1}\right]$
c_p	specific heat capacity air $\left[\text{kJ kg}^{-1}\ {}^{\circ}\text{C}^{-1}\right]$
D	discharge interception storage [mm]
D_s	drainage storage [mm]
D_{smax}	maximum drainage storage [mm]

d_r	inverse earth-moon distance [−]
e_s	vapour pressure at saturation [kPa]
e_a	actual vapour pressure [kPa]
E_p	potential evaporation [mm]
E_i	actual evaporation interception storage [mm]
E_s	substrate evaporation $\left[\text{kg m}^{-2}\ \text{s}^{-1}\right]$ [mm for Equation (17)]
ET	actual evapotranspiration [mm]
G	soil heat flux $\left[\text{MJ m}^{-2}\right]$
G_{plant}	soil heat flux plants $\left[\text{MJ m}^{-2}\right]$
G_{sc}	solar constant $\left[\text{MJ m}^{-2}\ \text{min}^{-1}\right]$
G_{sub}	soil heat flux substrate $\left[\text{MJ m}^{-2}\right]$
H	sensible heat flux density $\left[\text{MJ m}^{-2}\right]$
h_c	crop height [m]
H_r	relative air humidity [−]
h_{sub}	Substrate thickness [mm] [m for Equation (19)]
I	Substrate resaturation [mm]
i	Substrate resaturation velocity $\left[\text{mm period}^{-1}\right]$
J	number of day of the year [−]
k	von Karman constant [−]
L_m	longitude [rad]
L_z	longitude at center of time zone west of Greenwich [rad]
MO	Monin–Obukhov's stability parameter [−]
n	measured sunshine duration [h]
N	rainfall [mm]
q_d	discharge drainage [mm]
q_s	discharge substrate [mm]
P	atmospheric pressure [kPA]
p	atmospheric density $\left[\text{kg m}^{-3}\right]$
p_a	water vapor density air $\left[\text{kg m}^{-3}\right]$
p_s	water vapor density substrate $\left[\text{kg m}^{-3}\right]$
ρ_{vs}	saturated water vapor density $\left[\text{kg m}^{-3}\right]$
r_a	aerodynamic resistance $\left[\text{s m}^{-1}\right]$
r_c	stomatal resistance $\left[\text{s m}^{-1}\right]$
r_{cmin}	minimum stomatal resistance $\left[\text{s m}^{-1}\right]$
r_s	substrate surface resistance $\left[\text{s m}^{-1}\right]$
PAI	plant area index [−]
PAI_e	plant area index Economy Roof [−]
PAI_r	plant area index Retention Roof [−]
q_d	outflow drainage layer [mm]
q_s	substrate drainage [mm]
R_a	extraterestric radiation [MJ m^{-2}]
R_i	Richardson number [−]
R_n	net radiation [MJ m^{-2}]
R_{ns}	shortwave net radiation [MJ m^{-2}]
R_{nl}	longwave net radiation [MJ m^{-2}]
R_s	solar radiation [W m^{-2}]
R_{so}	solar radiation at clear sky [W m^{-2}]
S_c	seasonal correction factor sun hours [h]
S_{max}	maximum interception storage [mm]
SFC	soil cover fraction [−]
SCF_i	Inverse soil cover fraction [−]
t	standard time mid period [−]
t_{dh}	maximum daylight hours [h]

t_{sh}	sun hours per day [h]
T_a	air temperature [°C][$K\ for\ R_{nsub},\ R_{nl},\ f(Temp), \varepsilon_a, MO,\ T_{kv}$]
T_s	substrate temperature [°C][K for R_{nsub}]
T_t	atmospheric transmission coefficient [−]
$T_{max,k}$	maximum air temperature during period [K]
$T_{min,k}$	minimum air temperature during period [K]
T_{kv}	virtual temperature [K]
TR	actual transpiration [mm]
TR_p	potential Transpiration [mm]
U_z	wind velocity $\left[\mathrm{m\ s^{-1}}\right]$
VPD	vapor pressure deficit [−]
w	sun angle mid period [rad]
w_1	sun angle start period [rad]
w_2	sun angle end period [rad]
w_s	sun hour angle [rad]
z	height above sea level [m]
z_h	height of air humidity measurements [m]
z_m	height of wind velocity measurements [m]
z_{oh}	roughness length for sensible heat flux [m]
z_{om}	roughness length for momentum [m]
z_t	height of temperature measurements [m]
α	albedo [−]
γ	psychrometric constant $\left[\mathrm{kPa\ ^\circ C^{-1}}\right]$
δ	sun angle [rad]
ε_a	atmospheric emissivity at clear sky [−]
ε_s	substrate emissivity [−]
ζ	atmospheric stability parameter [−]
θ	volumetric water content $\left[\mathrm{m^3\ m^{-3}}\right]$
θ_d	discharge substrate $\left[\mathrm{m^3\ m^{-3}}\right]$
θ_{fk}	volumetric water content at field capacity $\left[\mathrm{m^3\ m^{-3}}\right]$
θ_{wp}	volumetric water content at wilting point $\left[\mathrm{m^3\ m^{-3}}\right]$
θ_{Imax}	Maximum substrate resaturation $\left[\mathrm{m^3\ m^{-3}}\right]$
κ	extinction coefficient [−]
σ	Stefan–Boltzmann constant $\left[\mathrm{MJ\ K^{-4} m^{-2} d^{-1}}\right]$
λ	latent evaporative heat $\left[\mathrm{J\ kg^{-1}}\right]$
ψ_h	heat flux atmospheric correction factor [−]
ψ_m	momentum atmospheric correction factor [−]
Δ	slope of the saturation–vapor–pressure temperature curve $\left[\mathrm{kPa\ ^\circ C^{-1}}\right]$

Appendix A

Table A1. Summary of used equations.

	Equation	New/Adopted/Modified	Source
Extraterrestrial Radiation	$R_a = \frac{12(60)}{\pi} G_{sc} d_r[(w_2 - w_1)\sin(\varphi)\sin(\delta) + \cos(\varphi)\cos(\delta)(\sin(w_2 - w_1))]$ $w_1 = w - \frac{\pi t_1}{24}$ $w_2 = w + \frac{\pi t_1}{24}$ $w = \frac{\pi}{12}[(t + 0.06667(L_z - L_m) + S_c) - 12]$ $S_c = 0.1645\sin(2b) - 0.1255\cos(b) - 0.025\sin(b)$ $b = \frac{2\pi(J-81)}{364}$ $d_r = 1 + 0.033\cos\left(\frac{2\pi}{365} J\right)$ $\delta = 0.409\sin\left(\frac{2\pi}{365} J - 1.39\right)$ $\omega_s = arccos(-tan\varphi\ tan\delta)$	Adopted	[48]

Table A1. *Cont.*

	Equation	New/Adopted/Modified	Source
Short and Longwave Radiation	$R_n = R_{ns} - R_{nl}$ $R_{so} = (a_s + b_s)R_a$ $R_s = \left(a_s + b_s \frac{t_{sh}}{t_{dh}}\right) R_a$ $N = \frac{24\omega_s}{\pi}$ $R_{ns} = (1-\alpha)\left(a_s + b_s \frac{n}{N}\right) R_a$ $R_{\mathrm{nl}} = \sigma \cdot \left(\frac{\left(T_{\mathrm{max,k}}{}^4 + T_{\mathrm{min,k}}{}^4\right)}{2}\right) \cdot (0.34 - 0.14 \cdot \sqrt{e_{\mathrm{a}}}) \cdot \left(1.35 \cdot \left(\frac{R_{\mathrm{s}}}{R_{\mathrm{so}}}\right) - 0.35\right)$	Modified for timesteps < 24 h	[48]
Net Radiation Substrate	$R_{nsub} = (1-\alpha)R_s + \left\{[(1-0.84c)\varepsilon_a + 0.84c]\frac{\sigma}{24}T_a^4 - \varepsilon_s \frac{\sigma}{24}T_s^4\right\}$	Modified for timesteps < 24 h	[49]
Albedo Substrate	$\alpha = 0.25 \quad \theta < 0.1$ $\alpha = 0.35 - \theta \quad 0.1 \leq \theta < 0.25$ $\alpha = 0.1 \quad \theta > 0.25$	Adopted	[50]
Emissivity Substrate	$\varepsilon_s = \min(0.90 + 0.18\theta_0\,; 1.0)$ $\varepsilon_a = 1.24\left(\frac{e_a}{T_a}\right)^{\frac{1}{7}}$	Adopted	[50]
Cloud Cover	$c = \begin{cases} 0 & 2.33 - 3.33T_t \leq 0 \\ 2.33 - 3.33T_t & 0 < 2.33 - 3.33T_t < 1 \\ 1 & 2.33 - 3.33T_t \geq 1 \end{cases}$ $T_t = \frac{R_s}{R_a}$	Adopted	[51]
Meteorological Parameter	$e_s = 0.611 exp\left(\frac{17.27\ T_a}{T_a + 237.3}\right)$	Adopted	[52]
	$\Delta = \frac{4098\ e_s}{(T_a + 237.3)^2}$ $\gamma = \frac{c_p P}{\varepsilon\lambda} * 10^{-3}$ $\lambda = 2.501 - \left(2.361 * 10^{-3}\right) T_a$ $P = 101.3\left(\frac{293 - 0.0065z}{293}\right)^{5.26}$ $p = 3.468\frac{P}{T_{kv}}$ $T_{kv} = T_a\left(1 - 0.378\frac{e_a}{P}\right)^{-1}$	Adopted	[48]
Potential Transpiration	$TR_p = \frac{1}{\lambda}\left[\frac{\Delta(R_n - G)}{\Delta + \gamma\left(1 + \frac{r_c}{r_a}\right)} + \frac{\frac{pc_p(e_s - e_a)}{r_a}}{\Delta + \gamma\left(1 + \frac{r_c}{r_a}\right)}\right]$ $r_a = \frac{ln\left(\frac{z_m - d}{z_{om}}\right) * ln\left(\frac{z_h - d}{z_{oh}}\right)}{k^2 U_z}$ $d = \frac{2}{3}h_c$ $z_{om} = 0.123h_c$ $z_{oh} = 0.0123h_c$ $G = \begin{cases} 0.4e^{-\kappa PAI}R_n & R_n > 0 \\ 0.5R_n & R_n \leq 0 \end{cases}$	Adopted	[53] 22 September 2025 12:08:00 p.m.
Potential Evaporation	$E_p = \frac{1}{\lambda}\left[\frac{\Delta(R_n - G)}{\Delta + \gamma} + \frac{\frac{pc_p(e_s - e_a)}{r_a}}{\Delta + \gamma}\right]$	Adopted	[37]
Stomatal Resistance	$r_c = \frac{r_{cmin}}{0.5\ LAI} f(solar) f(wasser) f(DDD) f(temp)$	Adopted	[8]
	$f(solar) = 1 + e^{-0.034(R_s - 3.5)}$ $f(\theta) = \begin{cases} 1 & \theta > 0.7\theta_{fk} \\ \frac{\theta_{fk} - \theta_{wp}}{\theta - \theta_{wp}} & \theta_{wp} < \theta < 0.7\theta_{fk} \\ 1000 & \theta_{wp} > \theta \end{cases}$ $f(DDD) = \frac{0.4}{1 - 0.41 ln(e_s - e_a)} + 0.21$ $f(temp) = \frac{1}{1 - 0.0006(18 - (T_a - 273.15))^2}$	Adopted Adopted Modified Modified	[25]
Evapotranspiration Transpiration Evaporation Interception	$ET = E_i + TR$ $TR = \left(1 - \frac{C}{S_{max}}\right) TR_p$ $E_i = \min\left(E_p, E_p \frac{C}{S_{max}}\right)$	Modified	[42]
Interception	$\int N\,dt = \int E_i\,dt + \int D\,dt + \int_{t_1}^{t_2} dC$ $S_{max} = -0.33 + 0.44PAI$ $D = \max(0, C - S_{max})$	New	

Table A1. *Cont.*

	Equation	New/Adopted/Modified	Source
Evaporation Substrate	$E_s = \frac{\rho_s - \rho_a}{r_a + r_s}$ $\rho_s = \rho_{vs} H_r$ $r_{sub} = 34.5 \left(\frac{\theta}{\theta_{fk}} \right)^{-3.3}$ $r_a = \frac{1}{U_z k^2} \left[\ln \left(\frac{z_m - d + z_{om}}{z_{om}} \right) + \psi_m \right] * \left[\ln \left(\frac{z_h - d + z_{oh}}{z_{oh}} \right) + \psi_h \right]$ $MO = - \frac{C_a T_a U^{*3}}{k g H}$ $U^* = U_z k \left[\ln \left(\frac{z_m - d}{z_{om}} \right) + \psi_m \right]^{-1}$ $\zeta = \frac{z_m - d}{MO}$ Neutral Atmosphere ($\lvert T_a - T_s \rvert \leq 0.01K$): $\psi_m = \psi_h = 0$ Unstable Atmosphere $T_a < T_s$ *oder* $MO < 0$: $\psi_h = -2\ln \left(\frac{1 + \sqrt{1 - 16\zeta}}{2} \right)$ $\psi_m = -2\ln \left(\frac{1 + (1 - 16\zeta)^{0.25}}{2} \right) - \ln \left(\frac{1 + \sqrt{1 - 16\zeta}}{2} \right) + 2\arctan \left\{ (1 - 16\zeta)^{0.25} \right\} - \frac{\pi}{2}$ Stable Atmosphere $T_a > T_s$ *oder* $MO > 0$: $\psi_m = \psi_h = \begin{cases} 5\zeta & 0 < \zeta < 1 \\ 5 & \zeta > 1 \end{cases}$	Adopted	[37,43,49,54]
Sensible Heat Flux Substrate	$H = C_a \frac{T_s - T_a}{r_h}$ $r_h = \frac{\left[ln \left(\frac{z_m - d}{z_{oh}} \right) - \psi_{sh} \right] * \left[ln \left(\frac{z_t - d}{z_{om}} \right) - \psi_{sm} \right]}{k^2 * U_z}$ $\psi_{sm} =$ $2\ln \left[\frac{1 + \left(1 - 16R_i \right)^{\frac{1}{4}}}{2} \right] + \ln \left[\frac{1 + \left(1 - 16R_i \right)^{\frac{1}{2}}}{2} \right] - 2\arctan \left(\left(1 - 16R_i \right)^{\frac{1}{4}} \right) + \frac{\pi}{2}$ $\psi_{sh} = 2\ln \left[\frac{1 + \left(1 - 16R_i \right)^{\frac{1}{2}}}{2} \right]$ $R_i = \frac{g(T_s - T_a)(z - d)}{T_a U_z^2}$	Adopted	[50,55]
Water Content	$\theta = \frac{N * SCF_i - E_s * SCF_i - TR + D + I}{h_{sub}} - \theta_d$ $\theta_d = \max(0; \theta - \theta_{fk})$	New	
Substrate Temperature	$T_s = \frac{G_{sub} + G_{plant}}{C_a h_{sub}}$ $G_{sub} = R_{nsub} - H - \lambda E_s$	New	
Drainage and Storage	$I = \begin{cases} \min \left(\int i \, dt, D_s \right) & i \geq (\theta_{Imax} - \theta) h_{sub} \\ \min \left((\theta_{Imax} - \theta) h_{sub}, D_s \right) & i < (\theta_{Imax} - \theta) h_{sub} \\ 0 & \theta \geq \theta_{Imax} \end{cases}$ $D_s = \max(q_s - I - q_d, 0)$ $q_d = \max(D_s - D_{smax}, 0)$ $q_s = \theta_d h_{sub}$	New	

Table A2. Summary of all used constants.

Constant	Value
a_s	0.25
b_s	0.5
C_a	0.0012 MJ m^{-3} K^{-1}
c_p	0.000001013 kJ kg^{-1} $^{\circ}C^{-1}$
D_{smax}	5 mm for Economy Roof 28.5 mm for Retention Roof
G_{sc}	0.082
h_c	0.08 m for Economy Roof 0.15 m for Retention Roof
h_{sub}	60 mm for Economy Roof 100 mm for Retention Roof

Table A2. *Cont.*

Constant	Value
i	0.002 mm 5 min^{-1} for Economy Roof 0.005 5 min^{-1} for Retention Roof
k	0.41
L_z	6.056292504 rad
r_{cmin}	336 sm^{-1} for Economy Roof 168 sm^{-1} for Retention Roof
z	650 m
z_h	0.2 m
z_m	0.2 m
z_{oh}	0.0001 m
z_{om}	0.001 m
z_t	0.2 m
σ	4.903×10^{-9} MJ $K^{-4}m^{-2}d^{-1}$
κ	0.8
θ_{fk}	0.455 m^3 m^{-3}
θ_{Imax}	0.23 m^3 m^{-3} for Economy Roof 0.41 m^3 m^{-3} for Retention Roof
θ_{wp}	0.06 m^3 m^{-3}

References

1. Santamouris, M. Heat Island Research in Europe: The State of the Art. *Adv. Build. Energy Res.* **2007**, *1*, 123–150. [CrossRef]
2. Berardi, U. The Outdoor Microclimate Benefits and Energy Saving Resulting from Green Roofs Retrofits. *Energy Build.* **2016**, *121*, 217–229. [CrossRef]
3. Rowe, D.B. Green Roofs as a Means of Pollution Abatement. *Environ. Pollut.* **2011**, *159*, 2100–2110. [CrossRef]
4. Oberndorfer, E.; Lundholm, J.; Bass, B.; Coffman, R.R.; Doshi, H.; Dunnett, N.; Gaffin, S.; Kohler, M.; Liu, K.; Rowe, B. Green Roofs as Urban Ecosystems: Ecological Structures, Functions, and Services. *BioScience* **2007**, *57*, 823–833. [CrossRef]
5. Richter, M.; Dickhaut, W. Retentionsgründächer als multifunktionale blau-grüne Infrastrukturen—Ergebnisse eines Langzeit-Monitorings in Hamburg. In Proceedings of the Grün Statt Grau, Glattfelden, Switzerland, 14–15 November 2022; Eawag, Switzerland: Glattfelden, Switzerland, 2022; pp. 54–61.
6. Gößner, D.; Farkas, J.; Berger, D. Sind Zisternen mit intelligenter Steuerung als Überflutungsschutzspeicher nutzbar? Eine indikative Datenauswertung anhand von Praxisbeispielen. In Proceedings of the Urbanes Niederschlagswassermanagement: Herausforderungen—Möglichkeiten—Grenzen, Graz, Austria, 22–24 September 2024; Scientific Board der Aqua Urbanica: Graz, Austria, 2024.
7. Getter, K.L.; Rowe, B. The Role of Green Roofs in Sustainable Development. *HortScience* **2006**, *41*, 1276–1285. [CrossRef]
8. Sailor, D.J. A Green Roof Model for Building Energy Simulation Programs. *Energy Build.* **2008**, *40*, 1466–1478. [CrossRef]
9. Alexandri, E.; Jones, P. Temperature Reduction Effect of Vegetation Coverage on Building Surfaces. *Energy Build.* **2008**, *40*, 280–288.
10. Lundholm, J. Green Roofs and Urban Biodiversity. *Urban Habitats* **2006**, *4*, 54–66.
11. Madre, F.; Vergnes, A.; Machon, N.; Clergeau, C. Biodiversity of Extensive Green Roofs: Does Vegetation Composition and Substrate Depth Matter? *Landsc. Urban Plan.* **2014**, *122*, 93–101.
12. Mentens, J.; Raes, D.; Hermy, M. Green Roofs as a Tool for Solving the Rainwater Runoff Problem in the Urbanized 21st Century? *Landsc. Urban Plan.* **2006**, *77*, 217–226. [CrossRef]
13. Berndtsson, J.C. Green Roof Performance towards Management of Runoff Water Quantity and Quality: A Review. *Ecol. Eng.* **2010**, *36*, 351–360. [CrossRef]
14. Locatelli, L. and M., Ole and Mikkelsen, Peter Steen Modelling the Cooling Performance of a Green Roof System with Different Vegetation Types. *Build. Environ.* **2014**, *82*, 480–490. [CrossRef]
15. Zhang, G. and Z., Xin and Jin, Hong and Lin, Zhi Modelling Green Roof Water and Energy Dynamics Using EnergyPlus. *J. Build. Perform. Simul.* **2020**, *13*, 66–79.
16. Palla, A.; Gnecco, I.; Lanza, L.G. Compared Performance of a Conceptual and a Mechanistic Hydrologic Models of a Green Roof. *Hydrol. Process.* **2012**, *26*, 73–84. [CrossRef]

17. Liu, K.; Baskaran, B. Bas Thermal Performance of Green Roofs through Field Evaluation. In Proceedings of the First North American Green Roof Infrastructure Conference, Awards and Trade Show: Greening Roof-Tops for Sustainable Communities, Chicago, IL, USA, 29–30 May 2003; NRCC Report: Washington, DC, USA, 2003.
18. Cascone, S.; Coma, J.; Gagliano, A.; Pérez, G. The Evapotranspiration Process in Green Roofs: A Review. *Build. Environ.* **2019**, *147*, 337–355. [CrossRef]
19. Niachou, A. and P., Konstantina and Santamouris, Mattheos and Tsangrassoulis, Aris and Mihalakakou, George Analysis of the Green Roof Thermal Properties and Investigation of Its Energy Performance. *Energy Build.* **2001**, *33*, 719–729. [CrossRef]
20. Cirkel, D.; Voortman, B.; van Veen, T.; Bartholomeus, R. Evaporation from (Blue-)Green Roofs: Assessing the Benefits of a Storage and Capillary Irrigation System Based on Measurements and Modeling. *Water* **2018**, *10*, 1253. [CrossRef]
21. Cibelli, E. Sedum on the Onondaga County Convention Center Roof: Calculating the Fraction of Coverage of Sedum Species on an Extensive Green Roof in Syracuse, New York. Bachelor's Thesis, Syracuse University, Syracuse, NY, USA, 2021.
22. Gößner, D.; Kunle, M.; Mohri, M. Green Roof Performance Monitoring: Insights on Physical Properties of 4 Extensive Green Roof Types after 2 Years of Microclimatic Measurements. *Build. Environ.* **2025**, *269*, 112356. [CrossRef]
23. Takebayashi, H.; Moriyama, M. Surface Heat Budget on Green Roof and High Reflection Roof for Mitigation of Urban Heat Island. *Build. Environ.* **2007**, *42*, 2971–2979. [CrossRef]
24. Tabares-Velasco, P.C.; Srebric, J. A Heat Transfer Model for Assessment of Plant Based Roofing Systems in Summer Conditions. *Build. Environ.* **2012**, *49*, 310–323. [CrossRef]
25. Tabares-Velasco, P.C.; Zhao, M.; Peterson, N.; Srebric, J.; Berghage, R. Validation of Predictive Heat and Mass Transfer Green Roof Model with Extensive Green Roof Field Data. *Ecol. Eng.* **2012**, *47*, 165–173. [CrossRef]
26. de Munck, C.S.; Lemonsu, A.; Bouzouidja, R.; Masson, V.; Claverie, R. The GREENROOF Module (v7.3) for Modelling Green Roof Hydrological and Energetic Performances within TEB. *Geosci. Model Dev.* **2013**, *6*, 1941–1960. [CrossRef]
27. Decruz, A. Development and Integration of a Green Roof Model within Whole Building Energy Simulation. Ph.D. Thesis, University of Notingham, Nottingham, UK, 2016.
28. Gößner, D.; Mohri, M.; Krespach, J.J. Evapotranspiration Measurements and Assessment of Driving Factors: A Comparison of Different Green Roof Systems during Summer in Germany. *Land* **2021**, *10*, 1334. [CrossRef]
29. Ouldboukhitine, S.-E.; Belarbi, R.; Jaffal, I.; Trabelsi, A. Assessment of Green Roof Thermal Behavior: A Coupled Heat and Mass Transfer Model. *Build. Environ.* **2011**, *46*, 2624–2631. [CrossRef]
30. Djedjig, R.; Ouldboukhitine, S.-E.; Belarbi, R.; Bozonnet, E. Development and Validation of a Coupled Heat and Mass Transfer Model for Green Roofs. *Int. Commun. Heat Mass Transf.* **2012**, *39*, 752–761. [CrossRef]
31. Tian, Y.; Bai, X.; Qi, B.; Sun, L. Study on Heat Fluxes of Green Roofs Based on an Improved Heat and Mass Transfer Model. *Energy Build.* **2017**, *152*, 175–184. [CrossRef]
32. Hong, J.; Utzinger, D.M. Reducing the Heat Island Effect: A Mathematical Model of Green Roof Design. In Proceedings of the 17th Conference of IBPSA (Building Simulation 2021), Bruges, Belgium, 1 September 2021; Saelens, D., Laverge, J., Boydens, W., Helsen, L., Eds.; International Building Performance Simulation Association (IBPSA): Bruges, Belgium, 2021.
33. Pitha, U.; Zluwa, I.; Scharf, B.; Lapin, K.; Besener, I.-M.; Virgolini, J.; Kapus, S.; Preiss, J.; Enzi, V.; Jesner, L.; et al. *Leitfaden Dachbegrünung*; GERICS: Hamburg, Germany, 2021.
34. Brune, M.; Bender, S.; Groth, M. *Gebäudebegrünung Und Klimawandel. Anpassung an Die Folgen Des Klimawandels Durch Klimawandeltaugliche Begrünung*; Climate Service Center Germany: Hamburg, Germany, 2017.
35. Kottek, M.; Grieser, J.; Beck, C.; Rudolf, B.; Rubel, F. World Map of the Köppen-Geiger Climate Classification Updated. *Meteorol. Z.* **2006**, *15*, 259–263. [CrossRef] [PubMed]
36. Dunkerley, D.L.; Booth, T.L. Plant Canopy Interception of Rainfall and Its Significance in a Banded Landscape, Arid Western New South Wales, Australia. *Water Resour. Res.* **1999**, *35*, 1581–1586. [CrossRef]
37. Tabares-Velasco, P.C. Predictive Heat and Mass Transfer Model of Plant-Based Roofing Materials for Assessment of Energy Savings. Ph.D. Thesis, Pennsylvania State University, State College, PA, USA, 2009.
38. Feng, Y.; Burian, S.; Pardyjak, E. Observation and Estimation of Evapotranspiration from an Irrigated Green Roof in a Rain-Scarce Environment. *Water* **2018**, *10*, 262. [CrossRef]
39. Kemp, S.; Hadley, P.; Blanuša, T. The Influence of Plant Type on Green Roof Rainfall Retention. *Urban Ecosyst* **2019**, *22*, 355–366. [CrossRef]
40. Franzaring, M.; Anemou, M.; Hernandez Cubero, L.C.; Katsarov, I.; Kauf, Z.; Mohiley, A.; Steffan, L.; Fangmeier, A. *Untersuchungen zur Kühlwirkung und der Niederschlagsretention der extensiven Dachbegrünungsvegetation*; KLIMOPASS-Berichte; LUBW Landesanstalt für Umwelt, Messungen und Naturschutz Baden-Württemberg: Karlsruhe, Germany, 2014.
41. Knepper-Bartel, Y.-C. *Dachbegrünungsrichtlinie—Richtlinien für Planung, Bau und Instandhaltung von Dachbegrünungen*, 6th ed.; Forschungsgesellschaft Landschaftsentwicklung Landschaftsbau e. V. (FLL): Bonn, Germany, 2018.
42. Muzylo, A.; Llorens, P.; Valente, F.; Keizer, J.J.; Domingo, F.; Gash, J.H.C. A Review of Rainfall Interception Modelling. *J. Hydrol.* **2009**, *370*, 191–206. [CrossRef]

43. Camillo, P.J.; Gurney, R.J. A Resistance Parameter for Bare-soil Evaporation Models. *Soil Sci.* **1986**, *141*, 95–105. [CrossRef]
44. Allen, R.G.; Pereira, L.S.; Raes, D.; Smith, M. *Crop Evapotranspiration: Guidelines for Computing Crop Water Requirements*; FAO Irrigation and Drainage Paper 56; Food and Agriculture Organization of the United Nations: Rome, Italy, 1998; ISBN 0254-5284.
45. de Vries, D.A. Thermal Properties of Soils. In *Physics of Plant Environment*; van Wijk, W.R., Ed.; North-Holland Publishing Company: Amsterdam, The Netherlands, 1963; pp. 210–235.
46. Feng, C.; Meng, Q.; Zhang, Y. Theoretical and Experimental Analysis of the Energy Balance of Extensive Green Roofs. *Energy Build.* **2010**, *42*, 959–965. [CrossRef]
47. Deutsche Vereinigung für Wasserwirtschaft, Abwasser und Abfall e. V. (DWA). *Arbeitsblatt BWK-A 3-1/DWA-A 102-1, Dezember 2020: Grundsätze zur Bewirtschaftung und Behandlung von Regenwetterabflüssen zur Einleitung in Oberflächengewässer—Teil 1: Allgemeines*; Bund der Ingenieure für Wasserwirtschaft, Abfallwirtschaft und Kulturbau-BWK-e.V., Sindelfingen, Deutsche Vereinigung für Wasserwirtschaft, Abwasser und Abfall e.V.-DWA-, Hennef, Eds.; BWK-Arbeitsblatt; Fraunhofer IRB Verlag: Stuttgart, Germany, 2020; ISBN 978-3-96862-044-2.
48. Allen, R.; Pereira, L.; Raes, D.; Smith, M. *FAO Irrigation and Drainage Paper 56*; FAO: Rome, Italy, 1998.
49. Campbell, G.S.; Norman, J.M. *An Introduction to Environmental Biophysics*; Springer Science & Business Media: Berlin, Germany, 1977.
50. Van Bavel, C.H.M.; Hillel, D.I. Calculating Potential and Actual Evaporation from a Bare Soil Surface by Simulation of Concurrent Flow of Water and Heat. *Agric. Meteorol.* **1976**, *17*, 453–476. [CrossRef]
51. Simunek, J.; Sejna, M.; Saito, D.; Sakai, M.; van Genuchten, M. *The HYDRUS-1D Soft-Ware Package for Simulating the One-Dimensional Movement of Water, Heat Ans Multiple So-Lutes in Variably-Satured Media*; Version 4.17; Department of Environmental Sciences, University of California, Riverside: Riverside, CA, USA, 2013.
52. Tetens, O. *Über Einige Meteorologische Begriffe*; Zeitschrift für geophysik; Friedrich Vieweg & Sohn Akt.-Gesellschaft: Berlin, Germany, 1930.
53. Choudhury, B.J.; Idso, S.B.; Reginato, R.J. Analysis of an Empirical Model for Soil Heat Flux under a Growing Wheat Crop for Estimating Evaporation by an Infrared-Temperature Based Energy Balance. *Agric. For. Meteorol.* **1987**, *39*, 283–297. [CrossRef]
54. Brutsaert, W. The Roughness Length for Water Vapor Sensible Heat, and Other Scalars. *J. Atmos. Sci.* **1975**, *32*, 2028–2031. [CrossRef]
55. Barbagallo, S.; Consoli, S.; Russo, A. A One-Layer Satellite Surface Energy Balance for Estimating Evapotranspiration Rates and Crop Water Stress Indexes. *Sensors* **2009**, *9*, 1–21. [CrossRef] [PubMed]

Disclaimer/Publisher's Note: The statements, opinions and data contained in all publications are solely those of the individual author(s) and contributor(s) and not of MDPI and/or the editor(s). MDPI and/or the editor(s) disclaim responsibility for any injury to people or property resulting from any ideas, methods, instructions or products referred to in the content.